ISSN 2507-9174

De La Salle University

Journal of Computational Innovations and Engineering Applications

Vol. 2 No. 2

January 2018

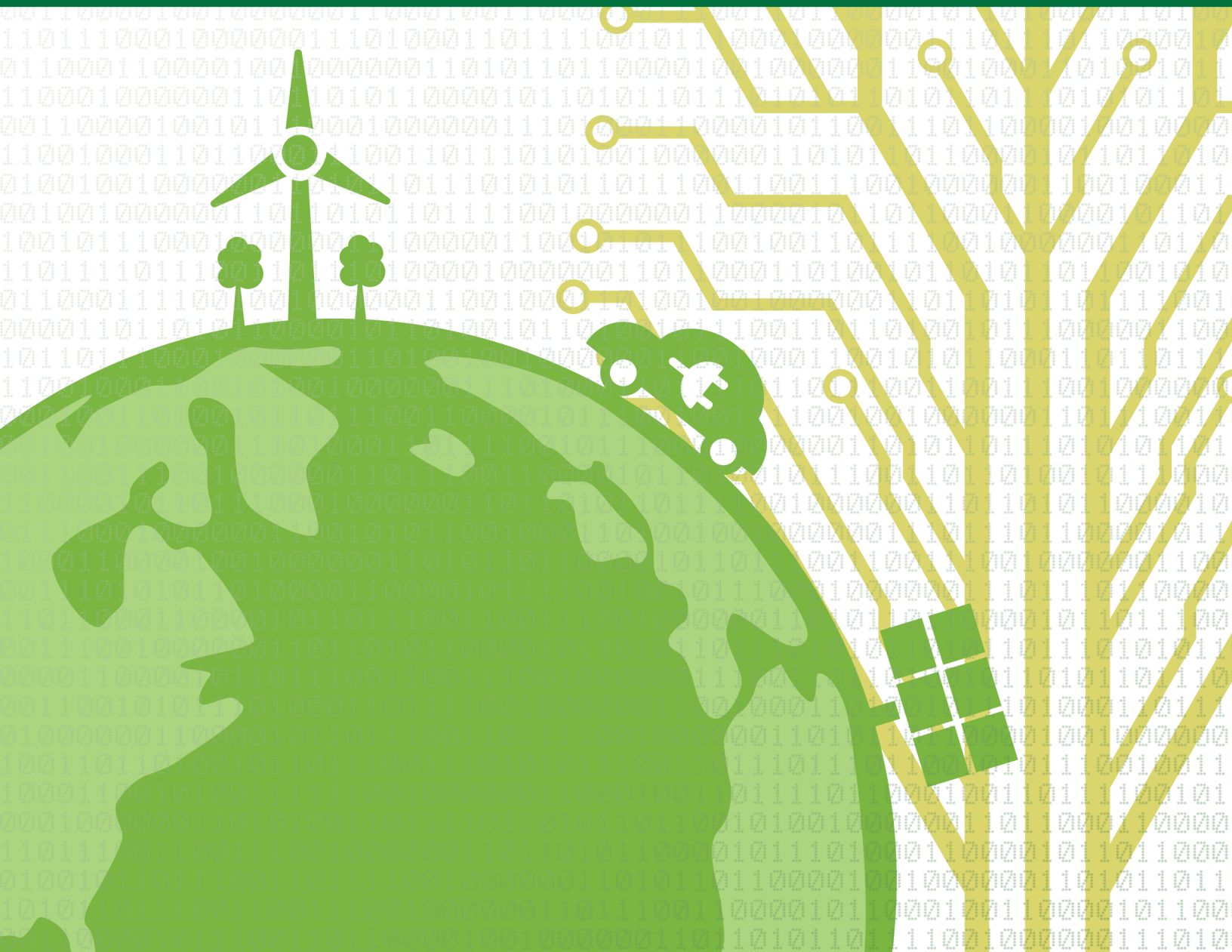

Editorial Board

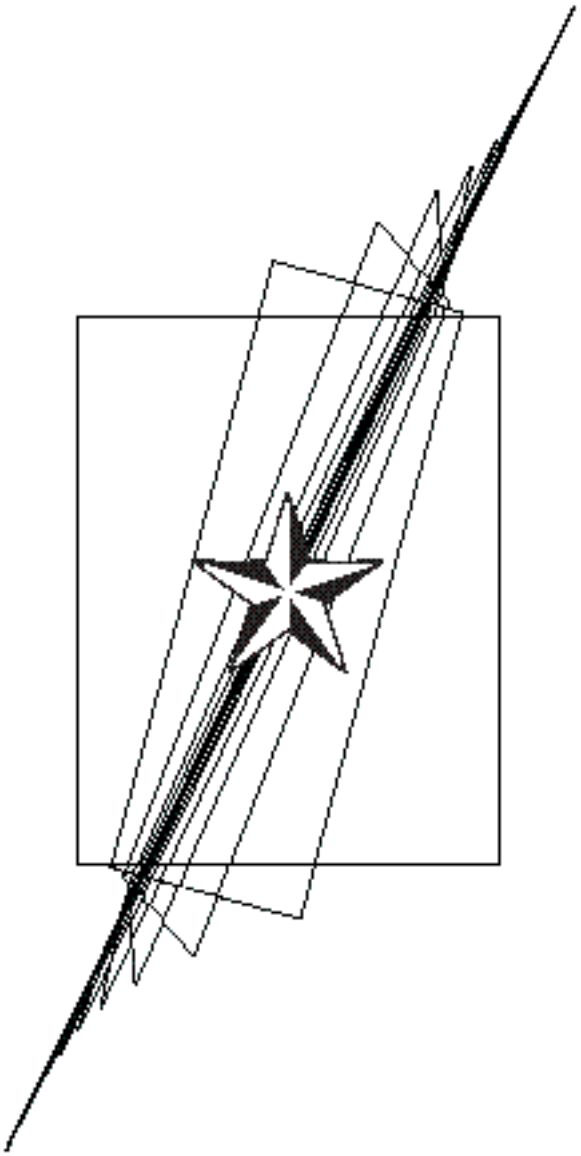

JOURNAL OF COMPUTATIONAL INNOVATIONS AND ENGINEERING APPLICATIONS

Volume 2 Number 2
2018

The **Journal of Computational Innovations and Engineering Applications (JCIEA)** is a peer-reviewed, open access journal of De La Salle University, Manila. The JCIEA aims to promote the development of new and creative ideas on the use of technology in solving different problems in different fields of our daily lives. The JCIEA solicits high quality papers containing original contributions in all areas of theory and applications of Engineering and Computing including but not limited to: Computational Applications, Computational Intelligence, Electronics and Information and Communications Technology (ICT), Manufacturing Engineering, Energy and Environment, Robotics, Control and Automation, and all their related fields. The JCIEA editorial board is comprised of experts from around the world who are proactively pushing for the development of research in these fields.

Annual Subscription Rates: Foreign libraries and institutions: US$60 (airmail). Individuals: US$50 (airmail). Philippine domestic subscription rates for libraries and institutions: Php1,800, individuals: Php1,300. Please contact Ms. Joanne Castañares for subscription details: telefax: (632) 523-4281, e-mail: dlsupublishinghouse@dlsu.edu.ph

ISSN 2507-9174

Published by De La Salle University Publishing House
2401 Taft Avenue, Manila 0922 Philippines
Telephone: (63 2) 523-4281 / 524-2611 loc 271
Fax: (63 2) 523-4281
Email: dlsupublishinghouse@dlsu.edu.ph
Website: http://www.dlsu.edu.ph/offices/publishing-house/journals.asp

The De La Salle University Publishing House is the publications office of De La Salle University, Manila, Philippines.

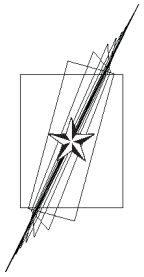

JOURNAL OF COMPUTATIONAL INNOVATIONS AND ENGINEERING APPLICATIONS

Table of Contents

From the Editor

The Journal of Computational Innovations and Engineering Applications (JCIEA) is a peer-reviewed and abstracted journal published twice a year by De La Salle University, Manila, Philippines. JCIEA aims to promote and facilitate the dissemination of quality research outputs that can push for the growth of the nation's research productivity. In its second volume, second issue, seven articles were selected to provide valuable references for researchers and practitioners in the field of environmental engineering, air quality monitoring, agricultural crop health assessment, healthcare engineering, assistive systems, machine learning, computer vision, video processing, wireless systems, motor controller for electric vehicles, and robotic systems.

The first article is "Air Quality Characterization Using *k*-Nearest Neighbors Machine Learning Algorithm via Classification and Regression Training in R". This paper aims to characterize air quality by using k-nearest neighbors machine learning algorithm to provide accurate sensor readings and calculations for an improved air quality index (AQI). The proposed methodology is implemented using a prototype of integrated gas sensors for data gathering. R programming, focusing on classification and regression training (caret) package for data processing, model development, and algorithm tuning, is utilized. The system is evaluated, and an accuracy of 99.56% is obtained.

The second article is "Assessment of Lettuce (*Lactuta sativa*) Crop Health Using Back Propagation Neural Network". Crop health assessment is important in ensuring high agricultural yield. The growth rate and productivity are factors that can help establish the expected yield by computing the crop assessment index. Using a romaine lettuce as test crop, a classification algorithm using color recognition and artificial neural network was developed for better crop quality assessment.

The third article is "Technology Acceptance Model for Breast Cancer Examination Assistant Using Computer Vision and Speech Recognition". This paper presents the development of a computer-assisted breast cancer examination using computer vision and speech recognition, with focus on user acceptance for improved technology penetration. Technology acceptance model (TAM) is used in the design concept and implementation of the breast examination assistant to rate its perceived usefulness (PU), perceived ease of use (PEOU), attitude (ATT), and behavioral intention to use (BI). Performance rating is based on Cronbach's α. Computer vision algorithm for BSE, speech recognition, and synthesis results in previous studies were highlighted to associate in TAM considerations.

The fourth article is "Performance Evaluation of HEVC With Intra-Refresh for Wireless Video Surveillance". This paper presents the result of the performance evaluation for a wireless video surveillance using the High Efficiency Video Coding (HEVC) standard. The video test sequences are converted into HEVC bit streams by the HM6.0 encoder. The HEVC bit streams were transmitted using a wireless network simulator setup for video surveillance. The effects of adjusting different parameters of the HEVC encoder, namely, the intra-refresh period and quantization parameter, were also evaluated in this paper.

The fifth article is “Comparison of High-Side and Synchronous Trapezoidal Control Using XMC-Based Brushless DC Motor Controller for Pedelecs”. This study aims to compare high-side and synchronous trapezoidal brushless DC (BLDC) control methods using an XMC-based motor controller for pedelecs. The electric bicycle implemented three different pedal-assist modes with varying human-to-motor power ratios and one throttle mode with the use of proportional-integral control. The study compares the efficiencies of two trapezoidal control methods through the throttle and pedal-assist mode. The data obtained shows that the high-side trapezoidal control is more efficient than the synchronous trapezoidal control in all modes implemented on the e-bike. This research opens possibilities to improve other BLDC control algorithms especially in terms of efficiency.

The sixth article is “Literature Review for the Design and Implementation of the Archer Robot”. This paper presents a literature review for the design and implementation of an archer robot capable of knocking an arrow to a standard recurved bow, drawing the arrow, and hitting a target. Ancient and current human-like mechanical archers using machine vision and intelligent controllers are discussed in this paper to serve as the ground work of the archer robot. Such robots with accurate and precise control systems are highly valued in automation and industrial processes.

The seventh article is “Design and Implementation of a Thermal-Based Exploration Mobile Robot”. Inaccurate control of industrial thermal processes occurs when there is no operator involvement in monitoring temperature set points. This paper examines the specifics of a temperature controlled mobile robot (MoBot) with the use of PIC16F877A microcontroller and LM 35 as temperature sensor. Experimental results showed that 98.31% accuracy of temperature readings from the sensor enabled the MoBot to properly work in different PWM values. The JCIEA editorial board expresses their warmest thanks and deepest gratitude to the distinguished authors for their outstanding contribution to JCIEA second volume, second issue. They likewise express profound appreciation to the peer reviewers for their assistance and cooperation.

Original research outputs are most welcome to JCIEA. There is no publication fee in this journal, and the research papers are assured of fair and fast peer review process. For further information, please visit www.dlsu.edu.ph/offices/publishinghouse/journals.asp.

Prof. Elmer P. Dadios, PhD
Editor-in-Chief, JCIEA

Air Quality Characterization Using *k*-Nearest Neighbors Machine Learning Algorithm via Classification and Regression Training in R

Timothy M. Amado

***Abstract* — Through the years, environmental health and protection have been ignored. However, because of recent phenomena such as climate change, people are slowly becoming aware of the environment. One of the main concerns nowadays is air pollution. To this avail, the U.S. Environmental Protection Agency (EPA) standardized air quality with the use of air quality index (AQI). However, AQI requires accurate sensor readings and complex calculation to obtain. Hence, the objective of this paper is to solve that problem by characterizing the air quality with regards to AQI through the use of *k*-nearest neighbors machine learning algorithm. The proposed methodology is implemented using a prototype of integrated gas sensors for data gathering. R programming, focusing on classification and regression training (caret) package for data processing, model development, and algorithm tuning, is utilized. The system is evaluated, and an accuracy of 99.56% is obtained.**

Keywords: **air quality characterization, AQI, KNN machine learning, sensor networks, r programming, caret**

I. Introduction

In the advent of the modernization age, the heightened awareness of people with regards to environmental and health protection puts air pollution as one of the main concerns of society. In fact, according to a report of the World Health Organization, air pollution has been the biggest environmental health risk [1]. Thus, several researches have been developed and pioneered to be able to mitigate the risks that air pollution brings to the environment.

Timothy M. Amado, Electronics Engineering Department Technological University of the Philippines–Manila. (email: timothy_amado@tup.edu.ph)

Air quality monitoring is one of the best ways to help fight against air pollution. By knowing the air quality, suggestions can be made in order to help alleviate its dangerous effects. Most of the air quality monitoring device relates the values they obtain to the air quality index (AQI). AQI is a system that standardized the levels and severity of polluted air. As the index increases, the more harmful the air would be for people, having the index of 500 being the most hazardous [2].

However, values obtained from the sensors do not show the immediate values of the AQI. And based on the available resources, calculation of sensor values relating to AQI can be somehow difficult to do. This can impose a problem when constructing prototypes of portable air quality monitoring devices.

The goal of this paper is to characterize the air quality by building a model that relates the sensor values to AQI. Machine learning is used to create the model through *k-nearest neighbor (KNN)* algorithm using R programming.

II. Related Works

This section presents the past studies done in the field of air quality monitoring.

Wang and Chen [3] developed a system that uses vehicular sensor networks (VSNs) to monitor the air quality in a city. In this study, the researchers proposed using VSNs to tactically monitor the air quality and develop an efficient data gathering and estimation (EDGE) mechanism. AQI is highlighted in this paper as the main standard for the monitoring accuracy.

Li and He [4] proposed an intelligent system for indoor air quality monitoring and purification. In this paper, the authors used wireless sensor networks to achieve the air quality monitoring, having an STC12C5A60S2 microcomputer as a core and MQ138 as the gas sensor. Air purification is achieved using a high-efficiency particulate air (HEPA) filter.

Molka-Danielsen et al. [5] presented a system using big data (BD) analytics on the analysis of the data of the

CO_2 levels on a logistics shipping base on Norway. The data were measured using wireless sensor networks, and the researchers used BD as a decision support system for the health and safety of the workers in the shipping industry.

A mobile and cost-effective platform for particulate matter (PM) air quality monitoring is proposed by Wu et al. [6]. The system uses lens-free microscopy to analyze the PM particles present in the air and machine learning to perform sizing and counting of the PM particles.

Chiwewe and Ditsela [7] suggested a method that can be used to estimate and predict different levels of pollutants, concentrating on the ozone. The authors used a multilabel classifier based on Bayesian networks machine learning algorithm to estimate the probability of the pollutants exceeding a certain threshold based on the AQI.

III. THEORETICAL BACKGROUND

This section details the theoretical knowledge used by the researchers in characterizing air quality of air. The first part gives a background about AQI, a standardization of U.S. Environmental Protection Agency (EPA) for air quality. The second part gives a run-through of the KNN machine learning algorithm.

A. AQI

After the conceptualization of the problem needed to be solved in this study, published papers, journals, and articles are consulted. Most notable studies are cited in section II of this paper.

Figure 1 shows the standard for AQI published by the U.S. EPA. The AQI is the main basis of the characterization done in this paper. It shows the levels of health concern as well as the color symbol for each AQI range.

Air Quality Index (AQI) Values	Levels of Health Concern	Colors
When the AQI is in this range:	*..air quality conditions are:*	*...as symbolized by this color:*
0 to 50	Good	Green
51 to 100	Moderate	Yellow
101 to 150	Unhealthy for Sensitive Groups	Orange
151 to 200	Unhealthy	Red
201 to 300	Very Unhealthy	Purple
301 to 500	Hazardous	Maroon

Fig. 1. AQI with color symbols and levels of health concerns [3].

According to U.S. EPA, there are six levels of air quality/pollution. Recommendations are given by the U.S. EPA in the event that certain values of AQI are observed [8].

AQI shows that air quality is standardized; however, it is not clear in the EPA article how these AQI ranges relate to exact sensor values. Hence, actual values of AQI cannot be displayed in situations where a standalone air quality monitoring device is used. Some literature provides this information as in the paper of Wang and Chen [3], where they used (1) to relate sensor values to AQI range:

$$I_k = \frac{I_{\text{high}} - I_{\text{low}}}{B_{\text{high}} - B_{\text{low}}}\left(C_k - B_{\text{low}}\right) + I_{\text{low}} \tag{1}$$

where B_{high} is a breakpoint $\geq C_k$, the average concentration of the pollutant, B_{low} is a breakpoint $\leq C_k$ and $I_{\text{high}}/I_{\text{low}}$ denotes the AQI value for $B_{\text{high}}/B_{\text{low}}$. I_k is the AQI of a given pollutant. The highest I_k calculated will be the AQI of the air being monitored [8].

B. KNN Machine Learning Algorithm

The KNN machine learning algorithm refers to a nonparametric supervised machine learning algorithm that utilizes both the nominal and numerical attributes of data by selecting the most common attribute between the KNNs or by getting the average of the values of the KNNs. This machine learning algorithm is one of the top 10 most important data mining algorithms [9].

To identify which of the attributes from the k instances in the training data set is the most similar to a new input, distances are measured. The most commonly used distances in KNN algorithm are the Euclidean distance (2), Manhattan distance (3), Minowski distance (4), and Hamming distance for the discrete data.

$$d = \sqrt{\sum_{i=1}^{k}\left(x_i - y_i\right)^2} \tag{2}$$

$$d = \sum_{i=1}^{k}\left|x_i - y_i\right| \tag{3}$$

$$d = \left(\sum_{i=1}^{k}\left(\left|x_i - y_i\right|\right)^q\right)^{1/q} \tag{4}$$

As per the appropriate value of k, algorithm tuning can be done choosing what value tailor-fits to the requirement of the given training set. The following algorithm shows the implementation of KNN machine learning [10].

Algorithm 1: *k*-Nearest Neighbors machine learning algorithm pseudocode

Input: Dataset E, Instance to classify x, Value k;

1: Calculate $d(x, x_i)$, i =1, 2, ..., n; where d denotes the Euclidean distance between the points.
2: Arrange the calculated n Euclidean distances in non-decreasing order.
3: Let k be a positive integer, take the first k distances from this sorted list.
4: Find those k-points corresponding to these k-distances.
5: Let k_i denotes the number of points belonging to the i^{th} class among k-points i.e. $k \geqslant 0$.
6: If $k_i > k_j \; \forall \; i \neq j$ then put x in class i.

Output: x_n

Aside from the simplicity of implementation, KNN is a very good algorithm for characterization if the data set is small. It has a very good predictive power and can accommodate data sets even without prior knowledge of the structure of data, which is very much applicable in the proposed methodology of this paper.

IV. METHODOLOGY

In this paper, the authors propose a method of characterization of the air quality in reference to the AQI set by the U.S. EPA.

A. Hardware Development

To be able to gather data for the construction and training of the model to be used in the machine learning algorithm, the researchers built a prototype of the air quality monitoring device consisting of an integrated array of sensors, an Arduino microcontroller, and an exhaust fan. The sensors used in this study are an air temperature sensor, a humidity sensor, and MQ2, MQ135, and MQ5 gas sensors. Table I shows the detailed specifications of each sensor used in constructing the hardware.

TABLE I
SENSORS USED FOR HARDWARE DEVELOPMENT

Sensor	Description
DHT 11	Temperature and relative humidity sensor module for Arduino
MQ2	General combustible gas sensor (methane, butane, smoke)
MQ5	Natural gas sensor (H_2, LPG, CH_4, CO, alcohol)
MQ135	General air quality sensor (NH_3, NOx, CO_2, benzene)

The sensors are selected based on their availability in the local market and compatibility with the Arduino microcontroller. These sensors will be enclosed in a compartment where the exhaust fan will also be installed. Holes are drilled facing the sensors to allow the sample air to go inside the device. Figure 2 shows the different layout views of the proposed system.

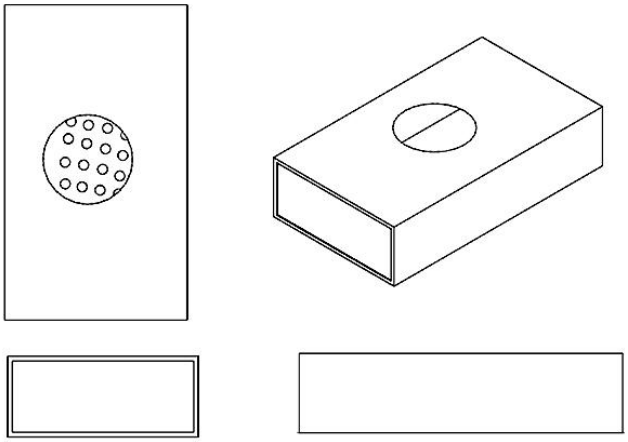

Fig. 2. Top, front, side, and isometric view of the chassis where the components of the prototype will be placed.

The prototype derives its power from a laptop computer when connected using a serial-to-USB connector. The data from the sensors are fetched by a script written in Python and written it in a comma-separated variable (CSV) file for every data collection session. A battery pack and SD card module can be installed on the system in the next iterations of the prototype.

B. Data Gathering

Next step after completing the project prototype is the data gathering. A certain scheme developed by the authors is used in gathering data since the proposed methodology will not be depending on the actual concentration readings of the sensors. Five environment conditions where air samples will be collected are chosen. These five conditions correspond to the AQI ranges stated in [3] except the "hazardous" condition (AQI $\geq$ 301). The researchers didn't choose an environment having this condition because of the health risks this AQI range might give. Table III shows the environmental condition for each AQI range/health concern cluster. These conditions are chosen based on readings from [3] and [8].

TABLE II
DATA GATHERING SCHEME

AQI Range	Levels of Health Concern	Environmental Condition
0–50	Good	Air-conditioned and properly ventilated room
51–100	Moderate	Non-air-conditioned room with poor ventilation
101–150	Slightly unhealthy	Outdoors beside a busy road
151–200	Unhealthy	Direct exposure to smoke from cars, trucks, motorcycles
201–300	Very unhealthy	Direct exposure to fumes of combustible gas, LPG, and fire

The data collection scheme that used in this paper includes deployment of the prototype on each of the environmental condition stated at Table II. A total of 150 sets of sensor data points are collected in each cluster.

C. Preprocessing, Development, and Training of the Model

This section presents the details and steps taken by the researchers in data preprocessing, development, and training of the KNN model.

1) Getting and cleaning the data. This is usually the first step of the development of every machine learning algorithm after the data has been gathered and collected. The data from the sensors are fetched into several CSV files per each cluster of observations. The data coming from the sensors are not organized. Missing values (NAs) can be encountered along the way. Also, because of the limitations of the Arduino microcontroller, the data obtained do not contain the environmental condition where the data are measured. This step takes care for all of those premises by getting and organizing the data from the CSV files, as well as cleaning them by removing any NAs and 0s. Finally, the environmental conditions where the data are measured are appended. All of these are accomplished using an R script.

2) Visualizing the data. This step involves several interactions with the R environment to give the researchers a thorough understanding of the data gathered. This involves getting plots for visual data representations, obtaining correlations, and viewing the summary of the overall data. These steps include the use of the `ggplot2` and `ggvis` packages in R.

3) Data slicing. After getting an overview of the data, the next step is to slice it into training set and testing set in preparation for training and tuning the resulting model. This is accomplished by using the classification and regression training `caret` package in R. In this paper, the authors adopted the standard 70% training and 30% testing data partition.

4) Data centering and scaling. Based on the results of the data visualization and overview, normalization, which include data centering and scaling, may be applied to the training set if the data ranges are nonuniform to standardize it. If the data are already uniform, this step may be skipped; however, in most of the cases, the data obtained need normalization in preparation for training. This is again achieved using the `caret` package in R.

5) Training the network. After data has been normalized, the KNN model can now be established. The `caret` package in R provides some useful tools to make it easier to establish and train a certain machine learning algorithm model. For the KNN, the training method that will be used to obtain the best model is the repeated cross-validation method.

In repeated cross-validation method, the training data are randomly divided into k sets or *folds* of approximately equal sizes. The KNN model is formed using all the samples except the first fold, after which the prediction error of the KNN is obtained using the first fold. The same process is repeated for each fold. The performance of the KNN model is calculated by averaging the errors obtained from the different folds.

In this paper, the researchers used the standard 10-fold, 10-repeats cross-validation method [11] in evaluating the performance of the KNN model.

6) Algorithm tuning. Algorithm tuning is a blind search methodology for the appropriate value for k to be used in the KNN algorithm. The `caret` package also provides a neat tool to employ algorithm tuning.

D. Testing and Evaluation

The KNN model will be tested using the test data set obtained from the partition of the original data set. The target accuracy is 95% to make it at par with the current KNN machine learning algorithms.

V. RESULTS AND DISCUSSION

This section presents the results of the methodologies done in section IV of this paper. This includes presentation of the actual hardware prototype, as well as the results of the data gathered together with the KNN model.

A. Project Prototype

The following images (Fig. 3) present the actual project prototype used in the data gathering phase of this paper.

Fig. 3. Different views of the protoype used in the data gathering phase.

The data can be read from the console of the Python IDLE. Because sensors take some time before stabilizing, data must be monitored in the console before being saved as CSV.

B. Overview of the Data

This section presents the overview of the data during the getting, cleaning, and visualization phases. All of the processes are done using R scripts and R packages.

Table III shows the head of the sampled cleaned data. Here, missing values are already removed from the data set, and categories are added based on the environmental condition where the data were originally measured.

The data frame is composed of 750 observation points with six variables corresponding to sensor values and the air quality classification.

Using the `ggvis` package, several plots are obtained to give a further visualization of the data at hand. Figure 4 shows several scatter plots relating sensor values to temperature.

TABLE III
HEAD OF THE SAMPLED CLEANED DATA

Obs. No.	Air Temp (°C)	Relative Humidity (%)	MQ2 (ppm)	MQ135 (ppm)	MQ5 (ppm)	Air Quality
551	30	73	34	95	117	Moderate
645	16	75	42	120	130	Good
411	32	66	46	123	188	S. Unhealthy
604	31	80	74	194	224	Unhealthy
727	29	84	139	265	239	V. Unhealthy
540	31	80	39	118	148	Moderate

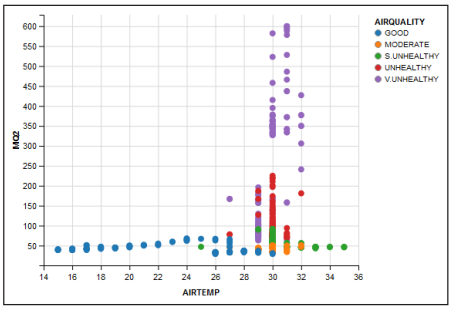

(a)

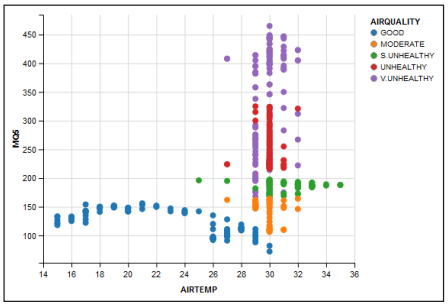

(b)

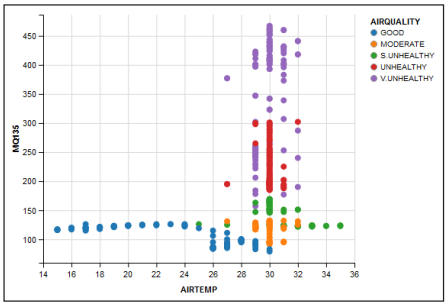

(c)

Fig. 4. Several scatter plots showing relationship of air temperature and sensor values: (a) air temperature versus MQ2, (b) air temperature versus MQ5, and (c) air temperature versus MQ135.

Based on the scatter plots, it can be observed that generally, for naturally low-temperature environments, air quality is "good" as indicated by a spread of blue points on the lower temperature section of each scatter plot. It can also be observed that for naturally high-temperature environments, high sensor values tend to appear. As for the clustering, it can be seen that only few outliers exist and majority of the data for each air quality condition tend to group up at specific portions of the plot. This implies that categorization using a machine learning model is very viable.

Figure 5 shows the smoothed curve of relationship between sensor values. The smoothed curve is obtained using the *locally weighted scatter plot smoothing* model or commonly called as the *LOESS model*. The LOESS model performs local fitting to give the best fit curve for data relationships. It is noted however that LOESS produces a model that does not result in an explicit form of an equation. However, prediction, interpolation, and extrapolation can be done by simulating the model [12].

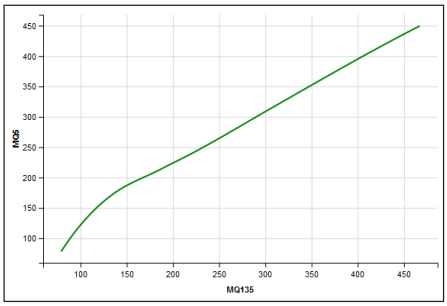

(a)

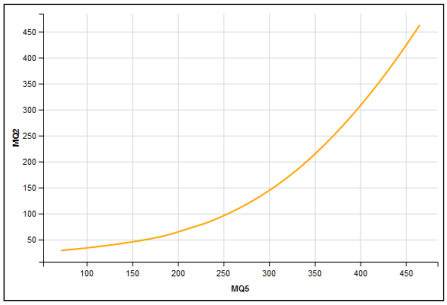

(b)

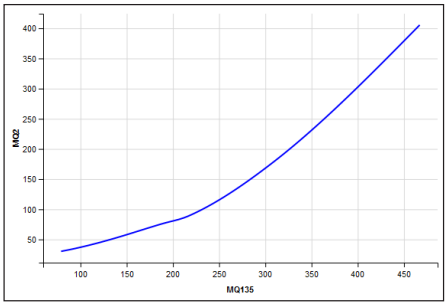

(c)

Fig. 5. Smoothed curve using the LOESS model: (a) MQ5 versus MQ135, (b) MQ2 versus MQ5, and (c) MQ2 versus MQ135.

It can be seen that as reading on a sensor increases, the other sensor values also increase. This means that there is a common component (a common gas that both sensors detect) between each sensor. It implies that as a future directive, principal component analysis may be employed to further characterize the data before applying a machine learning algorithm.

C. *Trained KNN Model Results*

After having a comprehensive overview and understanding of the data at hand, the development of the model comes next. This section presents the results of fitting and training a KNN machine learning algorithm for the characterization of air quality data. Training is done using the `caret` package.

Table IV shows the possible values of k obtained after algorithm tuning. The system automatically chooses the value of k based on the accuracy and kappa value of the model. Kappa is one of the machine learning metrics that is similar to classification accuracy but more useful when the distribution in of frequency in each class is nonuniform.

TABLE IV
ALGORITHM TUNING

k	Accuracy	Kappa
5	0.9959992	0.9949969
7	0.9958106	0.9947610
9	0.9954401	0.9942981
11	0.9937304	0.9921601
13	0.9899011	0.9873726
15	0.9893275	0.9866556
17	0.9885660	0.9857031
19	0.9889584	0.9861937
21	0.9887582	0.9859431
23	0.9883914	0.9854845

It can be seen from the figure that the best value is $k = 5$. The repeated cross-validation method for 10-folds and 10 repeats are used to map the accuracy of the model.

D. *Test and Evaluation Results*

The KNN model developed is tested using a test data set obtained from performing data slicing on the original data set. The overall accuracy for KNN model is 99.56%.

Moreover, Table V shows the overall statistics of the KNN model.

TABLE V
SUMMARY OF OVERALL MODEL STATISTICS

Accuracy	0.9956
95% Confidence interval	0.9755, 0.9999
No information rate (NIR)	0.2
p-Value (Acc > NIR)	$p < 2.2e\text{-}16$
Kappa	0.9944
Mcnemar's test *p*-value	NA

From Table V, the summary of the overall statistics of the model developed can be seen. Notable values here are the "no information rate," which basically means the largest class percentage in the data (which is 20% because there are five classes equally distributed). The *p*-value is obtained from a one-sided test taken to check if there is a significant difference for the accuracy when the data is considered only for the majority class. Since our *p*-value is small, it implies that the accuracy doesn't have a significant difference whether it came from the majority class or not. McNemar's test *p*-value is not applicable because the classes are sparse.

VI. CONCLUSIONS

Based on the data and results, the proposed method of characterization of the AQI using KNN machine learning algorithm is implemented successfully. A project prototype made up of an array of sensors is developed. A KNN machine learning model is established with 99.56% accuracy. Overall, the statistics of the model is excellent and accurate.

ACKNOWLEDGMENT

The author acknowledges Mapua University for the support in terms of access to the IEEE database that led to the vast improvement of this paper. The author would also like to thank the Department of Science and Technology – Philippine Council for Industry, Energy and Emerging Technologies for Research and Development (DOST-PCIEERD) for the Data, Connectivity and Intelligence: Data Science track training received, which proved to be a valuable asset that led to the fruition of this paper.

REFERENCES

[1] World Health Organization (WHO), "7 million premature deaths annu- ally linked to air pollution," Mar. 2014. [Online]. Available: http://www. who.int/mediacentre/news/releases/2014/air-pollution/en/.

[2] U.S. Environmental Protection Agency, "Air quality guide for particle pollution," US EPA, 2015.

[3] Y.C. Wang and G.W. Chen, "Efficient data gathering and estimation for metropolitan air quality monitoring by using vehicular sensor networks," *IEEE Trans. Veh. Technol.*, vol. 66, no. 8, pp. 7234–7248, 2017.

[4] Y. Li and J. He, "Design of an intelligent indoor air quality monitoring and purification device," in *2017 IEEE 3rd Information Technology and Mechatronics Engineering Conference (ITOEC)*, 2017, pp. 1147–1150.

[5] J. Molka-Danielsen, P. Engelseth, V. Olesnanikova, P. Sarafin, and R. Zalman, "Big data analytics for air quality monitoring at a logistics shipping base via autonomous wireless sensor network technologies," *2017 5th Int. Conf. Enterp. Syst.*, pp. 38–45, 2017.

[6] Y. Wu et al., "Mobile microscopy and machine learning provide accurate and high-throughput monitoring of air quality," in *2017 IEEE Conference on Lasers and Electro-Optics*, 2017.

[7] T. M. Chiwewe and J. Ditsela, "Machine learning based estimation of Ozone using spatio-temporal data from air quality monitoring stations," in *2016 IEEE 14th International Conference on Industrial Informatics (INDIN)*, 2016, pp. 58–63.

[8] U.S. Environmental Protection Agency, "Technical assistance document for the reporting of daily air quality—The air quality index (AQI)," US EPA, Dec. 2013.

[9] R. Agrawal, "*k*-nearest neighbor for uncertain data," *Int. J. of Computer Applications*, vol. 105, no. 11, pp. 13-16, 2014.

[10] J. M. Cadenas, M. C. Garrido, R. Martinez-Espana, and A. Munoz, "A more realistic *k*-nearest neighbors method and its possible applications to everyday problems," in *2017 IEEE International Conference on Intelligent Environments (IE)*, 2017, pp. 52–59.

[11] S. Borra and A. Di Ciaccio, "Measuring the prediction error. A comparison of cross-validation, bootstrap and covariance penalty methods," *Comput. Stat. Data Anal.*, vol. 54, no. 12, pp. 2976–2989, 2010.

[12] W. S. Cleveland, E. Grosse, and W. M. Shyu. "Local regression models," in *Statistical Models in S*, J.M. Chambers and T.J. Hastie, Eds. Wadsworth & Brooks/Cole, Pacific Grove, California, 1992.

Assessment of Lettuce (*Lactuta sativa*) Crop Health Using Backpropagation Neural Network

Ira C. Valenzuela,[1,]* Argel A. Bandala,[2] and Elmer P. Dadios[2]

***Abstract* — The determination of the healthiness of a crop is relevant in ensuring a high agricultural yield. The growth rate and the productivity are the factors that can help to establish the expected yield. This is done by computing the crop assessment index. The main objective of this study is to develop a simple color recognition algorithm using digital image processing techniques. This will eliminate subjectiveness in the classification of healthy and unhealthy lettuce. Moreover, this can help the farmers to assess the quality of the crops while growing them. The crop used in this study is romaine lettuce. The image processing was built using LabView Vision Assistant through RGB acquisition. The backpropagation of the artificial neural network was used to increase the efficiency of the system in assessing the quality of the lettuce. The total number of images used in the study is 280 wherein 15% were used for validation, 15% were used for testing, and 70% were used for training. The developed system proves to provide a better assessment of the lettuce crop health.**

Keywords: **lettuce, crop health assessment, ANN, backpropagation**

I. Introduction

The features that can determine the crop yield are its health and its seasonal progress. These are critical characteristics and are early indicators of the possible amount of crop yield, crop risk, and the degree of success or failure [1]. The determination of the healthiness of a crop is relevant in ensuring a high agricultural yield. The conceivable stresses that will cause low yield must be mitigated by the farmers at the early stage of the crop growth. Examples of these stresses are the parasite infestations, moisture deficiencies, and weed infestations. Growth rate and productivity are the factors that can help to establish the expected yield. This is done by computing the crop assessment index.

Traders of agricultural products are not usually in the field to personally monitor the growth and crop yield. They generally rely on the crop assessment index and other data that the farmers are giving to them in setting the price of the crops. These data are used for worldwide negotiation of trade agreements [2]. Also, this can help to locate future problems like the famine in Ethiopia. A significant drought was experienced during the 1980s and devastated a lot of crops. Humanitarian aid and relief efforts will be facilitated in advance when it is forecasted early [3].

The traditional way of assessing the crops' health is by visual inspection of its physical features. Possible diseases infecting the crops are seen through the discoloration on its surface. Also, the nutrient contents are measured in laboratories to check if these are sufficient [4]. Current technologies such as [5][6] involve the measurement of normalized differential vegetation index (NDVI). Hyperspectral images are captured and processed in a software [7][8][9]. These are done for large vegetation areas. In one study, the researcher proposed that to improve the color image feature, image normalization is done through color transfer process. The condition is that the data set should be uniform [10][11].

In this study, the crop to be modeled is a lettuce. *Lactuta sativa L*. or commonly known as lettuce as shown in Figure 1 is one of the most important salad crops and is grown worldwide. It originated from Asia. It can grow best in temperatures 45°F–80°F. It can also grow in hotter weather but for short intervals and taste bitter [12]. There are seven types of lettuce, but for this study, the romaine type of lettuce will be studied.

Fig. 1. Romaine lettuce.

[1]Ira C. Valenzuela, Technological University of the Philippines, Manila, Philippines (e-mail: patellaw@biust.ac.bw)

[2]Argel A. Bandala and Elmer P. Dadios De La Salle University, Manila, Philippines

The main objective of this study is to develop a simple color recognition algorithm using digital image processing and pattern recognition. This will eliminate subjectiveness in the classification of healthy and unhealthy lettuce. Moreover, this can help the farmers to assess the quality of the crops while growing it.

The rest of the paper is organized as follows: Section II explains how to extract the features and their analysis. This includes the data acquisition and experimental setup. Section III explains the structure of the network, the input and the output, and the criteria for the network. In Section IV, the data obtained from the training, validating, and testing are discussed. Finally, Section V gives conclusions.

II. FEATURE EXTRACTION AND ANALYSIS

Figure 2 illustrates the block diagram of the system. It consists of the different methods applied to obtain the desired output. The preprocessing is done on LabVIEW software.

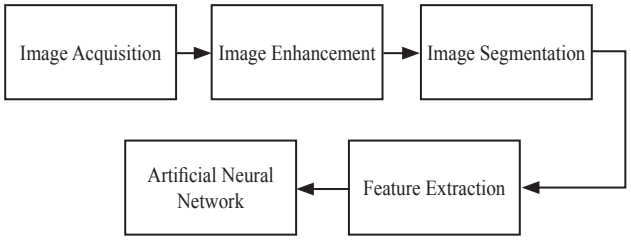

Fig. 2. Block diagram of the system.

A. Image Acquisition

Two hundred eighty (280) images of lettuce are gathered. These images include the quality classifications good and reject.

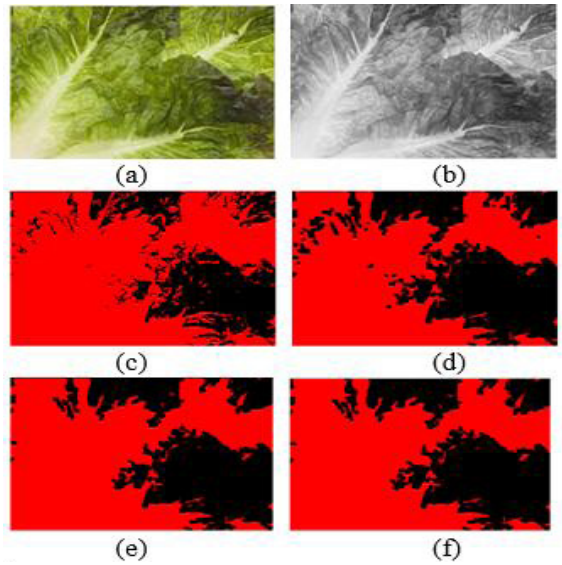

Fig. 3. Image processing of the sample lettuce leaf.

B. Image Enhancement

The purpose of enhancing the image is to reduce the noise present in the image and to adjust the image contrast. Color space conversion has been done also through translating the RGB values into HSV values. This is illustrated in Figure 3b. The image color is converted into HSV because of its similarity with the human eye perception. This is the mostly used color model in high-end image processing. The RGB color model is based on the three independent color planes, namely, red, green, and blue. And to state a certain color is to specify the amount of RGBs present on that particular color. On the other hand, the HSV color model is composed of hue, saturation, and value. The hue is measured from the red color, and saturation is the distance from the axis. This is shown in Figures 4a and 4b.

Figure 5a shows the actual image of the sample lettuce, while Figure 5b shows the separation of background image and foreground image. Figure 6a shows the RGB image of the lettuce, while Figure 6b shows the HSV image.

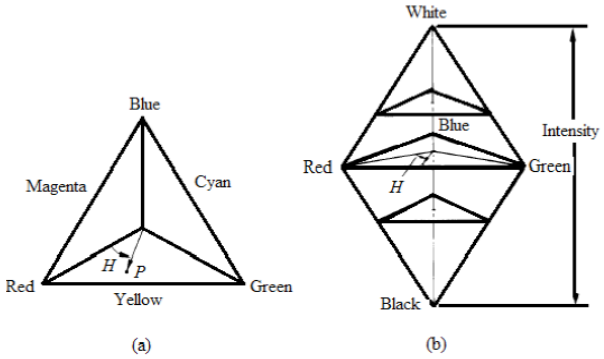

Fig. 4. (a) HSV color triangle and (b) HSC color solid.

(a) (b)

Fig. 5. (a) Sample lettuce (actual image) and (b) background and foreground separation images.

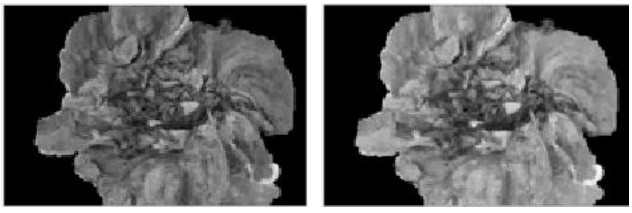

(a) (b)

Fig. 6. (a) RGB image and (b) HSV image.

The saturation and value have a range of 0–1. Zero (0) represents the black color while one (1) represents the white color. This is commonly used because of its ability to generate high-quality images. Saturation refers to the grayness of a color, and value refers to the brightness of the color. The RGB has been normalized using equation 1. The normalized HSV can be computed using equations 2, 3, 4, and 5.

$$r = \frac{R}{R+G+B};\ g = \frac{G}{R+G+B};\ b = \frac{B}{R+G+B} \quad (1)$$

$$h = \cos^{-1}\left\{\frac{0.5[(r-g)+(r-b)]}{\sqrt{(r-g)^2+(r-b)(g-b)}}\right\} \quad h \in [0,\pi] for\ b \le g \quad (2)$$

$$h = 2\pi - \cos^{-1}\left\{\frac{0.5[(r-g)+(r-b)]}{\sqrt{(r-g)^2+(r-b)(g-b)}}\right\}\ h \in [\pi,2\pi] for\ b > g \quad (3)$$

$$s = 1 - 3\cdot\min(r,g,b);\quad s \in [0,1] \quad (4)$$

$$v = \frac{R+G+B}{3\cdot 255};\quad v \in [0,1] \quad (5)$$

C. Image Segmentation

Figures 3c to 3f show how the image is segmented. This was done through setting a certain threshold and placing a mask. The image was then converted into black and white components to become a binary-level image. Figure 7a shows the binary image with noise. The small white components or blobs visible in the image are called noise. In Figure 7b, the noise was removed and retained only the defect.

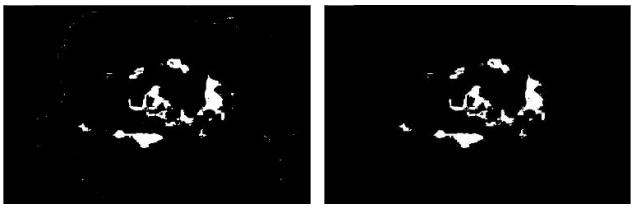

(a) (b)

Fig. 7. (a) Binary image (with noise) and (b) binary image (with defects).

D. Feature Extraction

To analyze the crop health of the lettuce, two parameters are extracted: (1) pixel area and (2) percent area/image area. The optimal performance of the ANN was achieved because of the heuristic analysis of the network.

III. Artificial Neural Network (ANN)

ANN is one of the commonly used computational models. It is patterned in the biological neural system of a mammal but in a smaller scale [13]. The layers of the neural network are composed of input, hidden, and output. The organization of these layers makes the network highly capable of predicting the outcomes with high accuracy. The backpropagation algorithm is added in this to provide a high accuracy and versatility in recognizing the defects in the lettuce crop base on their colors. The neural network served as the medium for identifying the quality of the lettuce.

A. Backpropagation Algorithm

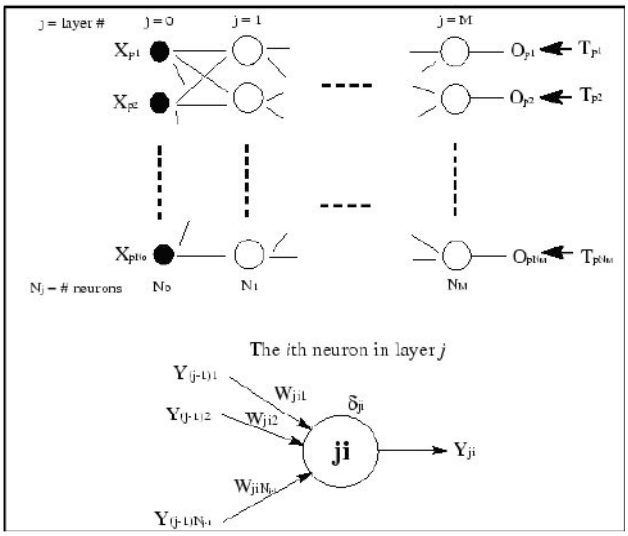

Fig. 8. Multilayer network of backpropagation ANN.

Equation 6 shows the Widrow–Hoff delta learning rule, which is the foundation of the backpropagation algorithm.

$$w = w_{old} + \eta\delta x \quad (6)$$

where $\delta = y_{target} - y$ and η is a constant that controls the learning rate (amount of increment/update Δw at each training step) [14].

Random prediction of outcome is initially made by neural network with the presented patterned images. With the delta leaning rule, adjustment of weights for improved performance becomes possible. It can predict the data correctly. This is repeatedly presented to the neural nets to minimize the error.

B. Design Architecture

The neural network was created in different combinations, with two input nodes, one hidden layer with varying number

of hidden nodes for each training, and one output node. Both the hidden and output layer neurons were activated by binary sigmoid activation function.

The basic training algorithm adjusts the weights in the steepest descent direction (negative of the gradient) [15]. However, it was later discovered that this process does not necessarily produce the fastest convergence. Hence, in this study, the scaled conjugate gradient algorithm (SCG) of [16] was used as the training algorithm. SCG avoids time consuming line search per learning iteration thus providing faster training with excellent test efficiency.

C. *Training and Classification*

The output is 1 if the lettuce has a good quality and no defect and 0 if the lettuce has defects. Two hundred eighty (280) images were extracted and divided into three sections. Of the images, 70% were used for training, 15% were used for testing, and the remaining 15% were used for validation. At the start of the training, weights and biases were randomly initialized. Also, the images were being inputted in a sequential manner. It was repeated until the required training number is obtained.

Three stopping criterions were set for the training of the network, that is, when the maximum iteration, minimum gradient, and maximum validation checks are reached. When these were reached, the neural network can be used for the quality assessment of the lettuce.

IV. RESULTS AND DISCUSSION

A. *Training*

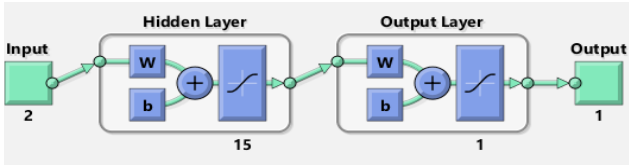

Fig. 9. Neural network architecture.

Figure 9 shows the architecture used for the neural network of the system. It is composed of two input layers, one hidden layer with 15 neurons, and one output layer.

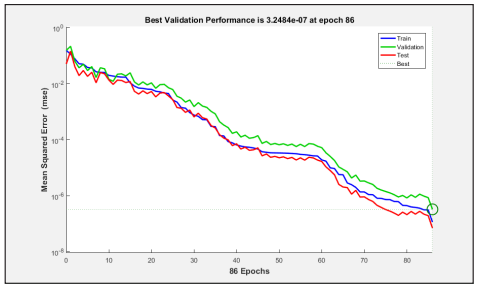

Fig. 10. Performance plot.

Figure 10 shows the performance plot of the trained neural network. For this training, the minimum required gradient was set to 1e-06. When the gradient has reached this value, the training has stopped at epoch 86 with a cross entropy value of 7.6814e-07. Good classification of the system is provided by the minimum cross entropy value.

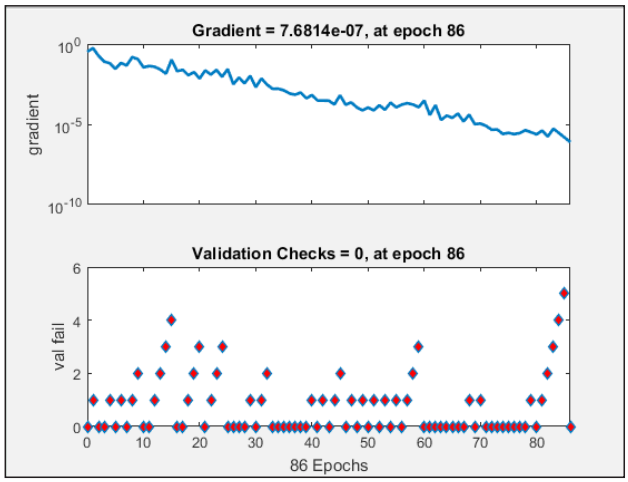

Fig. 11. State plot of lettuce health assessment.

In updating the values of the weights and biases, the gradient is used. The state plot for the training is shown in Figure 11. It illustrates the changes in the gradient value with respect to the epoch and the validation checks. For the 0th validation check, the gradient value is 7.6814e-07. The validation check ensures that the mean square error of the validations stops to decrease.

B. *Testing*

The traditional way of inspecting the defects in lettuce through visual gives a relatively high error due to different visual perceptions and lighting conditions. The use of the machine vision system with ANN has been studied to be an alternative way or the easiest way in identifying the quality of lettuce.

For the testing of the trained neural network, 20 samples are collected and used. The inputs of the system are the extracted values of RGBHSV components of the lettuce image. The actual classification of the samples is given as good (0) and reject (1). The N1 and N2 in output subheading of Table 1 correspond to the neuron 1 and neuron 2, respectively.

Figure 12 shows the comparison of the ANN output and actual value of the samples. With the 20 samples, a small difference was observed.

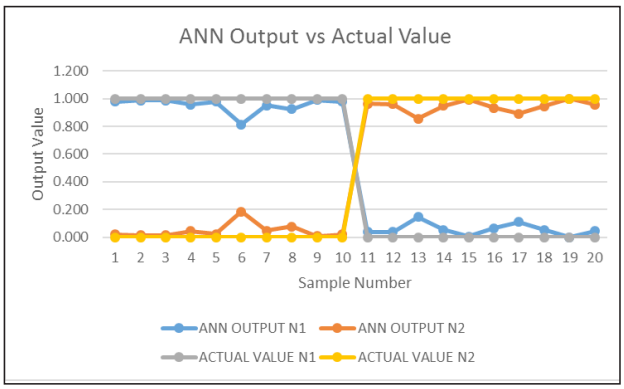

Fig. 12. Comparison of ANN output and actual value.

The relative error plot between the two outputs is shown in Figure 13. It is computed using equation 2. Relative error shows how good a measurement relative to the sample size is and is the ratio of the absolute error and the absolute value. It is important to determine the relative error to show how close the obtained data are to the target data. With the given samples, the mean relative error is 0.051.

$$Relative\ Error = \frac{Absolute\ Error}{Absolute\ Value} \tag{7}$$

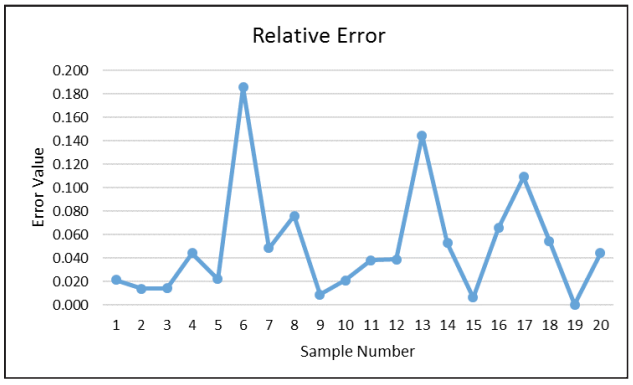

Fig. 13. Relative error plot.

V. CONCLUSION

The application of backpropagation neural network was successfully done on the assessment of lettuce crop health based on its color. RGB components of each image were obtained using RGB color feature extraction in LabVIEW. Based on the result, the system is capable of assessing the health of the lettuce with a minimum square error of 3.2484e-07.

ACKNOWLEDGMENT

The authors would like to acknowledge the financial support of the Department of Science and Technology–Engineering Research and Development for Technology.

REFERENCES

[1] "Crop condition monitoring, assessment and forecast," *Global Agricultural Crop,* 2016. [Online]. Available: http://www.gdacorp.com/crop-condition-and-health. [Accessed: Aug. 4, 2016].

[2] J. W. Rushing, *Improving the Safety and Quality of Fresh Fruits and Vegetables: A Training Manual for Trainers*. University of Maryland: Joint Institute for Food Safety and Applied Nutrition, 2010.

[3] "Crop monitoring and damage assessment," *National Resources Canada*, Nov. 25, 2015. [Online]. Available: http://www.nrcan.gc.ca/earth-sciences/geomatics/satellite-imagery-air-photos/satellite-imagery-products/educational-resources/14652. [Accessed: Aug. 4, 2016].

[4] S. N. Bartee, "Evaluation of crop health during late-season grainfill," *Helena*, Aug. 1, 2014. [Online]. Available: http://www.helenachemical.com/about-us/articles/evaluation-of-crop-health-during-late-season-grainfill/. [Accessed: Aug. 4, 2016].

[5] A. T. Nieuwenhuizen, "Automated detection and control of volunteer potato plants," Dissertation, Institute of Farm Technology, Wageningen University, 2009.

[6] F. D. Smedt, I. Billauws, and T. Goedeme, "Neural networks and low-cost optical filters for plant segmentation," *International Journal of Computer Systems and Industrial Management Applications*, vol. 3, pp. 804–811, 2011.

[7] R. Brivot and J. A. Marchant, "Segmentation of plants and weeds for a precision crop protection robot using infrared images," *IEEE Proceedings–Vision, Image and Signal Processing*, vol. 143, no. 2, pp. 118–124, 1996.

[8] A. Tellaeche, X. P. Burgos-Srtizzu, G. Pajares, and A. Ribeiro, "On combining support vector machines and fuzzy K-means in vision based precision agriculture," *World Academy of Science, Engineering and Technology*, vol. 28, pp. 33–38, 2007.

[9] D. S. Shrestha and B. Steward, "Segmentation of plant from background using neural network approach," in *Proceedings of ANNIE*, pp. 903–908, 2001.

[10] B. Garcia-Salgado and V. Ponomaryov, "Feature Extraction Scheme for a Textural Hyperspectral Image Classification using Gray-Scaled HSV and NDVI Image Features Vectors Fusion," 2016 International Conference on Electronics, Communications and Computers (CONIELECOMP) 2016, pp. 186–191.

[11] J. F. Molina, R. Gily, C. Bojacáy, G. Díazz, and H. Francox, "Color and size image dataset normalization protocol for natural image classification: A case study in tomato crop pathologies," in *Symposium of Signals, Images and Artificial Vision—2013: STSIVA—2013*. Bogota: IEEE, 2013, pp. 1–5.

[12] Juice Plus+, *Growing Guide: Lettuce.* Tower Garden, 2015.
[13] J. Burger, "Basic introduction to neural networks," 2010. [Online]. Available: http://pages.cs.wisc.edu/~bolo/shipyard/neural/local.html.
[14] K. Swingler, "Lecture 3: Delta Rule" 2012. [Online]. Available: http://www.cs.sur.ac.uk/courses/ITNP4B/lectures/kms/3-DeltaRule.pdf.
[15] M. Moller, "A scaled conjugate gradient algorithm for ast surpervised learning," *Neural Networks*, vol. 6, pp. 525–533, 1990.
[16] L. Wiedeman, "Information on the HSV color space." [Online]. Available: http://dcssrvl.oit.uci.edu/~wiedeman/cspace/me/infohsv.html.

Technology Acceptance Model for Breast Cancer Examination Assistant Using Computer Vision and Speech Recognition

Robert Kerwin C. Billones,* Melvin K. Cabatuan,[1] Laurence Gan Lim,[1]Edwin Sybingco,[1] Jose Santos Carandang VI,[1] Eric Camilo Punzalan,[1] Dennis Erasga,[1] Michael Ples,[1] Romeo Teruel,[2] Balintawak Sison-Gareza,[2] Ma. Ellenita De Castro,[1] Julien Carandang,[1] and Elmer P. Dadios[1]

***Abstract* — This paper presents the development of a computer-assisted breast cancer examination using computer vision and speech recognition, with focus on user acceptance for improved technology penetration. The study includes the development of algorithms for breast area detection and delineation and hand tracking during palpation. It uses speech recognition and audio feedback for better human–computer interaction during breast self-examination (BSE) performance. The technology acceptance model (TAM) is used in the design concept and implementation of the breast examination assistant to rate its perceived usefulness (PU), perceived ease of use (PEOU), attitude (ATT), and behavioral intention to use (BI). Performance rating is based on Cronbach's. Computer vision algorithm for BSE, speech recognition, and synthesis results in previous studies were highlighted to associate in TAM considerations. TAM results showed PU is 0.8887 (good), PEOU is 0.7817 (good), ATT is 0.7758 (good), and BI is 0.9378 (excellent).**

Keywords: **technology acceptance model, breast self-examination, computer vision, speech recognition**

I. Introduction

Breast cancer poses a major health care challenge, especially in developing countries. GLOBOCAN 2012 statistics indicated that the average breast cancer incidence and mortality rates in the Philippines are higher than the world average and Southeast Asia average [1] (see Table I). The steady rise in breast cancer incidence can be attributed the lack of public awareness and screening programs into the developing countries, which caused late diagnosis of the disease[2][3][4]. Nn-invasive computer-guided breast self-examination(BSE) technology was developed to promote breast cancer education, awareness, and self-care, which can help in early diagnosis of malignant breast tumors[5][6][7]. Introduction of such technologies [8][9][10][11][12][13] among target users still face roadblocks because of behavioral and societal acceptance. This paper addresses the technology acceptance of such sensitive technologies by providing audio-visual cues to users. It employs an interactive vision-based system with speech recognition. The measure of user acceptance was based from the technology acceptance model (TAM), which has criteria for perceived usefulness (PU), perceived ease of use (PEOU), attitude (ATT), and behavioral intention to use (BI). The measures were taken from the user's feedback after testing the system.

*Robert Kerwin C. Billones, De La Salle University, Manila, Philippines (e-mail: robert.billones@dlsu.edu.ph)

[1]Melvin K. Cabatuan, Laurence Gan Lim, Edwin Sybingco, Jose Santos Carandang VI, Eric Camilo Punzalan, Dennis Erasga, Michael Ples, and Romeo, Ma. Ellenita De Castro, Julien Carandang, and Elmer P. Dadios, De La Salle University, Manila, Philippines

[2]Romeo Teruel, Balintawak Sison-Gareza, University of St. La Salle, Bacolod, Philippines

II. Audio-visual Breast Self-Examination Training System

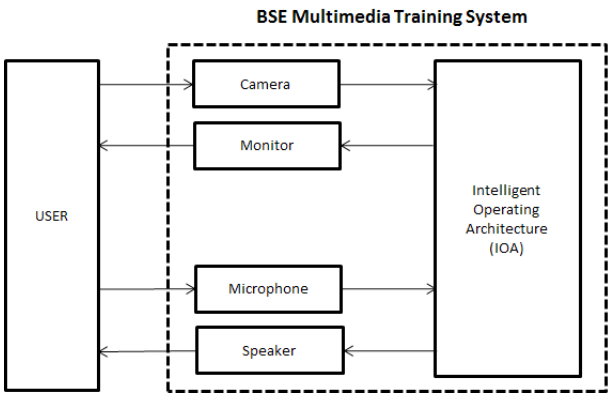

Fig. 1. Audio-visual BSE multimedia training system [14].

TABLE I
GLOBOCAN 2012 STATISTICS FOR BREAST CANCER [1]

Breast Cancer Statistics from GLOBOCAN 2012 (WHO-IARC) [1]									
Location	**Incidence**			**Mortality**			**5-year prevalence**		
	Number	**(%)**	**ASR (W)**	**Number**	**(%)**	**ASR (W)**	**Number**	**(%)**	**ASR (W)**
World	1671149	25.1	43.1	521907	14.7	12.9	6232108	36.3	239.0
Southeast Asia Region	239612	26.4	27.8	109631	19.8	12.9	734902	36	113.1
Brunei Darussalam	83	28.6	48.6	18	16.7	11.3	297	40	193.3
Cambodia	1255	15	19.3	585	10.2	9.3	4417	23.8	84.8
Indonesia	48998	30.5	40.3	19750	21.5	16.6	171005	41.7	187.7
Lao PDR	472	16.3	19	222	10.7	9.3	1663	28	76.8
Malaysia	5410	28	38.7	2572	24.7	18.9	18928	39.2	184.4
Myanmar	5648	17.2	22.1	2792	11.9	11.3	19734	27.6	105.3
Philippines	18327	33.2	47	6621	23.3	17.8	64046	44.6	201.5
Singapore	2524	32.6	65.7	628	19.6	15.5	9710	45	442.1
Thailand	13653	22.4	29.3	5092	13.8	11	54269	32.3	188.3
Vietnam	11067	20.3	23	4671	13	9.9	38713	32.2	109.7
Japan	55710	19	51.5	13801	8.9	9.8	246101	28	433.7

A simple block diagram of the BSE training system is shown in Figure 1. The intelligent operating architecture was discussed in detail in [14][15]. The system employs computer-vision, speech recognition, and synthesis functionalities for improve human–computer interaction.

A. Computer Vision (CV)

The CV systems are extensively used in computer-assisted BSE. Some algorithms developed are used for breast area detection, hand tracking, and palpation (pressure) level detection. Figure 2 shows the BSE performance test using a mannequin. Figures 3 and. 4 show delineation of the breast area (subdivided into smaller blocks) and hand tracking, respectively. Volunteer subjects were asked to perform BSE performance using the system.

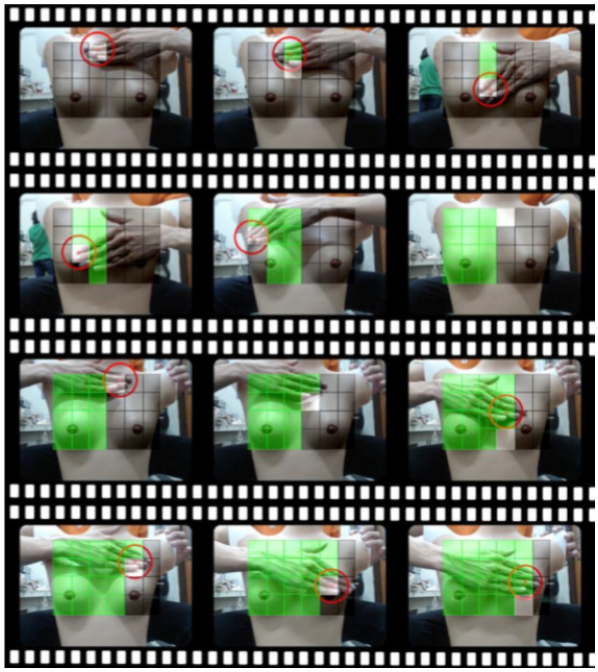

Fig. 2. BSE performance using a mannequin [15].

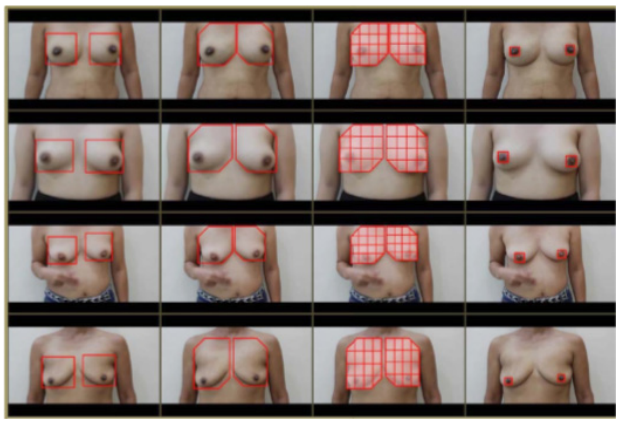

Fig. 3. Breast detection, delineation, division, and nipple detection and tracking [11].

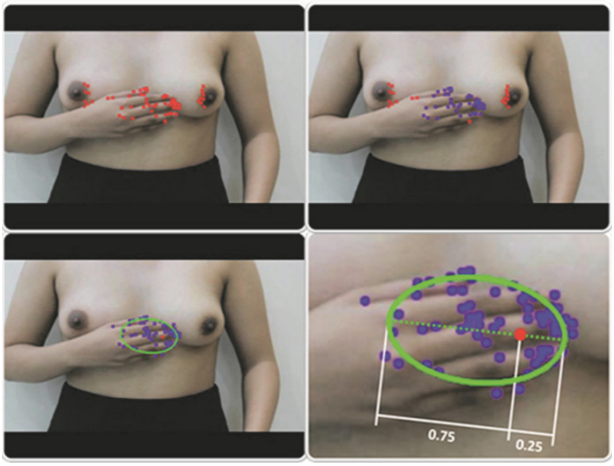

Fig. 4. Kanade–Lucas–Tomasi (KLT) feature tracker for hand tracking [12].

B. Speech Recognition (SR)

The SR system is used for user commands during BSE performance (Fig. 5). This improves the functionality of the computer vision system by less body movement during the performance. The SR system has four states: 1) sleep state, 2) listening state, 3) active state, and 4) execute state. During the sleep state, the system does not acknowledge any speech commands except for the wake signal "Hello BEA." If the user issues the wake signal, the system enters the listening state. While in the listening state, the system waits for any valid command signals from the user. If the user issues a valid command, the system will enter the active state, in which a corresponding system enabling signals will be triggered. The system action will proceed to the execute state, to execute the action that is associated with the valid command.

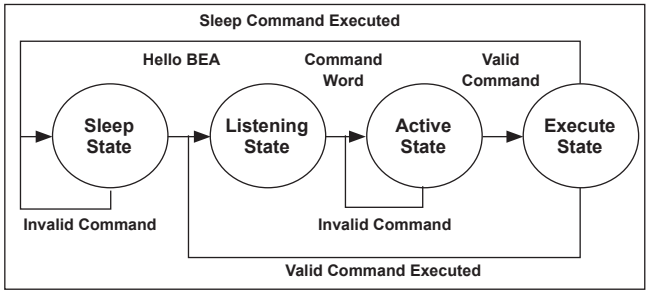

Fig. 5. Speech command recognition (sleep, listening, active, execute) [15].

III. TAM

TAM describes a user's intention to use a technology by evaluating its perceived usefulness (PU) and perceived ease of use (PEOU). The model is extensively used for forecasting acceptance, adoption and usage of information systems [16]. Based on the measurement of PU and PEOU, user ATT towards the technology can be estimated. The acceptance is the BI is derived from the results of PU, PEOU, and ATT (Fig. 6).

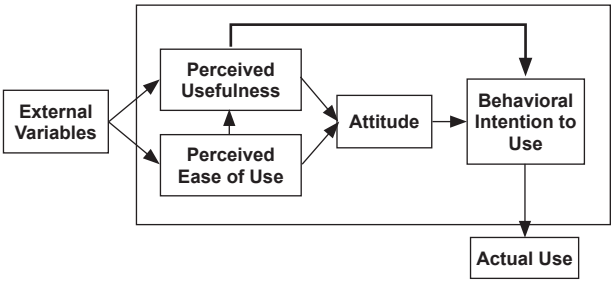

Fig. 6. TAM [16].

TAM reliability can be measured using Cronbach's α. Cronbach's α can be regarded as the probable correlation of two tests that measure the similar construct. It is implicitly assumed that the average correlation between a set of items is an accurate estimate of the average correlation between all items in a certain construct. Cronbach's α is a function of the number of items in a test, the average covariance between item pairs, and the variance of the total score. A quantity that is a sum of K components (*K-items* or *testlets*) is measured, such as $X = Y_1 + Y_2 + Y_3 + \ldots + Y_k$. Then, the formula for Cronbach's α is stated below:

$$\alpha = \frac{K}{K-1}\left(1 - \frac{\sum_{i=1}^{K} \sigma_{Y_i}^2}{\sigma_X^2}\right) \quad (1)$$

whereas the σ_X^2 variance of the total test scores and $\sigma_{Y_i}^2$ is the variance of component *i* for the current sample of person. Cronbach's α generally increases as the intercorrelations between test items increase. This shows an estimate of the internal consistency of the reliability of test scores. If α is equal to 0, this means that the true score is not measured at all (only error component). If α is equal to 1.0, this means that all items measure only the true score (no error component). Cronbach's α values and its meaning is shown in Table II.

TABLE II
CRONBACH'S α

Cronbach's α	Internal Consistency
$\alpha \geq 0.9$	Excellent (high-stakes testing)
$0.7 \leq \alpha < 0.9$	Good (low-stakes testing)
$0.6 \leq \alpha < 0.7$	Acceptable
$0.5 \leq \alpha < 0.6$	Poor
$\alpha < 0.5$	Unacceptable

IV. METHODOLOGY

A. Breast Examination Assistant (BEA) User Interface

BEA interface is developed to provide better user experience and ease of use of the system. Figure 7 shows the main user interface with different user options. It can be navigated using speech commands. Figure 8 shows a simulated BSE performance with the assistance of BEA.

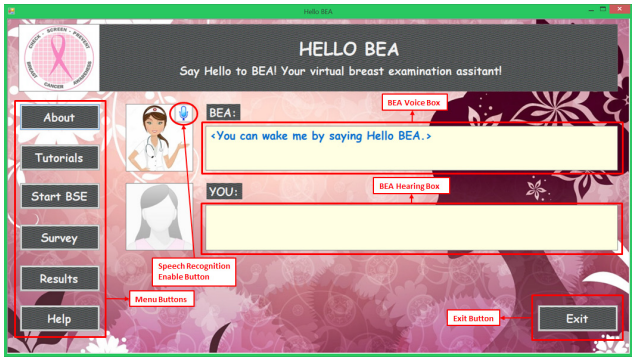

Fig. 7. BEA main interface.

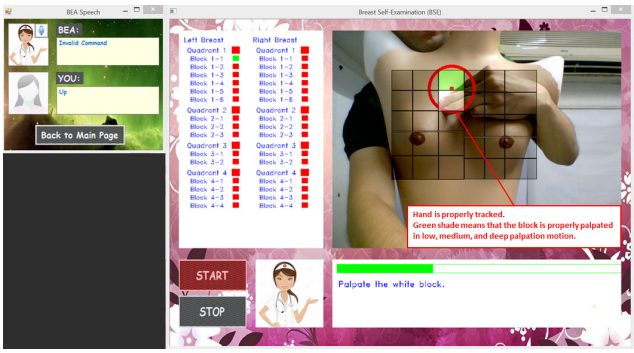

Fig. 8. BSE performance while assisted by BEA [15].

B. BEA Testing

During initial stage of development, BEA was tested using a mannequin (Fig. 9). Deployment was done with the help of volunteers. Sixteen volunteers agreed to test the BEA interface, out of which only four volunteers agreed in performing actual BSE (Fig. 10). The other 12 users only agreed to test the interface and speech recognition and synthesis functions.

C. BEA Survey

A built-in survey is incorporated in the BEA application. This survey can be taken after testing BEA (Fig. 11). Data gathered from the survey are used to validate the TAM for the BEA application. The survey questions and results are shown in the appendix.

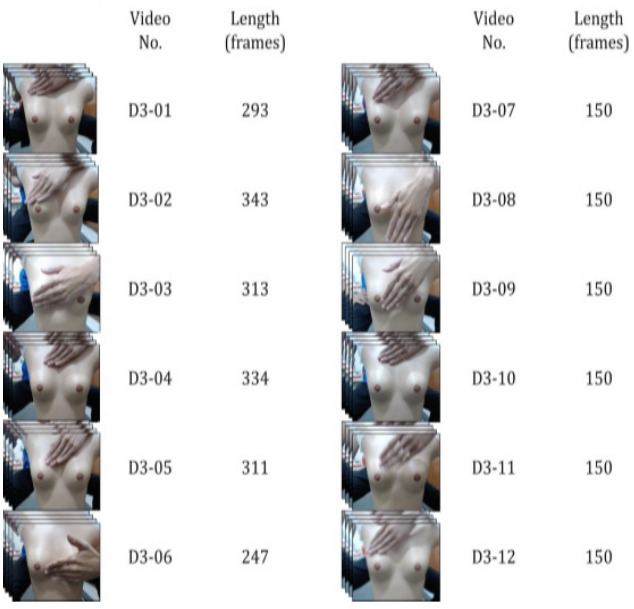

Fig. 9. Experimental BEA test setup using a mannequin.

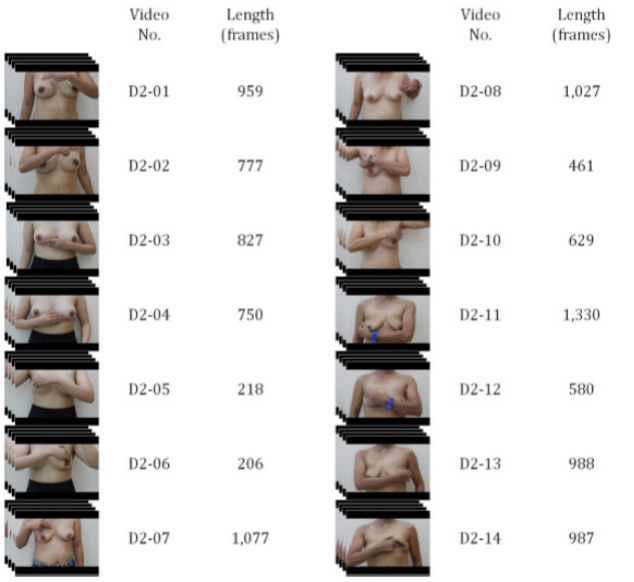

Fig. 10. Actual BEA test setup with volunteers.

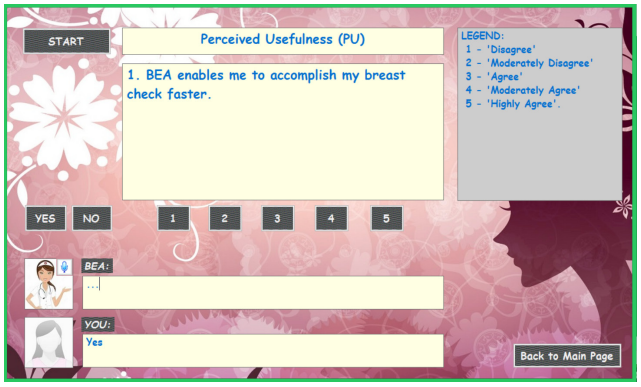

Fig. 11. BEA survey menu.

V. EXPERIMENT AND RESULTS

A. *Results for Computer Vision*

Table III shows the experiment results for computer vision algorithms.

TABLE III
COMPUTER VISION ALGORITHM RESULTS

Algorithm	Accuracy
Breast area identification (using F1-score)	95.30%
Nipple detection (using F1-score)	94.30%
Hand tracking (using F-score)	94.61%
Palpation detection	93.00%

B. *Results for Speech Recognition*

Figure 12 shows the experiment results for speech recognition.

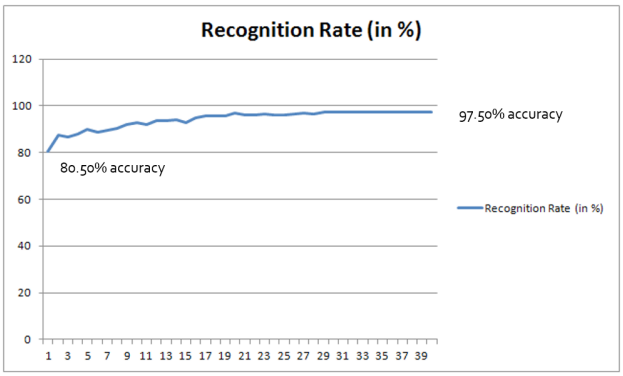

Fig. 12. Speech recognition results.

C. *BEA TAM Results*

The result of descriptive statistics shows the age information and the general breast health awareness of the survey participants. The respondents have an average (mean rating) age of 27.5 years. This is a young set of participants. Of the respondents,18.75% belong to the 20-years-and-younger age group, 56.25% belong to the 21-to-30-years age group,12.5% belong to the 31-to-40-years age group,6.25% belong in the 41-to-50-years age group, and 6.25% belong to the 51-to-60-years age group. There are no respondents in the 60-years-and-older age group. The general questions consist of four items that determine the breast health awareness of each participant. For the four items, there is a total of 24 (37.5%)"yes" responses and 40 (62.5%) "no" responses. A "yes" response is converted into the numerical value of 1. A "no" response is converted into numerical value of 0. The mean rating for the general questions is 0.375. These data show that the level of breast health awareness among the participants is low.

The general questions section has a Cronbach's α value of 0.8177. The test items used for general questions has good consistency and reliability. The PU rating has a Cronbach's α value of 0.8887. The test items used for PU have good consistency and reliability. The PU mean rating is 3.705. The participants agree to moderately agree on the usefulness of the system. The PEOU rating has a Cronbach's α value of 0.7817. The test items used for PEOU has good consistency and reliability. The PEOU mean rating is 4.2125. The participants moderately agree to highly agree on the ease of use of the system. The ATT rating has a Cronbach's α value of 0.7758. The test items used for ATT have good consistency and reliability. The ATT mean rating is 3.8125. The participants have "agree" to "moderately agree"ATT

towards the system. The BI rating has a Cronbach's α value of 0.9378. The test items used for BI have high consistency and reliability. The BI mean rating is 3.525. The participants have "agree" to "moderately agree" BI.

VII. Conclusion

Sixteen female users participated in testing the BEA system. The BEA system is given a common name, Hello BEA, for the graphical user interface. This allows for a friendlier term for the system. After each trial, a survey was conducted to assess the system's performance. The measure used for system performance is the TAM using Cronbach's α. This analyzes the PU, PEOU, ATT, and BI. The model is extensively used for forecasting acceptance, adoption and usage of information systems. Cronbach's α is used to measure the consistency of the test items used in the survey. Cronbach's α generally increases as the inter-correlations between test items increase. Results showed good consistency and reliability for the test items used in the survey. The general questions section has a Cronbach's α value of 0.8177. The PU rating has a Cronbach's α value of 0.8887. The PEOU rating has a Cronbach's α value of 0.7817. The ATT rating has a Cronbach's α value of 0.7758. The BI rating has a Cronbach's α value of 0.9378. Mean ratings showed a favorable response from the participants. The PU mean rating is 3.705. The participants agree to moderately agree on the usefulness of the system. The PEOU mean rating is 4.2125. The participants moderately agree to highly agree on the ease of use of the system. The ATT mean rating is 3.8125. The participants have "agree" to "moderately agree" ATT towards the system. The BI mean rating is 3.525. The participants have "agree" to "moderately agree" BI. The conduct of the survey can also be improved by evenly distributing participants for all age groups. The current user evaluation data have a young set of participants. Participants for the 31-to-40-years, 41-to-50-years, 51-to-60-years, and 60-years-and-older age groups can be increased to better test the TAM for the BEA system. It is also recommended to further improve the BEA GUI. A survey for the BEA GUI can be included to know the user acceptability of the human–computer interface.

References

[1] WHO | IARC, "GLOBOCAN World Health Organization International Agency for Research on Cancer," 2012. [Online]. Available: http://globocan.iarc.fr/Pages/fact_sheets_population.aspx.

[2] P. Ramakant, E. S. Forgach, J. Rendo, J. M. Chaparro, C. S. Basurto, M. Margaritoni, and G. Agarwal, "Breast cancer care in developing countries," *World Journal Surgery,* vol. 33, no. 10, pp. 2069–2076, 2009.

[3] D. Parkin, C. Ngelangel, D. Esteban, L. Gibson, M. Munson, M. Reyes, A. Laudico, and P. Pisani, "Outcome of screening by clinical examination of the breast in a trial in the Philippines," *International Journal of Cancer,* vol. 119, no. 1, pp. 149–154, 2006.

[4] M. Salagar, P. Kulkarni, and S. Gondane, "Educating and creating social awareness for sensitive topics using mobile applications," in *IEEE Conference Publications, 2013 IEEE International Conference in MOOC Innovation and Technology in Education (MITE),* pp. 335–336, 2013.

[5] S. Chen, Q. Cheng, R. Naguib, and A. Oikonomou, "Hand pressure detection among image sequence in breast self-examination multimedia system," *IEEE Conference Publications, International Forum on Information Technology and Applications, 2009. IFITA '09,* vol. 3, p. 127, 2009.

[6] A. Oikonomou, S. Amin, R. Naguib, A. Todman, and H. Al-Omishy, "IRiS: An interactive reality system for breast self-examination training," in *Engineering in Medicine and Biology Society, 2004. IEMBS '04. 26th Annual International Conference of the IEEE,* vol. 2, 2004.

[7] N. Talib, N. Zakaria, and S. Ramadass, "Teleconsultations in breast self-examination (BSE) practice: Alternative solution for early detection of breast cancer," *IEEE Conference Publications, International Symposium on Information Technology, 2008. ITSim 2008,* vol. 1, pp. 1–7, 2008.

[8] M. Cabatuan, E. Dadios, and R. Naguib, "Computer vision-based breast self-examination palpation pressure level classification using artificial neural networks and wavelet transforms," in *TENCON 2012—2012 IEEE Region 10 Conference,* 2012.

[9] M. Eman, M. Cabatuan, E. Dadios, and L. G. Lim, "Detecting and tracking female breasts using neural network in real-time," in *TENCON 2013—2013 IEEE Region 10 Conference (31194),* 2013.

[10] J. Jose, M. Cabatuan, E. Dadios, and L. Gan Lim, "Depth estimation in monocular breast self-examination image sequence using optical flow," in *Humanoid, Nanotechnology, Information Technology, Communication and Control, Environment and Management (HNICEM), 2014 International Conference on*, 2014.

[11] R. A. A. Masilang, M. K. Cabatuan, E. P. Dadios, and L. G. Lim, "Computer-aided BSE torso tracking algorithm using neural networks, contours, and edge features," in *TENCON 2014—2014 IEEE Region 10 Conference,* 2014.

[12] R. Masilang, M. Cabatuan, and E. Dadios, "Hand initialization and tracking using a modified KLT tracker for a computer vision-based breast self-examination system," in *Humanoid, Nanotechnology, Information Technology, Communication and Control, Environment and Management (HNICEM), 2014 International Conference*, 2014.

[13] R. Billones and E. Dadios, "Hiligaynon language 5-word vocabulary speech recognition using Mel frequency cepstrum coefficients and genetic algorithm," in *Humanoid, Nanotechnology, Information Technology, Communication and Control, Environment and Management (HNICEM), 2014 International Conference*, 2014.

[14] R. K. C. Billones and E. P. Dadios, "Intelligent operating architecture for audio-visual breast self-examination multimedia training system," *IEEE TENCON 2015,* pp. 1–6, 2015.

[15] R. K. C. Billones, E. P. Dadios, and E. Sybingco, "Design and development of an Artificial Intelligent System for audio-visual cancer breast self-examination," *Journal of Advanced Computational Intelligence and Intelligent Informatics,* vol. 20, no. 1, pp. 124–131, 2016.

[16] F. Damanhoori, N. Zakaria, L. Y. Hooi, N. A. H. Sultan, N. A. Talib, and S. Ramadass, "Understanding users' technology acceptance on breast self examination teleconsuItation," in *8th International Conference on High-capacity Optical Networks and Emerging Technologies,* pp. 374–380, 2011.

Survey Results for Hello BEA Application			
	Cronbach's α	**Mean**	**Standard Deviation**
General Questions			
1. Did you perform breast self-examination before?	0.8177	0.375	0.484123
2. Did you attend any seminar or campaign about breast health care before?		0.3125	0.463512
3. Did you consult any doctors about breast health care before?		0.125	0.330719
4. Did you think that breast self-examination is a good practice?		0.6875	0.463512
TOTAL (General Questions)		0.375	0.4354665
PU			
1. BEA enables me to accomplish my breast check faster.	0.8887	3.25	0.75
2. BEA enables me to accomplish my breast check more effectively.		3.5	0.866025
3. BEA brings conveniences in helping me in getting breast health care information that I need.		4	0.612372
4. BEA helps me to follow up closely my breast health condition.		3.75	0.559017
5. BEA increases my breast health care awareness.		4.625	0.484123
6. BEA enhances my breast health condition.		2.875	0.780625
7. Overall I find the Hello BEA application useful to me.		3.9375	0.826797
TOTAL (PU)		3.705	0.696994
PEOU			
1. The Hello BEA application is easy to use.	0.7817	4.25	0.75
2. The Hello BEA application is easy to learn and operate.		4.25	0.661438
3. The Hello BEA application takes a lot of effort to be skillful in using it.		3.9375	0.747391
4. The interaction with BEA is clear and understandable.		4.0625	0.747391
5. Overall the Hello BEA application is easy to use.		4.5625	0.496078
TOTAL (PEOU)		4.2125	0.680459
ATT			
1. Using Hello BEA application for my breast health care is a good idea.	0.7758	3.75	0.901388
2. Using Hello BEA application for my breast health care is unpleasant.		3.9375	0.747391
3. Using Hello BEA application is beneficial for my breast health care.		3.75	0.661438
TOTAL (ATT)		3.8125	0.770072
BI			
1. Assuming I have the chance to use Hello BEA application, I intend to use it.	0.9378	3.5625	0.704339
2. Given that I have the chance to use Hello BEA application, I predict that I would use it.		3.5625	0.704339
3. Whenever possible, I intend to use Hello BEA application as often as needed.		3.125	0.927025
4. To the extent possible, I intend to use Hello BEA application frequently.		3.125	0.927025
5. I intend to recommend others to use the Hello BEA application.		4.25	0.829156
TOTAL (BI)		3.525	0.818376

Performance Evaluation of HEVC With Intra-Refresh for Wireless Video Surveillance

Jason Jake E. Tan,[1] Edison A. Roxas,[1] Angelo R. dela Cruz,[1] Argel A. Bandala,[2] and Ryan Rhay P. Vicerra[2,*]

***Abstract* — This paper presents the result of the performance evaluation for a wireless video surveillance using the High Efficiency Video Coding (HEVC) standard. The video test sequences are converted into HEVC bit streams by the HM6.0 encoder. The HEVC bit streams were transmitted using a wireless network simulator setup for video surveillance. The wireless network setup introduced error to the HEVC bit stream. Common wireless transmission losses include cross traffic and multipath fading. The intra-refresh error resilient technique is utilized in the HEVC encoder to mitigate the effects of wireless channel. Finally, the effects of adjusting different parameters of the HEVC encoder, namely, the intra-refresh period and quantization parameter were also evaluated in this paper.**

Keywords: **HEVC, wireless video surveillance, packet loss**

I. Introduction

Wireless video surveillance has many applications including security, identification, monitoring, etc., and is used in many establishments. However, wireless transmission comes with some typical problems for data transmission. One of these problems is that wireless networks are more prone to noise compared to wired networks. The noise can be caused by obstruction, signal attenuation and interference, etc. [1]. In order to obtain high-quality videos in a wireless environment, error robustness is required [2]. Another problem that comes with video surveillance is that videos take up large amount of data. These videos must be efficiently compressed in order to reduce the amount of data [3]. It is also a must for a video surveillance to have real-time access. Therefore, it is important for video surveillance encoders to have low computational complexity in order for the video to have minimal delay [1][2].

For efficient compression, High Efficiency Video Coding (HEVC) is the most preferable to use. HEVC standard was made by a partnership called Joint Collaborative Team on Video Coding [2]. The partnership includes ITU-T Video Coding Experts Group and the International Organization for Standardization and the International Electrotechnical Commission Moving Picture Experts Group [2]. HEVC standard can provide better coding efficiency and also provides up to 50% bit-rate savings for the same video quality relative to the previous standards including H.264 [2][3].

The software that we adopted to simulate HEVC is the Test Model under Consideration (TMuC, version HM6.0) [4][5][6]. We use HM6.0 to encode and decode test sequences. The encoded sequences are subjected to noise simulated under Network Simulator 2 (NS2). We modify the HEVC decoder to implement a non-motion compensated error concealment technique. Results show the effects of packet loss on HEVC videos during transmission. The performance of HEVC with intra-refresh over wireless video surveillance was evaluated through the simulations. The results of the simulations measures the objective quality of the video based on its peak signal to noise ratio (PSNR) [7].

The rest of the paper is organized as follows. Section II discusses the design considerations including video transmission architecture and configurations. Section III discusses wireless network model used and the configurations for its simulation. Section IV discusses the results of the experiments, and Section V concludes the paper and also includes recommendations for future works.

II. Design Considerations

The architecture for the simulated video transmission is shown in Figure 1. The first block consists of the input

[1]Jason Jake E. Tan, Edison A. Roxas, Angelo R. dela Cruz, University of Santo Tomas, Manila, Philippines

[2]Argel A. Bandala, and Ryan Rhay P. Vicerra, De La Salle University, Manila, Philippines (e-mail: ryan.vicerra@dlsu.edu.ph)

video sequence. The input video sequence is then encoded using an HEVC encoder. After encoding, the encoded video sequence is transmitted over a wireless network. On the other end, the transmitted video sequence will now be decoded by a video decoder and then be reconstructed [4].

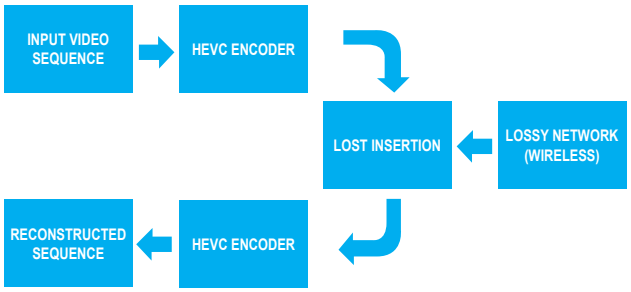

Fig. 1. Video transmission architecture.

Video compression efficiency of HEVC is achieved by exploiting the redundancy of information in both the spatial (within a frame) and temporal dimensions (among neighboring frames) of the video. Due to the high correlation within and among neighboring frames, predictive coding schemes are employed to exploit this redundancy. A predictive coding scheme includes motion estimation and compensation, which are both key parts of video compression.

Almost all video coding standards use these coding schemes such as the MPEG series and the most recent HEVC. While the predictive coding schemes are able to reach high compression ratios, they are highly susceptible to the propagation of errors. The illustration of error propagation over time is shown in Figure 2.

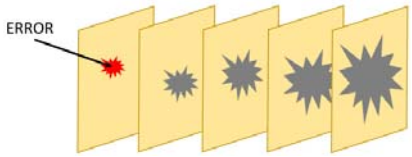

Fig. 2. Illustration error propagation over time. Image concept taken from [8].

Because of the low error robustness of HEVC, the use of an error resilient technique is needed [9]. Among the various error control schemes of video encoders, the intra-refresh method is preferred because of its low complexity implementation and its efficiency in reducing transmission distortion [10][11].

This method can effectively mitigate the error propagation due to packet loss and improve the video quality significantly [7].

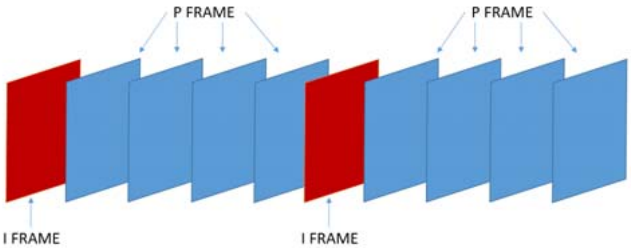

Fig. 3. Illustration of insertion of I-frames to minimize error propagation over time. Image concept taken from [8].

HEVC divides a picture, or a video frame, into coding tree blocks, or CTBs, and it is arranged in a raster order. Much like the previous standards, a sequence of CTBs can be put together to form a slice. Therefore, a picture can be divided into a different number of slices. It is very much possible to make the whole picture a slice, in which it has its specific network abstraction layer (NAL) unit [4][12].

One reason that makes video coding standards a lossy compression is the quantization parameter (QP). The QP determines the quantity of spatial details retained. The quality of the decoded video is proportional to the amount of spatial detail saved, with or without errors. A low QP ensures that most spatial details are saved albeit with a high storage requirement, while a high QP decreases the spatial details but now requires less storage space.

A. Video Sequences

Three video test sequences are used to represent a wide range of motion intensity. The Akiyo test sequence represents a video sequence with a minimal amount of motion. The female reporter is reading news only by moving her lips and eyes. The Foreman test sequence represents a video sequence with high motion content. The Foreman video contains a monologue of a man, and at the end, there is a continuous scene change. Meanwhile, the Container sequence has medium motion but high spatial texture and parallel to many object boundary edges. For our experiments, these three video sequences are used for the entire simulation. Figure 4 shows a sample frame of each video sequence.

(a) (b) (c)

Fig. 4. Sample frame of each video sequence (a) Akiyo, (b) Container, and (c) Foreman.

These video sequences are in CIF (352 × 288) resolution [3] in YUV format [9], which contains 300 frames. In a wireless video surveillance, Akiyo can represent a video with minimal movements from a static camera. For Container, it characterizes a video with a constantly moving environment from a static camera. And for Foreman, it can represent a video with a dynamic camera.

B. Configuration

The HEVC encoder is configured in such a way that a single frame is treated as a single slice. This makes the size of the slice matched to that of the maximum transmission unit (MTU) of the network in which the video is streamed [7]. Finally, the encoder sets the NAL unit to the MTU, where a NAL unit represents a packet ergo represents a video frame.

The reference software for encoding and decoding video test sequences using HEVC is called HM (HEVC Test Model) [11]. The purpose of an HM encoder is mainly to provide a common reference implementation of an HEVC encoder [13].

The configurations used for the HM encoder are as follows. The HM encoder that we used was HM version 6.0. HM provides various configuration profiles with different specifications. From the profiles provided, intra main configuration was used in encoding. All 300 frames of the video sequences were encoded with a frame rate equal to 30. A sequence of I-frame and P-frames were encoded. An I-frame is an encoded video frame in which it is independently decoded. It basically contains all the information to decode itself albeit it requires more storage requirement. On the other hand, a P-frame is an encoded video frame where a predictive coding scheme was used. It is highly dependent on information of its neighboring frame to be decoded. It contains less information making it require less storage.

For the application of the intra-refresh method, an I-frame will be encoded at specified intervals. The intra periods were set to 10, 20, 30, 40, and 50. The QP is set to typical values of 22, 27, 32, and 37 in video encoding [14].

III. WIRELESS NETWORK

The typical network topology used in wireless video surveillance is a mesh topology [1]. A mesh topology could achieve high system performance. Its benefits include a good data throughput, power efficiency, and conservation of energy.

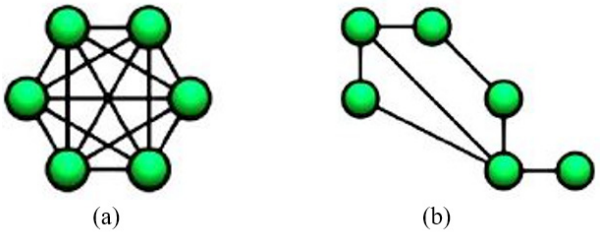

Fig. 5. Sample structure for mesh topology: (a) full mesh and (b) partial mesh. Image taken from [15].

The simulation of a wireless network was observed using NS2 as shown in Figure 6. In a mesh network, a 2-Mbps constant bit-rate traffic flows from node 0 to node 19. The distance of nodes for outdoors is around 80 to 90 m, and the distance of nodes for inside the building is around 15 to 18 m [16].

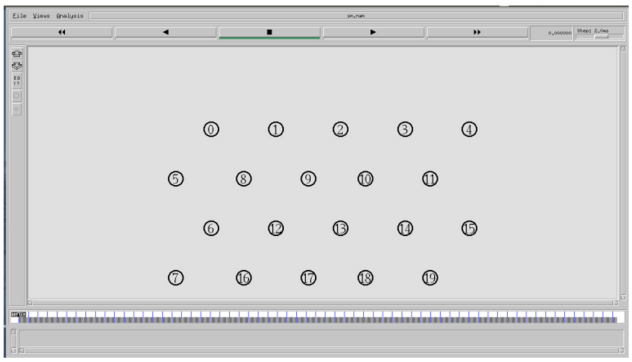

Fig. 6. Screenshot of mesh topology in NS2.

From the typical values of path loss and shadowing deviation in a wireless network environment, we used the following configurations shown in Table I [16].

TABLE I
TYPICAL VALUES OF PATH LOSS BETA (B) AND SHADOWING DEVIATION (Σ_{DB}) FOR WIRELESS NETWORK ENVIRONMENT

ENVIRONMENT	β	σ_{db}(dB)
In building, obstructed – office, soft partition	4.0	9.6
In building obstructed – office, hard partition	4.0	7.0
Outdoor – outdoor	2.7	4.0

An NS2 trace file will be generated from the simulation wherein the error pattern of the given network can be acquired. The error pattern from the trace file was extracted via MATLAB. The error pattern obtained from the various network environment which comprises 1s (no error) and 0s

(with error), as shown in Figure 7. NAL unit loss software will be used for the insertion of loss in the HEVC bit stream file produced by the encoder [17].

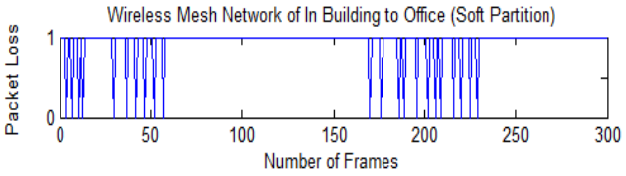

Fig. 7. Packet loss example of in building to office (soft partition) in wireless mesh network.

The HM decoder will be used in reconstructing the video with the HEVC bit stream file produced by the NAL unit loss software. In terms of error concealment, the decoder will copy the previous frame if the current frame is under error.

(a) (b)

Fig. 8. Decoded frame of Foreman (a) without error and (b) with intra period of 10 with transmission from in building to office (soft partition) in wireless mesh network.

In Figure 8 is the comparison of the sample frame from the decoded video without error and a video with error concealment introduced.

$$\mathrm{PSNR}(i,j) = 10\log_{10}\frac{\left(2^{P}-1\right)^{2}}{\mathrm{MSE}(i,j)} \quad (1)$$

$$\mathrm{MSE}(i,j) = \frac{1}{MN}\sum_{x=1}^{M}\sum_{y=1}^{N}\left[f_i(x,y)-g_j(x,y)\right]^{2} \quad (2)$$

Using equations (1) and (2), the PSNRs of the decoded video sequences are measured and analyzed [18].

IV. EXPERIMENTAL RESULTS

A. Encoding Complexity

To analyze the complexity introduced in encoding the video with intra-refresh method, varying the intra period values can determine the complexity of the encoder by observing its encoding time.

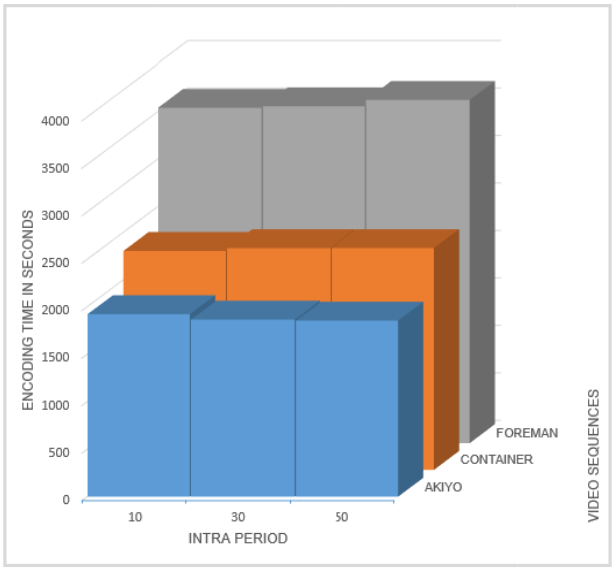

Fig. 9. Encoding time of all video sequences.

Increasing intra period means decreasing the number of intra frames encoded. In Figure 9, as the number of intra period increases (I-frames decrease), it can be observed that the encoding time increases because P-frames consume more time due to the predictive coding complexity.

In terms of motion intensity, high motion test sequences are longer to encode due to the search algorithm of the predictive coding. For the medium and high motion content video sequence, increasing intra period increases the complexity of the encoder. But for low motion content, I-frame used for prediction takes more time than generating the P-frames. The reason for this is that low motion content sequences have high temporal redundancy where the P-frames result to a relatively faster search algorithm than using an intra coded frame.

B. Bit Rate Versus QP

In wireless video surveillance, bitrate represents the required channel capacity to transmit the compressed sequences and the storage space required when storing the encoded video sequence.

QP adjusts how much spatial detail will be preserved. Lower QP means more spatial detail is saved while the intra period defines the frequency of I-frames.

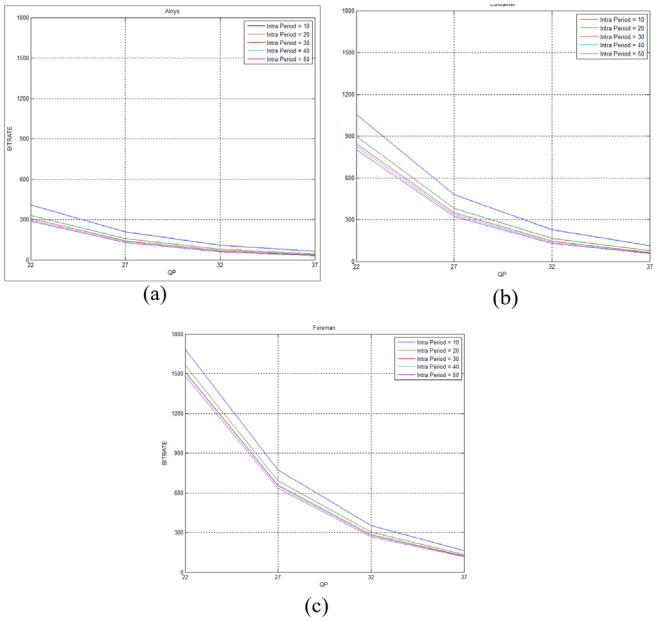

Fig. 10. Bitrate of video sequences with different QP values: (a) Akiyo, (b) Container, and (c) Foreman.

Figure 10 shows that lower QP means more spatial detail saved and thus more storage requirements. Foreman consumes more storage followed by Container then Akiyo. Videos with high motion content require more storage while low motion content requires less. Note also that higher frequency of I-frames consumes more storage.

C. *QP Versus PSNR for Different Intra Periods*

With no error, PSNR decreases as QP increases regardless of intra period due to the high level of quantization. In a lossy condition, the PSNR decreases but is somehow maintained to a certain value as QP increases. Figure 11 shows the QP versusPSNR for different intra periods for Foreman.

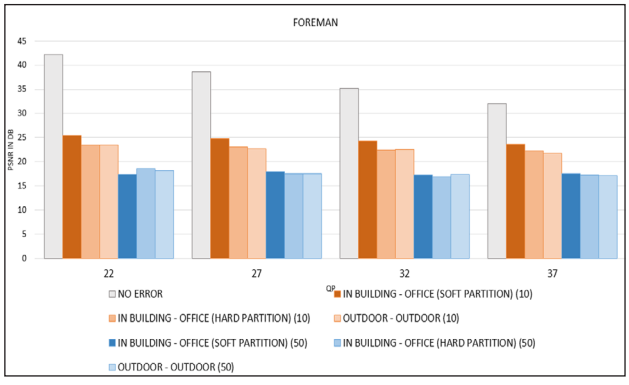

Fig. 11. Foreman with various configurations and different QP values with intra period set to 10 and 50.

Note that an intra period of 10 has less decrease in PSNR compared to an intra period of 50. Loss from quantization and network transmission causes minor variations from the results gathered for some cases in which a higher QP value produces a greater PSNR compared to lower QP values.

As quantization increases, the spatial detail decreases. So as the spatial detail decreases, the difference from the initial frame compared to the next frame is also reduced. Thus, after it underwent a lossy environment, some frames lost does not do any significant decrease in PSNR.

All tests show similar behaviors. But, in observing the PSNR of the decoded video without error, it can be perceived that the PSNR decreases as the QP decreases due to quantization.

D. *Intra Period Versus PSNR for Different Wireless Configurations*

Figure 12 shows the effect of quantization for the video sequences where it is observed to be greater for Foreman and less for Akiyo.

Using Foreman, there were averages of 42.11%, 69.11%, and 86.05% PSNR drop for intra periods of 10, 30, and 50, respectively. For intra periods from 10 to 30, there were averages of 18.50%, 16.21%, and 11.85% PSNR drop for Foreman, Container, and Akiyo, respectively.

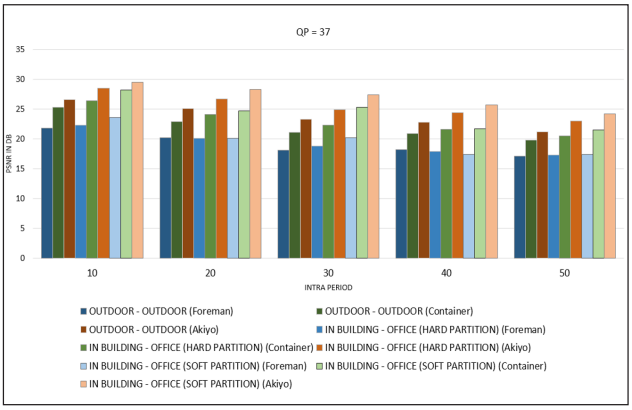

Fig. 12. Various configurations and different intra period values with QP set to 37 for all video sequences.

The decrease in PSNR when decreasing frequency of I-frame is more drastic for videos with higher motion content compared to those with less motion content.

E. *Subjective Quality*

At our discretion, the subjective quality shows that the effect of error is greater for high motion videos compared to low motion videos.

Fig. 13. Foreman with outdoor to outdoor configurations and intra period set to (a) 10, (b) 50, and (c) none.

In Figure 13, the tests show that a 6-dB decrease in PSNR between intra periods from 10 to 50 displays a significant effect on the quality of the video. Errors propagate greatly for an intra period of 50 compared to 10. This subjective quality supports the objective quality that there is a significant drop in PSNR for an intra period of 50 compared to 10.

V. Conclusion and Future Work

Storage requirement for encoded video sequence is affected by two major things. The first is by varying the QP. Increasing the value of QP reduces the storage space requirement at the expense of lesser spatial detail and lower video quality.

However, under lossy network, the difference in PSNR between different values of QP is at best tolerable. High motion video benefits greatly as it causes a significant decrease in storage requirement when increasing the QP. On the other hand, while low motion video also enjoys a decrease in storage requirement as QP increases, it is not as significant compared to high motion video.

The second is by varying the intra period or simply varying the frequency of I-frames in the encoded video sequence. Higher frequency of I-frames increases the storage requirement of the encoded video sequence. While it increases the storage requirements, its benefits lie in the error robustness it provides. Increasing the frequency of I-frames minimizes the effect of errors on the video quality when under a lossy network such as wireless channel.

It is safe to say that decreasing the frequency of I-frames equates to a decrease in video quality; however, there will come a point where the decrease is insignificant, if not tolerable. It is especially true for a video with low motion content compared to that with high motion content. The complexity introduced by changing the intra period is insignificant, and the complexity relies entirely on the performance of HEVC itself.

In summary, it is possible to vary the parameters of the encoder in which one of the requirements for a wireless video surveillance benefits without having to compromise the others significantly. The performance of HEVC with error resiliency techniques such as intra-refresh can be further evaluated by using the latest HM reference software with a different approach.

References

[1] Y. Ye, S. Ci, A. Katsaggelos, Y. Liu, and Y. Qian, "Wireless video surveillance: A survey," *Access, IEEE*, vol. 1, pp. 646–660, Sept. 18, 2013.

[2] Cisco, "Why go wireless." [Online]. Available: http://www.cisco.com/cisco/web/solutions/ small_business/resource_center/articles/work_from_anywhere/why_go_wireless/index.html. [Accessed: Apr.23,2015].

[3] G. Gualdi, A. Prati, and R. Cucchiara, "Video streaming for mobile video surveillance," *IEEE Transactions on Multimedia*, vol. 10, no. 6, Oct. 2008.

[4] J. Tan, C. Bello, J. Fajardo, and A. dela Cruz, "Performance evaluation of HEVC over delay-prone wired networks," in *IEEE, 2015 International Conference on Humanoid, Nanotechnology, Information Technology, Communication and Control, Environment and Management (HNICEM)*, pp. 1–5, Dec.9–12, 2015.

[5] S. Wenger, "Loss robustness report (AHG14)," JCT-VC Document, JCTVC-H0014, Feb. 2012.

[6] S. Oudin et al, "Block merging for quadtree-based video coding," in *2011 IEEE International Conference on Multimedia and Expo (ICME)*, pp. 1–6, July 2011.

[7] J. Nightingale, Q. Wang, and C. Grecos, "HEVStream: A framework for streaming and evaluation of High Efficiency Video Coding (HEVC) content in loss-prone networks,"*IEEE Transactions on Consumer Electronics*, vol. 58, no. 2, May 2012.

[8] A. Vetro, J. Xin, and H. Sun, "Error resilience video transcoding for wireless communications," *IEEE Wireless Communications*, vol. 12, no. 4, pp. 14–21, Aug. 2005.

[9] P. Seeling, M. Reisslein, and B. Kulapala, "Network performance evaluation using frame size and quality traces of single-layer and two-layer video: A tutorial," *Communications Surveys & Tutorials, IEEE*, vol. 6, no. 3, pp. 58–78, Dec. 1, 2009.

[10] G. Correa, P. Assuncao, L. Agostini, and L. da Silva Cruz, "Performance and computational complexity assessment of high-efficiency video encoders," *Circuits and Systems for Video Technology, IEEE Transactions on*, vol. 22, no. 12, pp. 1899–1909, 2012.

[11] Fraunhofer, Heinrich Hertz Institute, "High Encoding Video Coding (HEVC)." [Online]. Available: http://hevc.hhi.fraunhofer.de. [Accessed: Jan. 17, 2016].

[12] "HEVC test model under consideration (TMuC) revision 6.0," JCTVC Contribution HM 6.0, March 2012.

[13] F. Bossen, B. Bross, K. Sühring, and D. Flynn, "HEVC complexity and implementation analysis" *IEEE Transactions on Circuits and Systems for Video Technology*, vol. 22, no. 12, Dec.2012.

[14] F.Bossen, "Common test conditions and software reference configurations," JCT-VC Document, JCTVC-G1200.

[15] ItrainOnline, "Wireless Basic Infrastructure Topology." [Online]. Available: http://www.itrainonline.org/itrainonline/mmtk/wireless_en/04_Infrastructure_Topology/04_en_mmtk_wireless_basic-infrastructure-topology_slides.pdf. [Accessed: Jan. 17, 2016].

[16] K. Fall and K. Varadhan, "The NS manual," May 2010.

[17] S. Wenger, "NAL Unit Loss Software," JCT-VC Document, JCTVCH0072, Feb. 2012.
[18] V. Pullano, A. Vanelli-Coralli, and G. Corazza, "PSNR evaluation and alignment recovery for mobile satellite video broadcasting," Advanced Satellite Multimedia Systems Conference (ASMS) and 12th Signal Processing for Space Communications Workshop (SPSC), 2012.

Comparison of High-Side and Synchronous Trapezoidal Control Using XMC-Based Brushless DC Motor Controller for Pedelecs

Jomel Lorenzo, Jr.,* Jean Clifford Espiritu, Kristofferson Reyes, Isidro Marfori, and Noriel Mallari

Abstract — **This study aims to compare high-side and synchronous trapezoidal brushless DC (BLDC) control methods using an XMC-based motor controller for pedelecs. The electric bicycle implemented three different pedal-assist modes with varying human-to-motor power ratios and one throttle mode with the use of proportional-integral control. The study compares the efficiencies of two trapezoidal control methods through the throttle and pedal-assist mode. The data obtained shows that the high-side trapezoidal control is more efficient than the synchronous trapezoidal control in all modes implemented on the e-bike. This research opens possibilities to improve other BLDC control algorithms especially in terms of efficiency.**

Keywords: **Android, telemetry, PID, BLDC motor, trapezoidal motor control, Cortex-M0**

I. Introduction

Electric bicycles—or e-bikes—are lighter and smaller compared to motorcycles, yet they can give the comfort of riding one. To be able to get these benefits, a good motor controller for the electric bicycle is needed. Currently, e-bikes available in the market can assist riders when pedalling. Unfortunately, they do not have the capability to process complex data from the e-bike [1]. The study aims to improve the e-bike by focusing on the refinement of the motor controllers.

Electric bicycles would normally have a hub motor, which may be brushed or brushless [2]. In this study, the brushless DC (BLDC) motor is used. BLDC motors have favorable characteristics such as high efficiency, high speed ranges, and high torque-to-size ratios. However, they require complex control methods to commutate the motor as it requires six pulse width modulation (PWM) signals to operate. The BLDC motor would interface with a 32-bit microcontroller, which controls the MOSFETs (metal–oxide–semiconductor field-effect transistors) in order to adaptively drive the motor.

One similar study about pedelecs implemented smart features using an off-the-shelf motor controller from the market. However, the motor controller is treated as a black box, and the response of it is unpredictable [12]. This study designed the motor controller to control the motor's response effectively depending on the status of the e-bike.

From the previous study "Adaptive Speed and Power Control for a Pedelec Using an ARM Cortex-M0 Microcontroller," the motor controller already implemented three modes of pedal assist (executive, mid, and sport) that control the target power depending on human input and throttle mode, which control the target speed of the user [6]. This study implemented two trapezoidal BLDC control signals to the motor controller and compared the difference of the two control methods in terms of efficiency of different modes discussed from the previous study.

II. Design Consideration and Methodology

A. Infineon XMC 32-Bit ARM Microcontroller

The researchers used Infineon's XMC1302 with a 32-bit ARM Cortex-M0 microprocessor inside (Fig. 1). This microcontroller is used specifically for motor control by having the hardware capable of giving PWM signals of over 20kHz [8].

Jomel Lorenzo, Jr.,* Jean Clifford Espiritu, Kristofferson Reyes, Isidro Marfori, and Noriel Mallari, De La Salle University-Laguna

*(e-mail: jomel_lorenzo@dlsu.edu.ph)

Fig.1. XMC1302 boot kit microcontroller.

B. BLDC Motor Control Using MOSFETs

The commutation of the BLDC motor functions appropriately by applying the concept of an inverter. Basically, an inverter is a switching control that converts direct current to alternating current or vice versa [3]. There are several types of inverters; however, one of the types of inverters used to drive a BLDC motor is the full-wave three-phase inverter. The inverter consists of six switching devices similar to the diagram shown below (Fig. 2) [5]. These MOSFETs are controlled with a pulse controller, which generates switching pulse signals. The signals generated consist of varying PWM, which controls the switching MOSFETs.

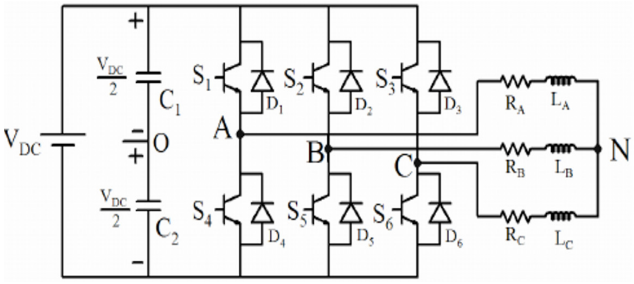

Fig. 2. Three-phase inverter.

C. High-Side and Synchronous Trapezoidal BLDC Control Methods

The BLDC motor has its advantages; however, it requires complex algorithms to operate [3]. Using a three-phase inverter made of MOSFETs, the operation of the BLDC motor can be controlled using PWM signals to move the motor to its desired position. Hall sensors would determine the current position of the motor [15]. Table I and Figure 3 show the high-side trapezoidal control signals applied in the inverter for proper commutation of the BLDC motor while Table II and Figure 4 show the synchronous trapezoidal control signals that have the same function of high-side with an additional inverted PWM in the low-side MOSFETs [10][11].

TABLE I
HIGH-SIDE COMMUTATION PATTERN WITH HALL SENSOS

No.	Hall Sensor			Input MOSFET Gate Signals					
	U	V	W	UH	UL	VH	VL	WH	WL
1	L	L	H	L	L	PWM	L	L	H
2	L	H	H	PWM	L	L	L	L	H
3	L	H	L	PWM	L	L	H	L	L
4	H	H	L	L	L	L	H	PWM	L
5	H	L	L	L	H	L	L	PWM	L
6	H	L	H	L	H	PWM	L	L	L

TABLE II
SYNCHRONOUS COMMUTATION WITH HALL SENSORS

No.	Hall Sensor			Input MOSFET Gate Signals					
	U	V	W	UH	UL	VH	VL	WH	WL
1	L	L	H	L	L	PWM	iPWM	L	H
2	L	H	H	Pwm	iPWM	L	L	L	H
3	L	H	L	PWM	iPWM	L	H	L	L
4	H	H	L	L	L	L	H	PWM	iPWM
5	H	L	L	L	H	L	L	PWM	iPWM
6	H	L	H	L	H	PWM	iPWM	L	L

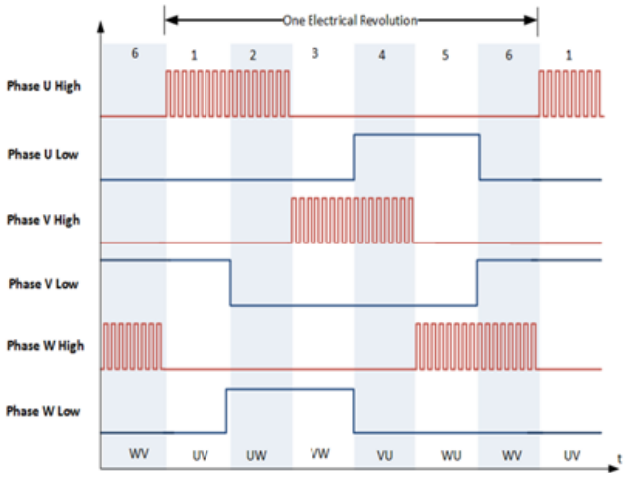

Fig. 3. High-side trapezoidal control signals.

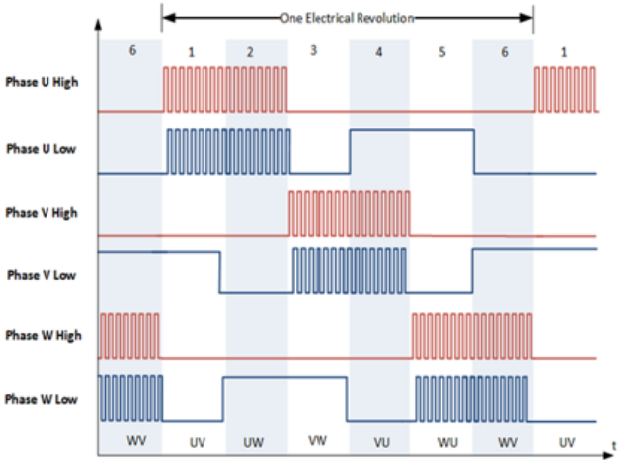

Fig. 4. Synchronous trapezoidal control signals.

D. Dead Time

Dead time is necessary in implementing the synchronous control because two PWMs are used in the same phase in the inverter [9]. Without the dead time, the high-side and low-side MOSFETs will be shorted; thus, a high current will flow, which in turn will destroy the MOSFETs. The researchers implemented a 150-ns dead time in the signals to prevent the short circuit from happening. Figures 5 and 6 show implemented dead time in the signals, and they also show that the point of intersection of the two signals will not trigger the MOSFET to be switched on. Therefore, the MOSFETs in the inverter will not generate a short circuit during operation.

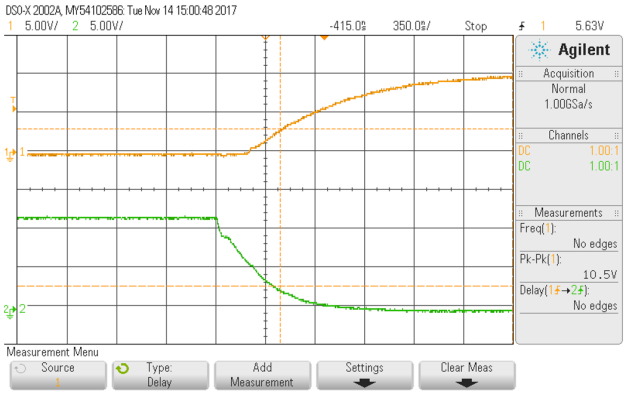

Fig. 5. Dead time in rising edge of the signal for high-side MOSFET and falling edge of the signal for low-side MOSFET.

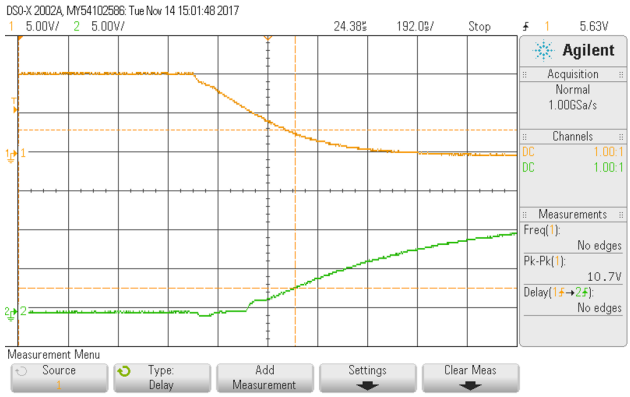

Fig. 6. Dead time in falling edge of the signal for high-side MOSFET and rising edge of the signal for low-side MOSFET.

E. Vehicle Kinematic Formula and Theoretical Power Computation

Power is needed to move the electric bicycle at any given speed. Equation 1 shows the factors that affect the required power to move the electric bicycle [4]. The human or the motor must exert more power when riding uphill, over rough roads, and in windy places.

$$P_{theo} = \frac{P_{drag} + P_{fric} + P_{hill}}{Eff} \quad (1)$$

Equation 1 can be expanded to consider the characteristics of the e-bike and the rider resulting to Equation 2. The efficiency can be computed when P_{theo} is equated to input power (P_{in}), which is equal to the product of battery current and voltage.

$$P_{theo} = \frac{0.5\left(pAV^2C_D\right)V + \left(\left(m_B + m_R\right)gC_R\right)V + \left(m_B + m_R\right)g\left(V\sin\theta\right)}{eff} \quad (2)$$

where

V = *velocity (m/s)*
m_V = *weight of the bicycle (kg)*
m_D = *weight of the rider (kg)*
g = *acceleration due to gravity (9.8 m/s²)*
C_{RR} = *coefficient of rolling resistance (unitless)*
p = *air density (1.2 kg/m³)*
A = *bicycle and rider frontal area (m²)*
C_D = *coefficient of drag*
θ = *inclination angle in degrees from horizontal plane*
Eff = *e-bike efficiency ($0 < Eff \leq 1$)*

F. Pedal-Assist and Combining Human Power and Motor Power

Pedal-assist is a concept that is achieved only when the motor is stimulated when the user is pedaling the electric bicycle. In order to detect if the user is pedaling the electric bicycle, a cadence sensor using hall magnets is utilized. To improve the response further, a torque sensor is used to determine the input human power into the system. Since the human power is identified, it is now possible to implement more advanced control algorithms that target a specific ratio between the human power and the motor power. The three ratios used for this study are the executive, mid, and sports modes. Executive mode makes the motor do 70% of the power output while the human is only 30% of the power output. Mid mode ensures that both the motor and the human equally contribute to the total power of the system. Sports mode makes the human do 70% of the power output while the motor only does 30% of the power output.

$$P_h = \tau * (2\pi * \omega)(3) \quad (3)$$

where

P_h = human power (W)
τ = torque (Nm)
ω = cadence (rps)

$$\tau = F * \frac{r}{\pi} \int_{-\frac{\pi}{2}}^{\frac{\pi}{2}} \cos(x)\, dx \quad (4)$$

where

τ = torque (Nm)
F = human force (N)
r = crank radius (m)

G. Speed Control

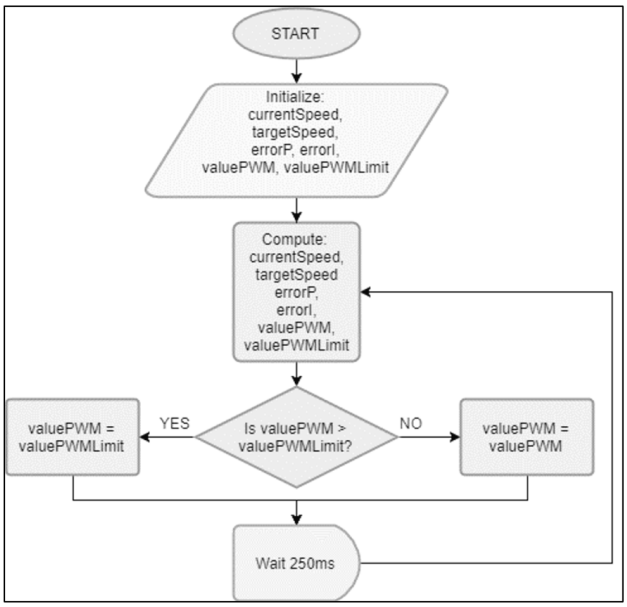

Fig. 7. Flowchart for speed control.

In this section, the researchers implemented a proportional-integral speed control algorithm for throttle mode that will target the desired speed of the user and maintain its current speed when the target speed is reached. See flowchart used in targeting speed for throttle mode (Fig. 7) [6].

A. Power Control

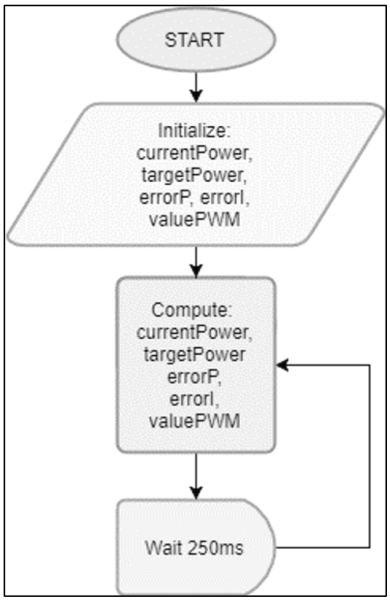

Fig. 8. Flowchart for power control.

In this section, the researchers implemented proportional-integral power control algorithm for pedal-assist mode. The target power will be adjusted depending on the mode used by the user and its peddling behavior. See flowchart used in controlling the motor power for pedal-assist mode (Fig. 8) [6].

I. MOSFET Characteristics

The researchers used IPP04N12N13G, a MOSFET that is capable of blocking 120 V during off condition and can let 120 A pass during on condition [13]. The battery voltage used in the study is 36 V, and choosing a breakdown voltage for a MOSFET must be twice of its input as a rule of thumb. This MOSFET can also be applied to 48-V battery systems.

J. Gate Driver Response Time and Determination of Switching Frequency

In this study, an Infineon MOSFET gate driver (MGD), 2EDL05N06PF, is used for translating the switching signals from the microcontroller to a higher voltage to fully drive the MOSFET [14]. MGDs are important in the circuit as they provide isolation to the high-power side and the low-power side of the circuit. In addition to that, they can support 20-kHz PWM frequency as an input by adjusting the value of the bootstrap capacitor to 1 uF. Figure 9 shows the circuit configuration of a MGD in one phase.

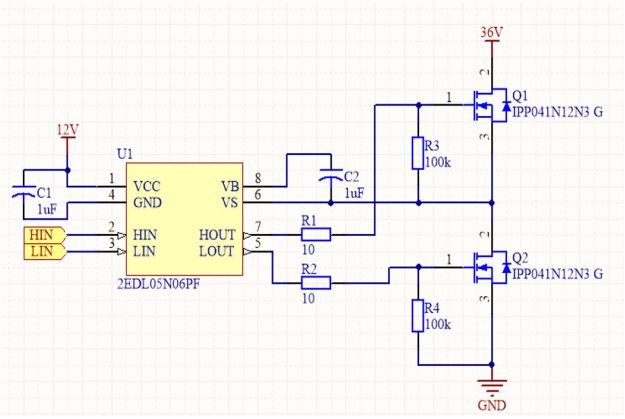

Fig. 9. MOSFET gate driver configuration.

III. RESULTS AND DISCUSSION

This section contains the efficiency testing of the two trapezoidal BLDC control methods. The testing setup was done on a flat road to eliminate the power needed to overcome slopes.

A. High-Side Trapezoidal

Figures 10, 11, and 12 show the efficiency of the e-bike operating in three pedal-assist modes using high-side trapezoidal control. The calculated average efficiency is 78.01%, which indicates efficient motor control of the system.

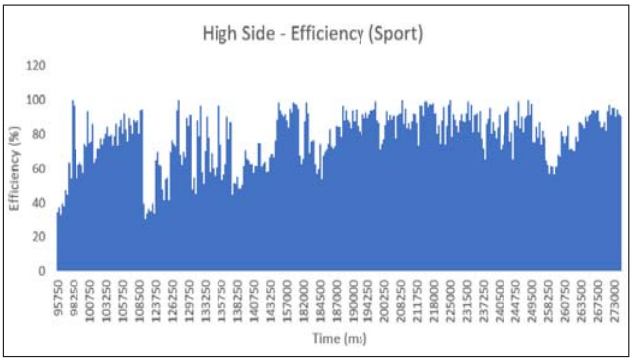

Fig. 10. Efficiency versus time (sports mode, high-side).

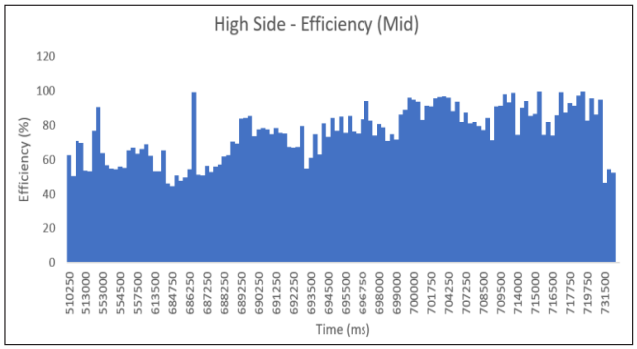

Fig. 11. Efficiency versus time (mid node, high-side).

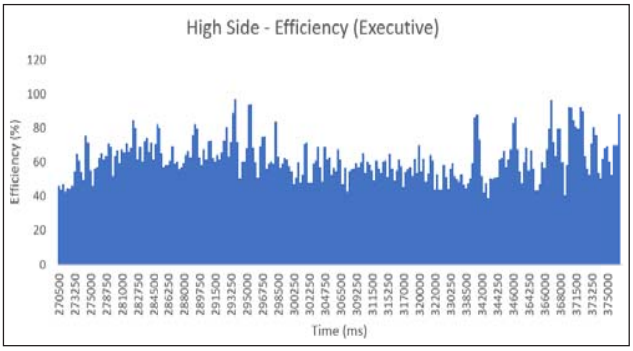

Fig. 12. Efficiency versus time (executive mode, high-side).

Likewise, Figure 13 shows the efficiency of the e-bike when operating in smart throttle. The calculated average efficiency in this case is 70.11%. This was attained through the use of an advanced state machine algorithm.

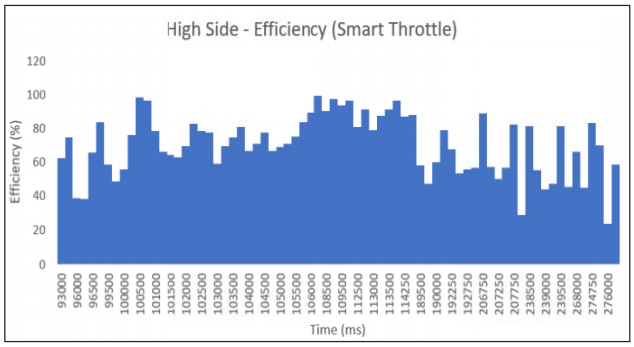

Fig. 13. Efficiency versus time (smart throttle, high-side).

B. *Synchronous Trapezoidal Control*

In the synchronous trapezoidal control method, Figures 14, 15, and 16 show the efficiency of the e-bike using the same testing setup in the high-side, and it is operated also in three pedal-assist modes, while Figure 17 shows the efficiency in the throttle mode that also used the same algorithm in the high-side.

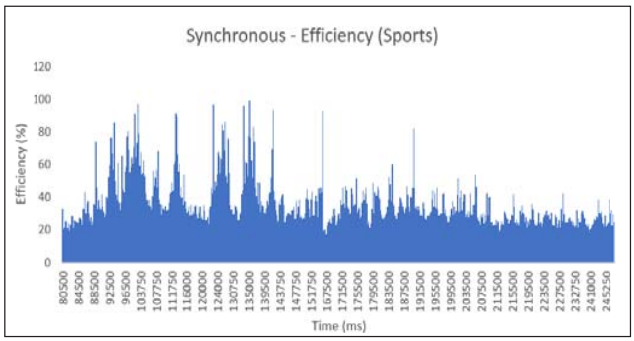

Fig. 14. Efficiency versus time (sports mode, synchronous).

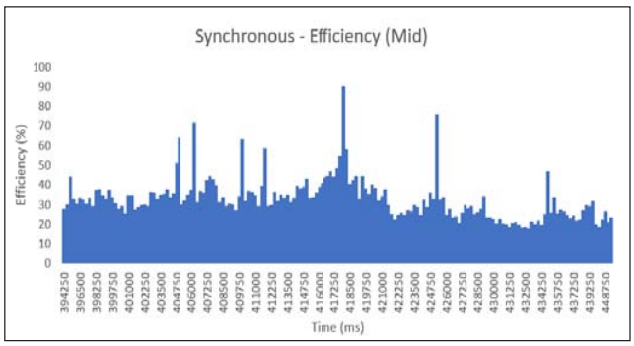

Fig. 15. Efficiency versus time (sports mode, synchronous).

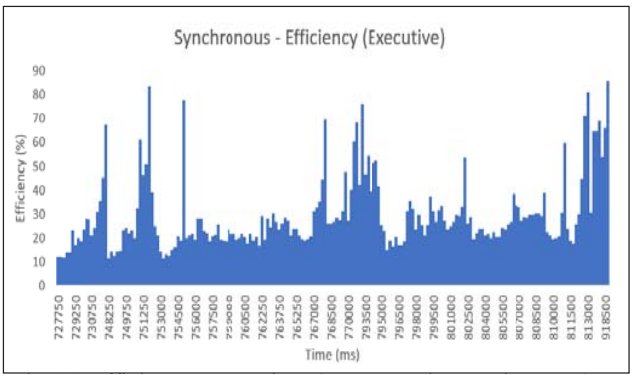

Fig. 16. Efficiency versus time (sports mode, synchronous).

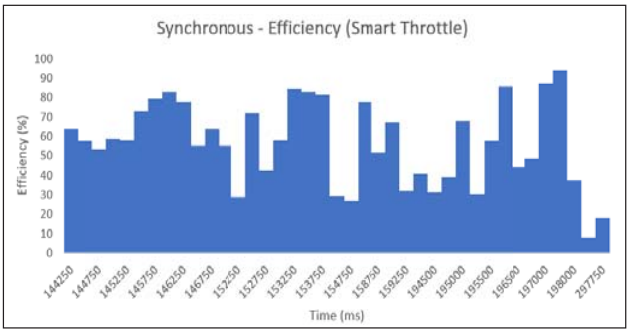

Fig. 17. Efficiency versus time (sports mode, synchronous).

C. *Comparison of the Two Control Methods*

Each graph in the data obtained from two trapezoidal control methods was used to get the average of the values in order to compute for efficiency of the system in each mode. Table II shows the summary of the efficiencies from two trapezoidal control methods.

TABLE III
SUMMARY OF DATA FOR THE EFFICIENCY OF BOTH CONTROL METHODS

Mode	Synchronous	High-Side
Sports	36.5%	78.01%
Mid	32.7%	75.41%
Executive	29.27%	61.97%
Throttle	56.25%	70.11%
Average	**38.68%**	**71.375%**

CONCLUSIONS

In summary, the study was able to compare two trapezoidal control methods in terms of efficiency. It was found that high-side trapezoidal control is more efficient than the synchronous trapezoidal control by a factor of 2,

whereas the average of efficiency across all modes of high-side control method is 71.38% while the average efficiency of synchronous control method is 38.68% across all modes. This result shows that if the e-bike is used in synchronous control and it only traverses 10 km in one full charge of the battery, then operating it using the high-side control method could travel 20 km in one full charge of the battery because of its efficiency. When driving the motor, the synchronous control method produces louder acoustic noise compared to the high-side trapezoidal control. This was caused by high torque ripple present in synchronous control, which is inefficient in flat roads [7].

At the end of the study, the researchers were successful in implementing two BLDC control methods and comparing their difference in terms of efficiency to determine the best control method to be used for the e-bike.

V. Recommendation

The researchers recommend adjusting the dead time, which can change the response of the synchronous trapezoidal control. Also, adding smart features such as Bluetooth connectivity to the smartphone and battery prediction will improve the overall response of the e-bike.

Acknowledgment

The researchers would like to thank Mr. Antonio and Infineon for giving us support through the power MOSFETs and the XMC1300 Boot Kit. We would also like to thank Engr. Noriel Mallari for assisting us with the leap from Arduino to an industry-grade microcontroller. Finally, we would like to thank Nyfti Inc. for providing the bicycle chassis used for the study.

References

[1] "About Us | Faraday Electric Bikes," *Faraday Bikes*, 2017. [Online]. Available: https://www.faradaybikes.com/about/. [Accessed: Oct. 6, 2017].

[2] "Sine-wave controllers, making hub-motors super quiet," *ElectricBike.com*, 2017. [Online]. Available: https://www.electricbike.com/sine-wave/. [Accessed: Oct. 7, 2017].

[3] T. Rahman, S. Motakabber, and M. Ibrahimy, "Design of a switching mode three phase inverter," *2016 IEEE International Conference on Computer and Communication Engineering (ICCCE)*, pp. 155–160, 2016.

[4] A. Gross, C. Kyle, and D. Malewicki, "The aerodynamics of human-powered land vehicles," *Scientific American*, vol. 249, no. 6, pp. 142–152, 1983.

[5] T. Erfidan, S. Urgun, and B. Hekimoglu, "Low cost microcontroller based implementation of modulation techniques for three-phase inverter applications," *MELECON 2008—The 14th IEEE Mediterranean Electrotechnical Conference*, pp. 541–546, 2008.

[6] K. Reyes, J. Lorenzo, J. Espiritu, P. Sacdalan, N. Mallari, and I. Marfori, "Adaptive speed and power control for a pedelecusing an ARM Cortex-M0 Microcontroller," 2017.

[7] L. Jianjun, X.Yongxiang, and J.Zou, "A study on the reduction of vibration and acoustic noise for brushless DC motor,"*in 2008 International Conference on Electrical Machines and Systems,* pp. 561–563*,* 2008.

[8] Infineon, "XMC1300 Microcontroller Series for Industrial Applications ARM Cortex-M0 32-bit processor core," XMC1302 Datasheet, May 2014.

[9] K. Denny, "PWM control and dead time insertion," *Hackaday.io*, 2018. [Online]. Available: https://hackaday.io/project/3176-gator-quad/log/11741-pwm-control-and-dead-time-insertion. [Accessed: Jan. 1, 2018].

[10] Texas Instruments, "DRV8308 Brushless DC Motor Controller," Texas Instruments Incorporated, Feb. 2014. [Revised: Nov. 2017].

[11] Renesas. "BLDC motor control algorithms," *Renesas Electronics Singapore*, 2018. [Online]. Available: https://www.renesas.com/en-sg/solutions/key-technology/motor-control/motor-algorithms/bldc.html. [Accessed: Jan. 1, 2018].

[12] N. Mallari, J. Macaraig, D. Navarrete, and I. Marfori, "Smart motor controller using model-based algorithm for control of pedal-assisted electric bicycle," 2016.

[13] Infineon, "2EDL05N06PF EiceDRIVER™ Compact High voltage gate driver IC," Infineon Technologies, Jan. 2016.

[14] Infineon, "IPP041N12N3 G OptiMOS Power-Transistor," Infineon Technologies, April 2014.

[15] J. Zhao and Y. Yu, "Brushless DC motor fundamentals application note,"*Monolithic Power Systems, Inc.* , 2011.

Journal of Computational Innovations and Engineering Applications 2(2) 2018: 36–48

Literature Review for the Design and Implementation of the Archer Robot

Alexander C. Abad* and Elmer P. Dadios

***Abstract* — This paper presents a literature review for the design and implementation of the Archer Robot that is capable of knocking an arrow to a standard recurved bow, drawing the arrow, and hitting a target. Ancient and current human-like mechanical archers, machine vision, and intelligent controllers that can be the bases for the future Archer Robot are discussed in this paper.**

Keywords: **Archer Robot, archery, artificial intelligence, machine vision**

I. Introduction

Humans have a long history of creating something that looks and moves like a human [1]. One of the earliest accounts of human-like automaton (a machine that can move by itself, plural form: automata [2]) was written in the Lie Zi text in China, which dates back to the third century B.C. [3,4]. Inside the text is a story about King Mu of Chou, who encountered Yen Shih, an artificer who presented a life-like humanoid (human resembling) automaton that can sing and act. The king was astonished by the skills of the humanoid robot. The humanoid even winked its eye and made advances to the ladies that made the king very angry and want to execute the artificer. Due to fear of death, the artificer destroyed the humanoid automaton and showed to the king that it is just made of leather, wood, glue, and lacquer, colored with white, black, red, and blue. The king was convinced and delighted with the skill of the artificer that he exclaimed, "Can it be that human skill is on a par with that of the great Author of Nature?" [4].

In the following centuries, many human-like automata or moving dolls and statues were developed such as the automaton of Hero of Alexandria (100 A.D.), the humanoid automaton of Al-Jazari (1200), the humanoid automaton of Leonardo da Vinci in the late 15th century, the Jacquet-Droz's family of androids in Europe, and the mechanical dolls of Japan, known as "karakuriningyo," both developed in the 18th century [1, 5].

Human-like automata flourished in the 20th century. Humanoid animatronics systems with programmable human-like movements synchronized with audio became an attraction at theme parks. These systems were fixed open-loop without sensing their environment. Later on, with the advancement of digital computing, humanoid animatronics were incorporated with the ability to sense, control, and actuation at the end of the 20th century [1]. Automata with a closed-loop system were later called "robots." The term *robot* was derived from *robota*, which means subordinate labor in the Slav languages. The term was first introduced by Karel Capek in his play "Rossum's Universal Robots (R.U.R.)" in 1920 [5].

The 21st century has been labeled by many roboticists as the "age of the robots." Intelligent autonomous machines will gradually substitute for many automatic machines [6]. These robots are not only programmed to do certain tasks but are capable of learning from their environment. Humans' dream of creating something like them in movement and thinking is becoming a reality in the field of humanoid robotics. This area of research is like a "mirror" that can help us reflect and understand ourselves relative to motion, sensing, perception, and thinking.

Eye–hand coordination has been mastered by humans through experience. Humans are capable of estimating depth and distance of objects within their reach. In the field of robotics, visual servoing is the counterpart of eye–hand coordination. Robust and intelligent algorithms are needed to perform efficient, repeatable, and accurate control of robotic arms to perform tasks such as putting an arrow to a bow and pulling it to shoot a target.

Generally, even humans have difficulty in tracking and shooting an object within the environment. This human ability to adapt and to adjust body movements in order to shoot a target is difficult to incorporate in a robotic system.

The Archer Robot in this study will use a standard recurved bow used in archery competition. It will be designed to knock an arrow to a bow, draw the arrow,

Alexander C. Abad* and Elmer P. Dadios, De La Salle University, Manila, Philippines

*(e-mail: alexander.abad@dlsu.edu.ph)

and hit a static target. It will use artificial intelligence algorithms for control and machine vision (MV) for its feedback. The robot will have a static lower body but with an upper body capable of pivoting to the left or right by turning its waist.The Archer Robot will track and shoot the official 80-cm target spot face based on the FITA beginners' manual [7]. The shooting of a static target will be characterized at different distances relative to the Archer Robot. Distances will be 6 m (FITA Red Feather), 8 m (FITA Gold Feather), 10 m (FITA White Feather), 14 m (FITA Black Feather), and 18 m (FITA Blue Feather—official FITA indoor distance) [7]. All testing will be held indoors to neglect wind resistance.

II. Significance of the Archer Robot

The Archer Robot can be a very good platform for education. With regard to control systems, this study can contribute to the growing area of intelligent control. It can be a programming project wherein a robot can be treated as a black box to be programmed in order to display a concrete physical manifestation of the programming codes [8].

The Archer Robot can be a learning focus because a robot can stimulate students to be interested in science, technology, and engineering. It can promote life-long learning results in areas such as teamwork, problem solving, and self-identification with technology-focused careers [8]. This study can be a point of collaboration among engineering courses especially in the fields of mechanical engineering, electronics engineering, and computer engineering because it covers a wide area of knowledge and applications.

The Archer Robot can be a learning collaborator wherein a robot can enhance the learning process by imbibing dedication in learning. It can be a source of discovery and wonder for students [8].

The Archer Robot not only is for education but can also be for entertainment. Due to advancements in the field of robotics, educational robot tournaments are becoming popular [8]. Sooner or later, there will be an archer robot competition among different schools and universities. This study can be a very good platform in preparation for this future competition.

The feedback mechanism of the Archer Robot using MV can be used for industry applications and also for security and surveillance applications. The MV algorithm that will be developed in this study can be used in a manufacturing plant. This can be used in the industry for inspection of parts, color matching, gauging, quality checking, and robotic guidance for picking up or segregating a moving object in a conveyor belt. In military, it can also be used in the interception of flying attackers such as drones.

III. Review of Related Literature

This section focuses on research regarding human-like archer automata, humanoid archer robots, and some robotic arms that can play like humans. It also covers research on machine control and MV.

1) Archer Automata

a) Karakuriyumiiridōji, ("bow-shooting boy") by Hisashige Tanaka:

Fig. 1. *Karakuriyumiiridōji,* ("bow-shooting boy") by Hisashige Tanaka [10].

Kakakuri can be translated as "a tricky mechanical device or gadget" [9]. It is a self-operating wooden puppet equivalent to Western automata with clockwork mechanisms [10]. Figure 1 shows the whole setup of the Japanese archer automata created by Hisashige Tanaka (1799–1881) [10], inventor and founder of Shibaura Engineering Works (a predecessor of Toshiba) [9].

Yumi-iri Doji has four small arrows in a case at his side and removes each arrow one by one into his bow and shoots by pulling back on the bow. The whole process is shown in Figure 2, which is lifted from [9, 10]. A YouTube video link of a*karakuri* can be found in [11].

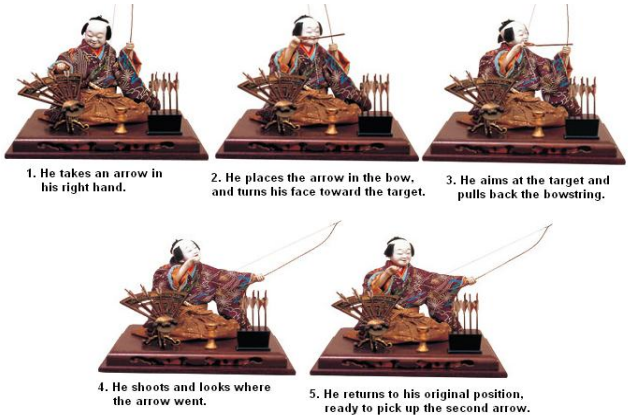

Fig. 2. *Karakuriyumiiridōji,* ("bow-shooting boy") steps in shooting [9, 10].

b) Samurai Archer by Hideki Higashino:

According to [12], Hideki Higashino is one of the few remaining craftsmen who continue the Japanese *karakuri* tradition that dates back 200–300 years to the Edo period. His *karakuri* samurai archer shown in Figure 3 can draw arrows, put them in the bow, and pull it to shoot a target. These steps are very similar to Figure 2.2, but the archer is in a standing position and the arrow can stick to the target. A video of this *karakuri* samurai archer is accessible through the links provided in [12, 13].

Fig. 3. Samurai archer by Hideki Higashino [13].

c) Yabusame ("Horseback Archer") Karakuri by Tsuyoshi Yamazaki:

Another version of archer *karakuri* is the *yabusame* or the horseback archer made by retired engineer Tsuyoshi Yamazaki. This *yabusamekarakuri* was the first-prize winner in the "World Karakuri Contest" in the 2005 World Expo, Nagoya, Japan [14]. Shown in Figure 4 is a *karakuri* archer riding a horse and shooting three targets. The archer is moving horizontally as it shoots the target. A video clip of this *karakuri* in action is available in the link provided in [15].

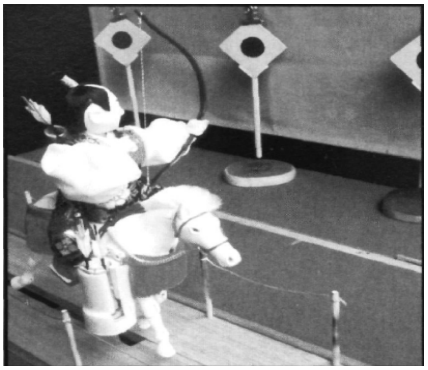

Fig. 4. *Yabusamekarakuri* by Tsuyoshi Yamazaki [14].

2) Toylike Humanoid Archer Robot

a) Hammerhead:

This lightweight (less than 3kg) humanoid robot of the Osaka Sangyo University Waling Project [15] demonstrated its arrow shooting capability during the 16th Robo-One Championship held last 2009 in Toyama City, Japan [16]. This archer robot shot an arrow at a glass plate target. The arrow has a suction cup tip and was able to stick on the glass plate when Hammerhead shot it [17]. Shown in Figure 5 is a snapshot of Hammerhead from a YouTube video [18].

Fig. 5. Hammerhead in the 16th Robo-One Championship [18].

b) i-SOBOT Archer:

i-SOBOT is a 6.5-inch humanoid robot thatis certified as "The World's Smallest Humanoid Robot in Production" by the Guinness World Records [19]. Figure 6 shows an i-SOBOT archer capable of shooting an arrow. A video clip is available on YouTube [20].

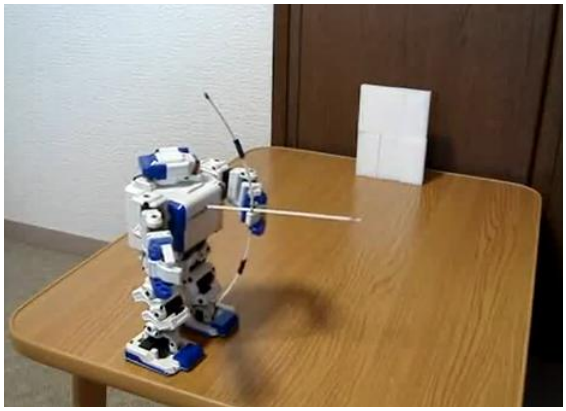

Fig. 6. i-SOBOT Archer [20].

c) The iCub Archer:

The 53-degrees of freedom (DOF) humanoid robot iCub shown in Figure 7 was programmed with a learning algorithm called ARCHER (Augmented Reward CHainEd Regression) to hold the bow, release the arrow, and learn by itself to aim and shoot arrows at the given target. It was able to learn to hit the target in only eight trials [21]. The paper [21] and the video [22] of iCub Archer were presented at the 2010 IEEE-RAS International Conference on Humanoid Robots, Nashville, TN, USA. Unlike the karakuri archers [9–15] that can put arrows to the bow, iCub used a loaded bow.

Fig.7. iCub Archer Robot [22].

So far, toy-like archer automata and archer robots were presented above. The bow and arrow used are not official archery tools. Though not related to archery, life-size robots with human-like skills are presented in the next sections. They can be a great source of motivation for the future Archer Robot.

3) Robots With Dexterous Arms

The following are robots with dexterous arms performing some human tasks with flexibility, mobility, and agility. Most of them are being used by different universities as an educational platform. All of them utilize an MV feedback system for closed loop control.

a) Sword Wielding Robots:

Inspired by the movie *Star Wars*, the Yaskawa Company showed at the 2009 International Conference on Robotics and Automation (ICRA), in Shanghai, two industrial robots with "lightsabers" performing a choreographed motion of sword wielding with each other [23]. Shown in Figure 8 is a snapshot from [24] for the "Jedi vs Sith" robotic arm demonstration.

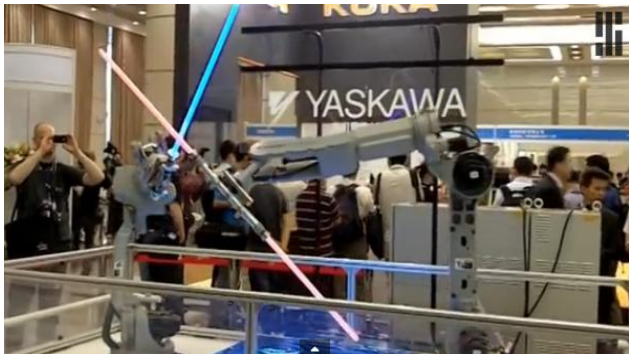

Fig. 8. "Jedi vs Sith" [24].

Another sword wielding performed by a robot was demonstrated in 2011 by students at Stanford University under the supervision of Prof. Oussama Khatib. This robot, called "Jedibot," has been programmed to attack and to defend versus a human opponent. Using a Kinect sensor, it can track the motions of color-coded foam swords [25, 26]. A snapshot of "Jedibot" from a Stanford video clip [27] is shown in Figure 9.

Fig. 9. "Jedibot" [27].

The "Jedibot" is just one of the projects in Khatib's Experimental Robotics course at Stanford. Other robot projects include a robotic arm that plays golf, a robotic arm that can write, and a robotic arm that can cook hamburgers [25].

b) "Wu and Kong":

Two life-size humanoid robots, Wu and Kong, developed at Zheijiang University in China, were able to play table tennis. The two robots were designed to have ball tracking technology, accurate identification, location prediction, motion modeling, and balance [28]. A snapshot of Wu and Kong from a Reuters video clip [29] is shown in Figure 10.

Fig. 10. Wu and Kong [29].

c) Motoman SDA10 Robot:

The Motaman SDA10 is an industrial dual-arm robot created by Yaskawa Electric Corporation and has been programmed to perform many complex tasks [30–33]. Figure 11 is a snapshot from a YouTube video clip [31] showing how the Motoman SDA10 cooks *okonomiyaki*. The cooking ability of the robot was demonstrated at the Food Machinery and Technology Expo in Tokyo 2008 [33]. The Motoman SDA10 cook in Figure 2.11 was developed by Prof. Paul Rybski and a pair of graduate students from Carnegie Mellon University. They used a $20,000 laser navigation system, sonar sensors, and a Point Grey Bumblebee 2 stereo camera that functions as the eyes of the robot [33].

Fig. 11. Motoman SDA10 cooking [31],

In another video clip recorded in 2008 [32], with a snapshot in Figure 12, the Motoman SDA10 was able to assemble a camera and take a picture at the end of the task.

Fig. 12. Motoman SDA10 assembles a camera [30].

d) Rollin' Justin:

Rollin' Justin is a mobile humanoid robot with two arms. It is designed for research on sophisticated control algorithms for complex kinematics and mobile two-handed manipulation and navigation. It has 3 DOF in the torso, 7 DOF in each arm, 12 DOF in each hand, and 2 DOF in its head [34]. This robot is capable of catching flying balls and preparing coffee. It is capable of carrying out dynamic and sensitive tasks [35]. Justin can catch not only one ball but two balls thrown at the same time. A snapshot from a video clip [36] of Justin is shown in Figure 13.

Fig. 13. Rollin' Justin catches two balls [36].

4) MVVersus Computer Vision

MV is not the same as computer vision (CV) [37]. In general, MV is more of a system utilizing CV. MV is more practical while CV is more theoretical. Although MV and CV relate to artificial vision systems, MV is more on the hardware architecture and application of a vision system, while CV is more on the software or algorithm aspect of MV. Table I, based on [37], shows a comparison between MV and CV. Entries in the MV column are related to a factory-floor machine.

TABLE I
COMPARING MV AND CV

Feature	MV	CV
Academic/practical motivation	Practical	Academic
Advanced in theoretical sense	Unlikely (practical issues are likely to dominate over academic matters).	Yes. Academic papers often contain a lot of "deep" mathematics.
Cost	Critical	Likely to be secondary of importance
Dedicated electronic hardware for high-speed processing	Very likely	No (by definition)
Designers willing to use nonlogarithmic solutions to solve problems	Yes (e.g., are likely to benefit from careful lightning)	No
In situ programming	Possible	Unlikely
Input data	A machine part, piece of metal, plastic, glass, wood, etc.	Computer file
Knowledge of human vision influences system design	Most unlikely	Very unlikely
Most important criteria by which a vision system is judged	(a) Ease of use (b) Cost effectiveness (c) Consistent and reliable operation	Performance
Multidisciplinary	Yes	No
Nature of an acceptable solution	Satisfactory performance	Optimal performance
Nature of subject	Systems engineering, practical	Computer science, academic (i.e., theoretical)
Operates free-standing	(a) Interactive prototyping system must be able to interact with its human operator (b) Factory floor (target machine) must be able to operate free-standing	May rely on human interaction
Operator skill level required	(a) Interactive prototyping system: medium/high (b) Factory floor (target machine) must be able to cope with low skill level	May be very high
Output data	Simple signal to control external equipment	Complex signal for human being
Speed of processing	(a) IPT enough for effective interaction (b) Real-time operation is very important for TM	Not of prime importance
User interface	Critical feature for IPT and TM	May be able to tolerate weak interface

Note. Entries in the MV column relate to the factory-floor target machine, unless otherwise stated [37].

In order to create an MV system, the person in charge must take into consideration different technologies such as the ones presented in Table II. The MV system is an integration of diverse technologies. The person in charge is a system engineer rather than a scientist [37].

TABLE II
TECHNOLOGIES NEEDED TO DESIGN AN MV SYSTEM [37]

Technology	Remarks
Mechanical handling	(i) Presenting objects to the camera for viewing (ii) Mounting camera and lights rigidly and without causing undue obstruction within the camera's field of view
Lightning	Critical part of any MV system
Optics	Lightning and optics can often convert a very difficult problem into a trivial one
Sensor	Camera, line-scan sensor, laser scanner, ultra-sonic sensor, x-ray sensor
Systems architecture design	Organization of the overall system
Analog and video electronics	Normally used principally for preprocessing
Digital electronics	To reduce the data rate
Algorithms and heuristics Software	CV normally claims these twoareas for itself. MV has a "legitimate interest" in them too.
Industrial engineering	Design for robustness in the hostile factory environment
Communications	(i) Networking to computers in company and other vision systems (ii) Connection to other factory machines, programmable logic controllers, etc.
User interface	Design for ergonomic interface to a human operator
Quality Control	Design for industrial, operational, and environmental
Production Engineering	Compliance with current working and quality-control practices. It may be possible to modify the product or process to make inspection easier/more reliable.

a) Active and Passive 3D Vision Systems

Depth perception is one of the most investigated aspects of biological and MV [38]. With depth perception, a three-dimensional (3D) view of the environment can be realized. The use of 3D information is vital in the field of robotics, especially in MV systems, in order to detect and avoid obstacles in a 3D workspace, to recognize objects, and to map environments [39]. Depth perception has been utilized for distance or range measurements. The development of accurate, low-cost, and compact vision-based range sensors is a dynamic area of research in the field of robotics. Vision systems for depth perception or range sensing techniques in the field of robotics can be classified as active or passive. Active range sensing uses a reflected beam of light coming from a light source, which is commonly a laser, while passive range sensing depends only on ambient light [40]. Laser range finders have been around for half a century. They were first used and demonstrated by John D. Myers in 1965 [41]. Direct and active range finding techniques in MV or CV involve light time-of-flight (TOF) estimation and triangulation systems [42]. Active triangulation is one of the first range imaging approaches used in robotics [39]. It is a well-established technique for measuring distance (range) to surfaces, which is composed of a light source and a camera placed at a certain lateral distance (baseline) from the source [43]. Active techniques, such as laser scanning and contrived lighting (striped light, grid coding, and moiré fringe contouring), intentionally project illumination into the scene in order to construct easily identifiable features and minimize the difficulty involved in determining correspondence [42, 44]. Depth perception using the triangulation technique is not only for active vision systems but has been also implemented in passive vision systems [44–46]. Triangulation in passive range finding techniques does not require structured illumination. Such techniques are much more flexible than the active ones [45]. In general, passive methods have a wider range of applicability since no artificial source of energy is involved and natural outdoor scenes (lit by the sun) fall within this category [42]. Depth perception via passive techniques can be monocular image-based or stereo-based. Monocular image-based range finding includes texture gradient analysis, photometric methods (surface normal from reflectance), occlusion effects, size constancy, and focusing methods [42]. On the other hand, the passive stereo ranging technique is also a triangulation technique with the same geometric characteristics as active

triangulation, except the range is computed by triangulation between the locations of matching pixels in images rather than between a known source and an observed pixel [39]. A taxonomy of vision techniques via optical sensor has been presented in [45] and is shown in Figure 14.

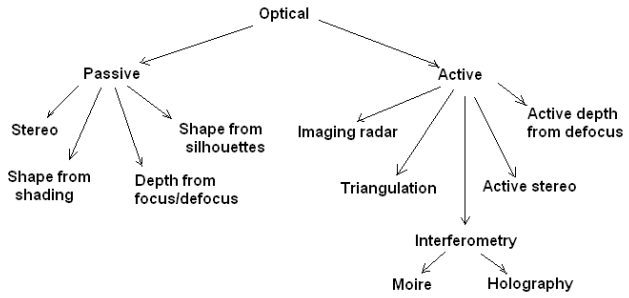

Fig. 14 Taxonomy of vision techniques [45].

The 3D scene reconstruction from projections on a 2D sensor is inherently ambiguous. In the field of robot vision, there are many proposed methods for depth perception such as stereoscopic vision, depth from motion parallax, and depth from oculomotor parallax [38]. Among these techniques, there have been many studies with regard to stereo vision, and some of them are discussed in the next section.

b) Stereo Vision

Range sensing is vital in the field of robotics to detect obstacles or target within the surrounding. Scanning lasers are the most widely used range sensor for robotics, but they are not the only way. There is an increasing popularity of stereo vision range sensing techniques for mobile robots. Compared to scanning lasers, stereo vision has passive camera sensors that are lightweight, power efficient, and low-cost. The cameras in stereo vision do have sensitive mirrors, and the optics found in scanning lasers make them more robust to vibration, shock, and the effect of strong magnetic fields. Stereo vision is well suited for use on moving platforms, unlike lasers that scan the environment in a sequential manner from which any movement during laser scanning can skew the results unless it is taken into consideration. The stereo vision technique produces dense 3D data, compared to the relatively sparse 2D data of a single 2D laser scan [47]. Stereo vision has been used in long-distance ranging [39] such as the one presented in [48], which is capable to detect 14 cm or 35.56 in obstacles at over 100 m (109.36 yards) for on-road obstacle detection. A study in [49] shows encouraging results comparing stereo vision performance with a laser rangefinder. It was reported that a stereo rangefinder (SRF) can be an alternative to a laser rangefinder (LRF) for operating at short–medium ranges in man-made environments.

c) Visual Servoing

Visual servoing means a closed-loop position control for a robot end-effector using MV. The term is generally called visual feedback [50]. A survey of visual servoing for manipulation can be found in [51], where it discusses theories, applications, and comparisons of the different visual approaches for robotic manipulation during the past three decades.

On the other hand, [50] presented a tutorial introduction to robotic servo control that focused on the fundamentals of coordinate transformations, image formation, feedback algorithms, and visual tracking.

Visual servoing is the use of CV data to control the motion of a robot. The vision data comes from a camera, which is mounted directly on the robot or on a fixed position in the workspace observing the robot. Visual servoing relies on image processing, CV, and control theory [52]. Generally, there are two camera configurations: eye-in-hand, wherein the camera is mounted on or near the end-effector, and eye-to-hand wherein the camera is at a distance from the robot manipulator capturing a panoramic vision of the environment [53]. According to [54], there are two basic approaches to visual servoing control, which are image-based visual servo (IBVS) and position-based visual servo (PBVS). In IBVS, the error signal that is measured directly in the image is mapped to actuator commands, while PBVS utilizes CV techniques to reconstruct a 3D workspace on which the actuator commands are computed. A hybrid method combining the advantages of IBVS and PBVS has been reported in [55] and is called 2D 1/2 visual servoing. It is based on the estimation of the camera displacement between the current and desired views of an object.

According to [52], the main goal of any vision-based control system is to minimize an error $e(t)$, defined by

$$e(t) = s[m(t), a] - s^* \tag{1}$$

where:

$m(t)$ = a set of image measurements (e.g., image coordinates, parameters of image segments);
$s[m(t), a]$ = a vector of k visual features computed using image measurements;
a = a set of parameters that represent potential additional knowledge about the system (e.g., coarse camera intrinsic parameters or 3D model of objects); and
s^* = a vector that contains the desired values of the features.

Visual servoing systems differ according to how s is expressed. In IBVS, s consists of a set of features that are immediately available in the image data, while in PBVS, s consists of a set of 3D parameters. Once s is selected, designing the visual control can be quite simple. One straightforward approach is to design a velocity controller based on the relationship between the time variation of s and the camera velocity. Let the spatial velocity of the camera be denoted by $u_c = (v_c, \omega_c)$ where v_c is the instantaneous linear velocity of the origin of the camera frame and ω_c is the instantaneous angular velocity of the camera frame. The relationship between the first derivative of s which is $\dot{s}$ and u_c is given by

$$\dot{s} = L_s u_c \tag{2}$$

where $L_s \in \mathbb{R}^{k\times 6}$ is called the interaction matrix related to s [52].

Shown in Figure 15 is the block diagram of a simple closed-loop visual servoing image-based system [52].

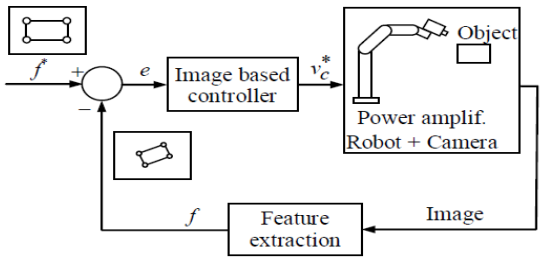

Fig. 15. Closed-loop visual servoing [52].

With regards to PBVS control, a 3D camera calibration is needed in order to map the 2D data of the image features to the Cartesian space data. Intrinsic (e.g., lens and CCD sensor properties) and extrinsic (e.g., relative pose of the camera system with respect to a generic world reference system) parameters of the camera must be evaluated. The extrinsic parameters matrix coincides with the homogeneous transformation between the camera and the object reference systems:

$$T_o^c = \begin{bmatrix} R_o^c & t_o^c \\ 0^T & 1 \end{bmatrix} (3) \tag{3}$$

where:

c = camera;
o = origin;
T_o^c = the homogeneous transformation matrix of the camera relative to the origin;
R_o^c = the rotation matrix of the camera relative to the origin; and
t_o^c = the translation vector of the camera relative to the origin [56].

5) Intelligent Robot Controller

Robot controllers based on mathematical descriptions such as differential equations, transfer functions, and first order vector matrix differential equations based on the state space method shown in the previous sections of this chapter can be classified as classical controllers. In the mid-1990s, Dr. Elmer Dadios suggested, demonstrated, and proved, using the flexible pole-cart balancing platform, that there are other techniques that can be used to control complex and highly nonlinear systems. At least three nonclassical or intelligent robot controllers were reported, presented, and effectively demonstrated, which are the fuzzy logic controller, genetic algorithm (GA)–based controller, and artificial neural network (ANN)–based controller and a combination of two of these intelligent controllers [57–60].

a) The Fuzzy Logic Controller

Zadeh introduced the concept of fuzzy sets in 1965 [61]. Fuzzy logic uses linguistic descriptions to describe complex systems. Information is described using fuzzy sets, which are made precise by defining associated membership functions. These membership functions enable the fuzzy system to interface with the outside world. The membership function output is real numbers ranging from 0 to 1. Fuzzy sets are combined with fuzzy rules to define specific actions in the form of a fuzzy associative matrix (FAM). Figure 16 shows the block diagram of the fuzzy logic system. It is composed of a fuzzifier, rules, an inference engine, and a defuzzifier. Once the rules are established, the fuzzy logic system can be considered as a mapping of inputs to outputs. Rules are collection of IF–THEN statements, e.g., IF the temperature is too hot, THEN fan speed is maximum. The fuzzifier maps crisp input numbers into fuzzy sets, which activates rules in terms of linguistics variables that have associated fuzzy sets. The inference engine generates output in terms of fuzzy values. It handles the way in which rules are combined. The defuzzifier maps the output in crisp numbers which are used for the control action [57, 60, 62].

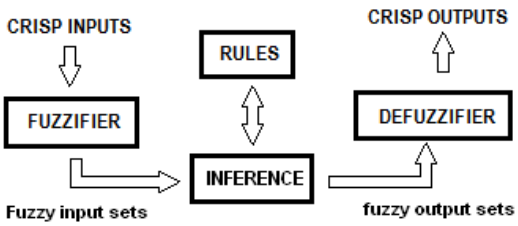

Fig. 16. Fuzzy logic system.

The effectiveness of fuzzy logic in controlling complex, highly dynamic, and nonlinear systems was demonstrated in a number of robot systems such as the micro soccer robots

with navigation, tracking, and obstacle avoidance capability [63–66], micro-golf robot [67], ball-beam balancing robot [62], and humanoid robot [68]. Fuzzy logic can also be applied in image processing for dynamic color object detection and recognition such as the ones reported by Reyes and Dadios [69,70].

b) Genetic Algorithm

Genetic algorithm (GA) is a type of evolutionary algorithm which is loosely based on Darwinian principles of biological evolution where it operates on a population of individual strings called chromosomes [71]. These chromosomes are possible solutions to the problem. Chromosomes have elements called alleles which can be encoded using binary alphabet, integers, or real numbers. GA begins with an initial set of randomly generated chromosomes, called population, which are evaluated using a fitness function in order to determine the level of correctness of a particular solution. Chromosomes are ranked relative to their fitness, and the top-ranking chromosomes are selected to form a mating pool from which a new set of chromosomes will be generated. Two chromosomes from the mating pool are selected for reproduction. Genetic operators such as crossover and mutation are applied to generate two children chromosomes. After several generations, the GA hopefully converges for an optimal solution to the problem [59,71,72]. Shown in Figure 17 is a sample GA process based on [72]:

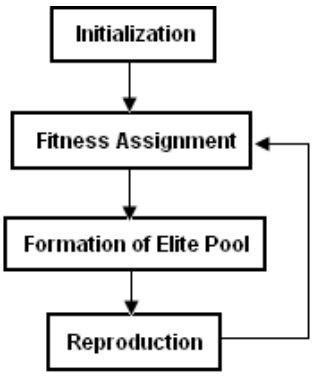

Fig. 17. GA process [94].

c) ANN

ANN is loosely based on biological neural cells. It is an information processing system composed of interconnected processing elements (PE) that is nonalgorithmic, nondigital, and intensely parallel [58]. The first layer is the input layer, and the last layer is the output layer. In between the input and the output layers is the hidden layer/s. The processing elements of an ANN are connected by a number of weighted links through which signals can flow. They translate different stimuli into a single output response. The transfer function of the PE is a mathematical expression that describes the translation of the input stimulus to the output response signal [58]. ANNs have been applied to solve different problems in control systems, image processing and robotics [58,73–75]. Shown in Figure 18 is an ANN general structure.

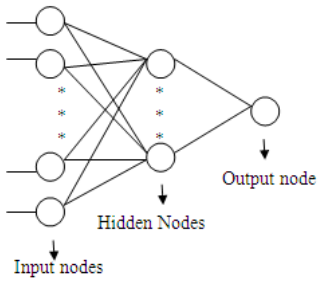

Fig. 18. ANN general structure.

6) Cost of Some Robotic Arms

Based on [52], commercial and custom-made robotic arms that cost over US$100,000 as of 2011 are the Barret WAM, Meka A2 arm, PR2 robot, DLR-LWR III arm, Schunk Lightweight Arm, Robonaut, Cog, Domo, Obrero, Twendy-One, and Agile Arm. But [76] also reported some low-cost robotic arms, such as the R17 arm of ST Robotics, whichcosts US$10,950;the arms of the Dynamaid robot, which have a total cost of at least US$3,500; and the KUKA youBot arm being sold for €14,000. Due to the high cost of robotic arms, [76] created a low-cost 7-DOF robotic arm that costs only US$4,135.

IV. CONCLUSIONS

This paper presented a review of related literature for the design and implementation of the Archer Robot. Discussions covered ancient and current human-like mechanical archers, MV, and intelligent controllers that can be used for the future Archer Robot. So far, the mechanical archers presented have an arrow already loaded in the bow. The future Archer Robot will be capable of knocking an arrow to a standard recurved bow, drawing the arrow, and hitting a target. There are toy-like archer robots and robots with dexterous arms, which will be the bases in the design and implementation of the Archer Robot.

ACKNOWLEDGMENT

The authors would like to thank the Engineering Research and Development for Technology (ERDT) of the Department of Science and Technology (DOST)–Philippines for funding this research as well as De La Salle University–Manila.

REFERENCES

[1] C. C. Kemp, P. Fitzpatrick, H. Hirukawa, K. Yokoi, K. Harada, and Y. Matsumoto, "Humanoids," in *Springer Handbook of Robotics*. Springer, June 2008.

[2] *Definition of "automaton,"* [Online], Available: http://www.merriam-webster.com/dictionary/automaton.

[3] N. Mavridis, A Review of Verbal and Non-Verbal Human-Robot Interactive Communication, Jan. 20, 2014, arXiv:1401.4994 [cs.RO]

[4] J. Needham, *Science and Civilisation in China: Volume 2*. Cambridge University Press, 1959, p. 53.

[5] B. Siciliano and O. Khatib (eds.), "Introduction," in *Springer Handbook of Robotics*. Springer, 2008.

[6] G. Veruggio and F. Operto, "Roboethics: Social and ethical implications of robotics," in *Springer Handbook of Robotics*, Part G, 2008, pp. 1499–1524.

[7] *FITA Beginners Manual*, [Online], Available: http://www.worldarchery.org/Portals/1/Documents/Development/Beginners_Manual/BeginnersManuel-e.pdf. [Accessed: May 19, 2014].

[8] D.P. Miller, I.R. Nourbakhsh, and R. Siegwart, "Robot for education,"in *Springer Handbook of Robotics*, Part F, 2008, pp. 1283–1301.

[9] Toshiba, *Right on target: From the arrow-shooting boy to the future of robotics*, [Online]. Available: http://eu.computers.toshiba-europe.com/Contents/Toshiba_teg/EU/WHITEPAPER/files/Visions-2006-05-Right-on-target-EN.pdf. [Accessed: January 3, 2018].

[10] S.Kuniko, "Robotic karakuridoll brings the 19th century back to life,"*Web Japan, NIPPONIA,*no. 38, September 15, 2006. [Online]. Available: http://web-japan.org/nipponia/nipponia38/en/feature/feature06.html.[Accessed: January 3, 2018].

[11] "The most famous Japanese "Karakuri" automata that have made 200 years ago,"*YouTube*, Jan. 16, 2008 [Video file]. Available: https://www.youtube.com/watch?v=i5zYK9FxORI. [Accessed: January 3, 2018].

[12] M. Allard ACS, "Karakuri" [Video file]. Available: http://vimeo.com/24412432. [Accessed: January 3, 2018].

[13] yumekarakuri, "Samurai Archer,"*YouTube*, Oct. 28, 2009 [Video file]. Available: https://www.youtube.com/watch?v=6b_U-u1Rb2k. [Accessed: January 3, 2018].

[14] "Mechanical music,"*Journal of the MBSI*, vol. 52, no. 4, July/August 2006. [Online]. Available: http://www.mbsi.org/journal/MBSI-2006-52-4/MBSI-2006-52-4-19.pdf

[15] 末松良一, "yabusame.avi, Yabusamekarakuri made by Tsuyoshi Yamazaki,"*YouTube*, Jan. 9, 2013 [Online]. Available: https://www.youtube.com/watch?v=-xTA0DaAV-c. [Accessed: January 3, 2018].

[16] "Hammerhead plays William Tell" [Video file]. Available: http://www.robots-dreams.com/2009/09/robo-one-demonstration-performance-was-awesome-video.html. [Accessed: June 6, 2014].

[17] "16th Robo-One Competition: Cool Pics and Videos" [Online]. Available: http://singularityhub.com/2009/10/08/16th-robo-one-competition-cool-pics-and-videos/. [Accessed: January 3, 2018].

[18] andonoblog,第16回ROBO-ONE in 富山予選：ハンマーヘッド,*YouTube*, Sep. 27, 2009 [Video file]. Available: https://www.youtube.com/watch?v=D8kK1SG3TnM.[Accessed: January 3, 2018].

[19] i-SOBOT [Online.] Available: http://www.isobotrobot.com/eng/about/whats/index.html. [Accessed: June 6, 2014].

[20] paxshikai, "i-SOBOT shoots an arrow,"*YouTube*, Jan. 5, 2008 [Video file]. Available: https://www.youtube.com/watch?v=gSI4f5CeU5o#t=33. [Accessed: January 3, 2018].

[21] P. Kormushev, S. Calinon, R. Saegusa, and G. Metta,"Learning the skill of archery by a humanoid robot iCub,"presented at 2010 IEEE-RAS International Conference on Humanoid Robots, Nashville, TN, USA, December 6–8, 2010.

[22] P. Kormushev, "Robot Archer iCub,"*YouTube*, Sep. 22, 2010 [Video file]. Available: https://www.youtube.com/watch?v=QCXvAqIDpIw. [Accessed: January 3, 2018].

[23] E.Ackerman, "Jedi vs. Sith in robot lightsaber duel," IEEE Spectrum article, May 10, 2011 [Online]. Available: http://spectrum.ieee.org/automaton/robotics/industrial-robots/jedi-vs-sith-in-robot-lightsaber-duel. [Accessed: June 6, 2014].

[24] IEEE, "Robot Lightsaber Duel,"*YouTube*, May 10, 2011 [Video file]. Available: https://www.youtube.com/watch?v=sLofEA_BvGY. [Accessed: January 3, 2018].

[25] E. Ackerman, "Stanford's 'JediBot' tries to kill you with a foam sword," IEEE Spectrum article, Jul. 18, 2011 [Online]. Available: http://spectrum.ieee.org/automaton/robotics/diy/stanford-robots-flip-burgers-play-jedi-make-your-life-complete. [Accessed: June 6, 2014].

[26] S. Anthony, "Lightsaber + Kinect + robotic arm = JediBot," July 18, 2011 [Online]. Available: http://www.extremetech.com/extreme/90204-lightsaber-kinect-robotic-arm-jedibot. [Accessed: June 6, 2014].

[27] Standford, "Students create 'Jedibot',"*YouTube*, Jun. 30, 2011 [Video file].Available: https://www.youtube.com/watch?v=VuSCErmoYpY. [Accessed: January 3, 2018].

[28] *Big size humanoid robots developed at Zhejiang University* [Online]. Available: http://www.zju.edu.cn/english/redir.php?catalog_id=279955&object_id=2036949. [Accessed: June 7, 2014].

[29] Reuters, "Chinese robots display ping-pong prowess," October 24, 2011 [Online]. Available: http://www.reuters.com/video/2011/10/23/chinese-robots-display-ping-pong-prowess?videoId=223838974. [Accessed: June 7, 2014].

[30] D. Melanson, "Cooking, camera-building skills," ENGADGET article,Dec. 2,2008 [Online]. Available: http://www.engadget.com/2008/12/02/motoman-sda10-robot-shows-off-its-cooking-camera-building-skill/. [Accessed: June 7, 2014].

[31] DigInfo TV, "A robot that cooks Japanese okonomiyaki pancakes :DigInfo,"*YouTube*, Jun. 16, 2009 [Video file]. Available: https://www.youtube.com/watch?v=nv7VUqPE8AE. [Accessed: January 3, 2018].

[32] saver020, "Motoman assembles camera,"*YouTube*, Nov. 27, 2008, Available: https://www.youtube.com/watch?v=PSuvFCPgwE8. [Accessed: January 3, 2018].

[33] IAN DALY, "Just like mombotused to make,"*The New York Times*, February 23, 2010 [Online].Available: http://www.nytimes.com/2010/02/24/dining/24robots.html?pagewanted=all&_r=0. [Accessed: June 8, 2014].

[34] Borst, C., et al., "Rollin' Justin—Mobile platform with variable base,"in *Proc. of the IEEE Int. Conference on*

Robotics and Automation ICRA, Kobe, Japan, 2009, pp. 1597–1598.

[35] B. Bauml et al., "Catching flying balls and preparing coffee: Humanoid Rollin' Justin performs dynamic and sensitive tasks,"in *Proc. of the 2011 IEEE Int. Conference on Robotics and Automation ICRA, Shanghai, 2011,* pp. 3443–3444.

[36] Hizook, "Rollin' Justin robot catches balls tossed in its direction,"*YouTube*, Apr. 27, 2011 [Video file]. Available: https://www.youtube.com/watch?v=R6pPwP3s7s4. [Accessed: June 8, 2014].

[37] B. G. Batchelor, "Coming to terms with machine vision and computer vision: They're not the same!" *Advanced Imaging*, Jan. 1999, pp. 22–24.

[38] F. Santini and M. Rucci, "Depth perception in an anthropomorphic robot that replicates human eye movements,"in *Proc. ICRA*, 2006, pp.1293–1298.

[39] M. Hebert, "Active and passive range sensing for robotics," in *Proceedings of the IEEE International Conference on Robotics and Automation (ICRA '00)*, pp. 102–110, San Francisco, Calif, USA, April 2000.

[40] S.F. El-Hakim, J.A. Beraldin, and F. Blais, "A comparative evaluation of the performance of passive and active 3-D vision systems," *SPIE Proc. 2646, St. Petersburg Conf. on Digital Photogrammetry*, pp. 14–25, June 1995.

[41] KIGRE, Inc., Laser transmitters and components [Online]. Available: http://web.mit.edu/ldewan/Public/laser/kigre_lasers.pdf. [Accessed: June 14, 2014].

[42] R.A. Jarvis, "A perspective on range finding techniques for computer vision,"in *IEEE Trans. Pattern Anal. Mach. Intell.,* 1983, pp. 122–139.

[43] D. Ilstrup and R. Manduchi., "Active triangulation in the outdoors: A photometric analysis," presented at the Fifth International Symposium on 3D Data Processing, Visualization and Transmission, 2010.

[44] J. Davis, R. Ramamoorthi, and S. Rusinkiewicz, "Spacetime stereo: A unifying framework for depth from triangulation," in *IEEE Computer Society Conference on Computer Vision and Pattern Recognition (CVPR)*, pp. 359–366, June 2003.

[45] B. Curless, "Overview of active vision techniques," Proc. SIGGRAPH 99 Course on 3D Photography, 1999.

[46] T.C. Strand, "Optical three-dimensional sensing for machine vision," *Optical Eng*., vol. 24, no. 1, pp. 33–40, 1985.

[47] S. Hrabar, P.I. Corke, and M. Bosse,"High dynamic range stereo vision for outdoor mobile robotics," in *ICRA*, 2009, pp. 430–435.

[48] T. Williamson and C. Thorpe, "A trinocular system for highway obstacle detection," in *Proc. IEEE International Conference on Computer Vision and Pattern Recognition,*1998.

[49] M. Antunes, J.P. Barreto, C. Premebida, and U. Nunes, "Can stereo vision replace a laser rangefinder?" in *IEEE/RSJ International Conference on Intelligent Robots and Systems (IROS)*, 2012, pp. 5183–5190

[50] S. Hutchinson, G. Hager, and P. Corke, "A tutorial on visual servo control," in *IEEE Transactions on Robotics and Automation*, vol. 12, pp. 651–670, October 1996.

[51] D. Kragic, and H. Christensen, "Survey on visual servoing for manipulation,"Technical Report CVAP259, January 2002.

[52] F. Chaumetteand S. Hutchinson, "Visual servoing and visual tracking," Part C24, in *Springer Handbook of Robotics*, 2008, pp. 563–583.

[53] P. Morgado, J. C. Pinto, J. M. M. Martins, and P. Gonçalves, "Cooperative eye-in-hand/stereo eye-to-hand visual servoing," in *Proc. of RecPad 2009—15th Portuguese Conference in Pattern Recognition, Aveiro, Portugal, 2009*.

[54] P. I. Corkeand S. A. Hutchinson, "Real-time vision tracking and control,"in*Proceeding of IEEE International Conference on Robotics and Automation*, 2000, pp. 622–629.

[55] E. Malis, F. Chaumette, and S. Boudet, "2-1/2-d visual servoing," *IEEE lhns. on Robotics and Automation*, vol. 15, pp. 238–250, Apr. 1999.

[56] G. Palmieri, M. Palpacelli, and M. Battistelli,"A comparison between position based and image based visual servoing on a 3 DOFs translating robot," in *AIMETA 2011 XX CongressoAimeta di MeccanicaTeorica e Applicata—Atti del congresso. Bologna, Italia, 12–15 Settembre, 2011.*Conselice (Ra):Publi&Stampa.

[57] E. P. Dadios and D. J. Williams, "Multiple fuzzy logic systems: A controller for the flexible pole-cart balancing problem," in *Proc. of the IEEE Robotics and Automation International Conference, Minneapolis, Minnesota USA, April 24–26, 1996. ICRA,*pp. 2276–2281.

[58] E. P. Dadios and D. J. Williams, "Application of neural network to the flexible polecart balancing problem," in *Proc. of IEEE Systems Man and Cybernetics, International Conference, Vancouver Canada*, Vol. 3, pp. 2506–2511, October 22–25, 1995.

[59] E. P. Dadios, P.S. Fernandez, and D.J. Williams, "Genetic algorithm on line controller for the flexible inverted pendulum problem,"*Journal of Advanced Computational Intelligence and Intelligent Informatics*, vol. 10, no. 2, 2006.

[60] E. P. Dadios and D. I. Williams, "A fuzzy-genetic controller for the flexible pole-cart balancing problem," in *Proc. of the IEEE 3rd International Conference on Evolutionary Computation (ICEC'96), Nagoya, Japan, May 20–22, 1996*.

[61] L. A Zadeh, *Fuzzy Sets, Information and Control*, vol. 8, pp. 338–353, 1965.

[62] E. P. Dadios, R. Baylon, R. De Guzman, A. Floren Lee, and Z. Zulueta, "Vision guided ball-beam balancing system using fuzzy logic," in *Industrial Electronics Society, 2000. IECON 2000. 26th Annual Conference of the IEEE 2000*, pp. 1973–1978, vol.3.

[63] O. Maravillas and E. P. Dadios, "Fuzzy logic controller for micro robot soccer game," in *Proc. of the 27th, Annual Conference of the IEEE Industrial Electronics Society (IECON'01), Hyatt Regency Tech Center,Denver, Colorado, USA*, pp. 2154–2159, Nov. 29–Dec. 2, 2001.

[64] E. Maravillas and E.P. Dadios, "Hybrid fuzzy logic strategy for soccer robot game," *Journal of Advanced Computational Intelligence and Intelligent Informatics*, vol. 8,no. 1, pp. 65–71, FUJI Technology Press, January 2004.

[65] E. Dadios and O. Maravillas, "Cooperative mobile robots with obstacle and collision avoidance using fuzzy logic," in *Proc. of 2002 IEEE Int. Symposium on Intelligent Control, Vancouver, Canada*.

[66] A. Abad, G. Abulencia, W. Pacer, E. Dadios, andN. Gunay, "Soccer robot shooter strategy," presented at the National Electrical, Electronics, and Computing Conference 2009, Science Discovery Center SM Mall of Asia, December 9–11, 2009

[67] K.G. B. Leong, S. W. Licarte, G. M. S. Oblepias,E. M. J. Palomado, E.P. Dadios, and N. G. Jabson, "The autonomous golf playing micro robot: With global vision and fuzzy logic controller,"*International Journal on Smart Sensing and Intelligent Systems*, vol. 1, no. 4, pp. 824–841, December 2008.

[68] J.J. Biliran, R. Garcia, J. Ng, and A. Valencia, *Quatrobot Humanoid Robot*, BSECE Thesis, De La Salle University–Manila, 2008.

[69] N.H.Reyes and E.P. Dadios, "A fuzzy approach in color object detection," in *IEEE International Conference on Industrial Technology, 2002. IEEE ICIT '02*, vol. 1, pp.232–237.

[70] N. Reyes and E. P. Dadios, "Dynamic color object recognition using fuzzy logic," *Journal of Advanced Computational Intelligence and Intelligent Informatics*, vol. 8, no. 1, pp. 29–37, 2004.

[71] E. P. Dadios and J. Ashraf, "Genetic algorithm with adaptive and dynamic penalty functions for the selection of cleaner production measures: A constrained optimization problem," *Journal of Clean Technologies and Environmental Policy*, vol. 8, no. 2, pp. 85–96.

[72] S. Barrido and E. P. Dadios, "Online robot tracking using genetic algorithms," in *Proceedings of the 17th IEEE International Symposium on Intelligent Control (ISIC '02),* pp. 479–484, Vancouver, Canada, October 2002.

[73] E. P. Dadios, K. Hirota, M. L. Catigum, A. C. Gutierrez, D. R. Rodrigo, C. A. G. San Juan, and J. T. Tan, "Neural network vision-guided mobile robot for retrieving driving-range golf balls,"*JACIII*, vol. 10, no. 2, pp.181–186, 2006.

[74] J. P. N. Cruz, M. L. Dimaala, L. G. L. Francisco, E. J . S. Franco, A. A. Bandala, and E. P. Dadios, "Object recognition and detection by shape and color pattern recognition utilizing artificial neural networks," in *2013 International Conference of Information and Communication Technology (ICoICT), IEEE*, pp. 140–144, March 20–22, 2013.

[75] L.S. Bartolome, A.A. Bandala, C. Lorente, and E.P. Dadios, "Vehicle parking inventory system utilizing image recognition through artificial neural networks," in *IEEE Region 10 Conference*, 2012, pp. 1–5.

[76] M. Quigley, A.T. Asbeck, and A.Y. Ng., "A low-cost compliant 7-DOF robotic manipulator,"in *ICRA*, pp. 6051–6058, IEEE, 2011.

Design and Implementation of a Thermal-Based Exploration Mobile Robot

Jay Robert B. Del Rosario,* Benjamin Emmanuel F. Tamonte, John Michael M. Ligan, Lyndon Vincent L. Ang, Darren Justin B. Cruz, and Chong We D. Tan

***Abstract* — Inaccurate control of the industrial thermal processes occurs when there is no operator involvement in monitoring temperature set points. This document will examine the specifics of a temperature controlled mobile robot (MoBot) with the use of PIC16F877A microcontroller and LM 35 as the temperature sensor for the input feed data. The project is primarily about acquiring the temperature measured by the sensor to determine the state and the speed of the mobile robot. The amount of temperature will dictate the state and the duty cycle of the mobile robot. Results show that the accuracy of the temperature sensor utilized in the project ended to 98.31% and the MoBot was able to work properly in different PWM values as triggered by the data from LM35.**

Keywords: **temperature, duty cycle, microcontroller, LM35 temperature sensor, mobile robot**

I. Introduction

A control system is basically a group of interconnected components that regulates and manages the actions or performance of a device or other systems. A control system was conceptualized to pave way for the increasing demand in efficiency, practicality, and convenience [1].

In the same manner, temperature-controlled devices were created for the efficiency, practicality, and convenience that they serve.

Applying the concept of a control system to our project led the group to the design and application of a temperature-controlled mobile robot (MoBot). Instead of the regular schemes wherein the power supplied to the MoBot is controlled by a simple off or on switch, the state and the duty cycle of the group's MoBot will be dependent and proportional to the input given by the LM35 temperature sensor.

The group's primary intent is essentially to design and create a temperature-controlled MoBot that would be able to vary in state and duty cycle depending on the temperature input provided by the sensor. Along with these objectives, the group would like to set upper and lower temperature bounds for the MoBot to work in.

The aim of the project is to work only in normal or room temperature conditions with variations of up to 5°C. This is to show the state and duty cycle of the MoBot in normal conditions and minimal temperature changes.

The MoBot's goal is to move away from places that have spiking temperature and anything that is connected to it. Most of the devices that are created require a certain temperature to operate and maintain its condition, though there are times that changing temperature is inevitable. One simple solution to this problem is to apply this MoBot or attach it to the devices. Once there is a spike in temperature, the MoBot is tasked to move away from that place and stop in a place that has its desirable temperature. Though the MoBot that we have created is just small with a direct current motor that is working only at 5 V, it could be attached to big devices and heavy components and be scaled up for heavier purposes.

Another application of the MoBot is for it to act like a heat sink. Instead of placing a wheel into the motors, it could be replaced with a fan that could dissipate heat. It could be placed in front or on top of the device that is overheating. This is an energy-conserving tool because it is not all the time that the device is overheating and needs to be cooled [2]. The PIC16F877A we have used in this project is programmed to operate only at a certain temperature.

If the desired temperature is met, it is programmed to stay idle and wait until the temperature changes so that the component could not operate anymore.

Jay Robert B. Del Rosario,* Benjamin Emmanuel F. Tamonte, John Michael M. Ligan, Lyndon Vincent L. Ang, Darren Justin B. Cruz, and Chong We D. Tan, De La Salle University, Manila, Philippines

*(e-mail: jay.delrosario@dlsu.edu)

II. Review of Related Literature

In an article entitled "Mobile Robot Temperature Sensing Application via Bluetooth," an LM 35 was also used in the acquisition of temperature data. According to the article, "ADC is used to convert the analog value from LM35z to 10 bits digital value." It also stated in the article that the acquired temperature value has a low error percentage [3]. Hence, the LM 35 is a very reliable temperature sensor.

A thesis paper from De La Salle University titled "Implementation of a Portable Automobile Exhaust Emission Analyzer" is about solving the problem of emission in our environment. The group who made the thesis aimed to create a device that would measure the emission of each vehicle so that the driver could gauge the emission of the car that he or she is using [4].

The group first connected the following things to create their device. The group members used the type T thermocouple of sensor that is connected to the analog-to-digital converter to monitor the oil temperature and whether the oil temperature is reaching 70°C. The temperature is proportional to the increase of the resistance in the sensor. The group connected it to a voltage divided and a comparator circuit using the LM741 operational amplifier.

The members of the group did many experiments that concluded that when the T thermocouple sensor detected that the oil temperature is 70°C, the corresponding resistance is 6.7 ohms.

So that the device could be used anytime and anywhere, the power supply connected to the device is the car battery. The device needs the car battery because the two devices need a lot of current that could easily drain the primary battery cell. The primary cell is connected to the PP3 9-V radio battery. The battery is used to satisfy the voltage required to power the voltage regulators [4].

The purpose of using an emission tester is to have data and to assess the acceptable values in the emission of the car; the car varies with two types of engine, namely, the gas engine and the diesel engine. Of course, the diesel engine has a higher tolerance for CO_2 emissions. There is also a classification on what year the engine's car is manufactured; older engines have a higher level of CO_2 emissions compared to those that are made in 1997 onwards. For gasoline engines, CO_2 emissions should be only 3.5% in volume for cars made in 1997 onwards and 4.5% in volume for cars made before that time. This paper is quite relevant to us as it also used a sensor and a programming component that determines the acceptable carbon dioxide emission of a vehicle and the device determines if the engine passed or not [4].

Another relevant paper is entitled "Robotic Arm Rehabilitation With Biofeedback for Filipino Stroke Patients." This paper states that the sensor used to take body temperature of patients is a thermistor, used to properly measure and compare variations of temperature measurements [5].

The thesis utilized a Z8-Encore microcontroller to control the motor with respect to the current state of the inputs as well as converting the measured analog temperature from the thermistor sensor to 10-bit binary number.

This thesis has similarities to our project because it also has a temperature-triggering device. The temperature determines the movement of the robotic arm. This group applied this concept in treating and aiding Filipino people who are suffering from stroke or whom we call stroke patients.

The difference of our project is instead of a moving robot that looks like a car, the thesis paper used a robotic arm that would move depending on the temperature recorded by the sensor. Another difference is this thesis has better devices that could help the society.

This thesis uses a robotic arm to conduct and motivate stroke patients to conduct different activities and to move around. The robotic arm also gathers information through the doctor's data and through real-time biofeedback. It also conducts its own evaluation on the patient's reaction and the patient's condition.

The paper "Global Fan Speed Control Considering Non-Ideal Temperature Measurements in Enterprise Servers" [6] describes that the function of a motor is somewhat similar to that of ours. It also shows a circuit that changes the speed of a fan, automatically and linearly, depending on the room temperature. The paper also states that the circuit shown has a high sensitivity and that the output RMS voltage can be changed from 120 V to 230 V. This entails a temperature range change from 22°C to 36°C. Therefore, this means a significant difference in speed is available. Another thing pointed out was that the change in speed varies linearly, not in steps.

Another article that we found related to the topic we proposed was entitled "Temperature Based DC Motor Speed" by Gary Royston George [7]. The article had the same idea as ours. It made use of an analog temperature sensor to determine the temperature that will control the speed of the motor. It was also said in the article that the microcontroller would create a pulsed width modulated (PWM) signal, which has changing duty cycles that are based on the temperature reading, and use that reading to change and vary the speed of the motor.

According to the article "Real Time Speed Control of a DC Motor by Temperature Variation Using LabVIEW and Arduino" [8], the use of DC fans has become widespread. These motors are used primarily in industries specifically for cooling in electronics, communication system, and other useful applications. Some DC fans allow for large

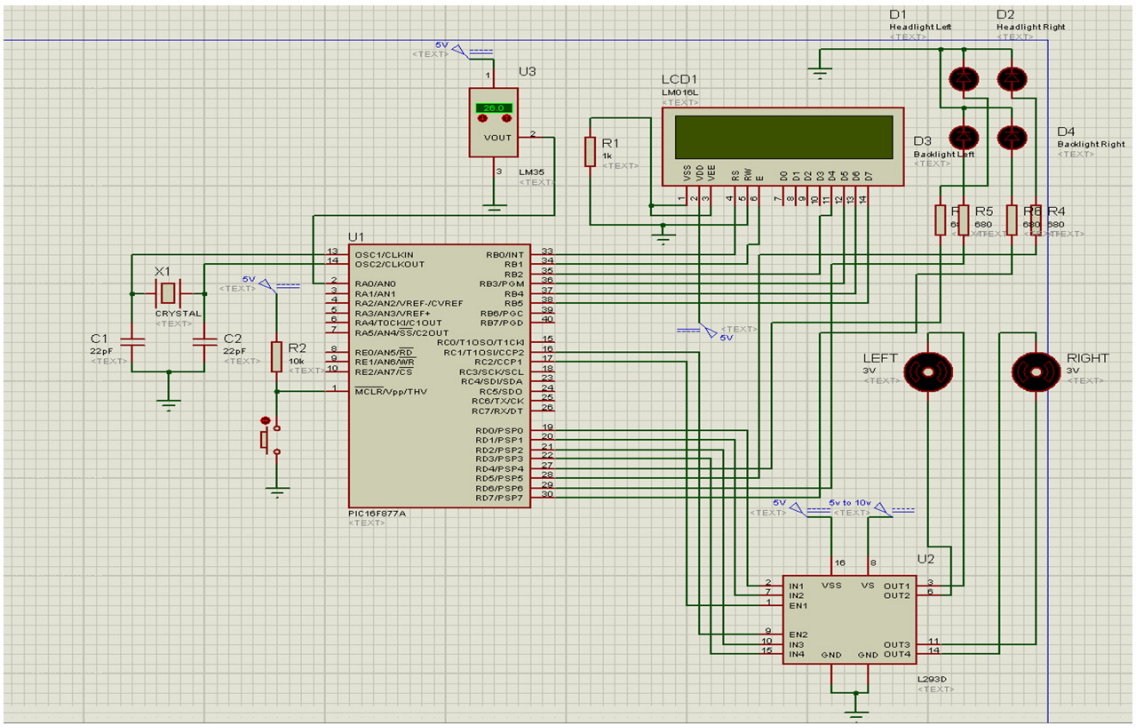

Fig. 1. Overall circuit diagram of the thermal-based exploration MoBot.

voltage-dependent speed variations, making them very popular where air moving noise or power consumption considerations are important.

According to the paper "A Novel Microcontroller-Based Sensor Less Brushless DC (BLDC) Motor Drive for Automotive Fuel Pumps" [9], PWM may be employed to vary the effective voltage in the armature of the motor. Pulse width modulation is simply controlled by short pulses of voltage or current. A pulse variation of pulses also varies the torque that a motor produces thus adjusting the speed or duty cycle of a motor.

III. DESIGN AND APPLICATION

To fundamentally implement the project, the group utilized a PIC16F877A as its main microcontroller. The group chose this microcontroller due to the number of I/O ports provided by this microcontroller that will suffice for the needed input and output components [10] and the ADC requirements of the project. Along with this microcontroller is a temperature sensor (LM35), 16 × 2 Alphanumeric LCD (LM016D), and H bridge motor drivers. The initial hardware implementation was done in a breadboard, and the final product, on a universal printed circuit board. Figure 1 shows the circuit diagram of the entire project.

A. LM 35—Precision Centigrade Temperature Sensors

The LM 35 is a precision centigrade temperature sensor that produces output voltages linearly proportional to the change in centigrade temperature. LM 35 can precisely sense temperature ranging from −55°C to 150°C. The LM 35 output voltage is approximately 10 mV per degree centigrade. As shown in Figure 2, the sensor should be supplied a minimum of 4 V and can potentially accept up to a maximum of 20 V [11].

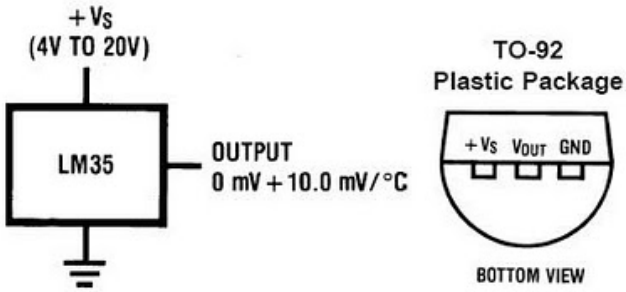

Fig. 2. Schematic diagram of temperature sensor [11].

The basic implementation of the LM 35 is to be placed across the body of the MoBot, preferably at a point where there is no interference with the sensor for accurate

measurement of temperature [12][13]. The sensor is then fed or connected to RA0 of Port A for the built-in analog-to-digital converter of the microcontroller. The group essentially aims to limit or set the bounds of the temperature for the MoBot to work in. The group ideally aims to work only on room temperature conditions ranging from 25°C to 35°C.

The group will also make the MoBot very sensitive as possible to show the performance of the MoBot in minimal temperature changes.

The measured temperature shall then be displayed into an LCD along with its corresponding voltage.

B. LM016L—16 × 2 Alphanumeric LCD

To accurately discern the voltage produced by the LM35 and to properly display the state and duty cycle of the MoBot, an LCD will be used to display the temperature measured by the sensor. The group used a 16 × 2 Alphanumeric LCD to properly and accurately display the produced parameters [14].

C. L293D—H Bridge Motor Driver and Pulse Width Modulation

L293D is basically an integrated circuit used to drive components that have inductive loads such as DC and stepping motors. Relying on the output voltage produced by the microcontroller will not be sufficient to drive a DC motor [15]. The L293D will also use to implement the phase width modulation of the MoBot. Pulse width modulation is basically a modulation technique that varies the width of a pulse to control the power supplied to electrical devices, especially to devices with inertial loads such as motors.

To implement the PWM of the MoBot, the group declared certain ranges of temperatures with their corresponding ranges of voltage readings to a certain PWM value. Given a temperature range of 25°C to 30°C, the group can set these temperatures to their corresponding PWM values. Say, 25°C to 26°C has a PWM of 0 (stop), 27°C to 28°C has a PWM of 128 (mid speed), and lastly a 29°C to 30°C has a PWM reading of 255 (max speed). Therefore, it is very crucial to determine the bounds or the limits that the group's MoBot can work in.

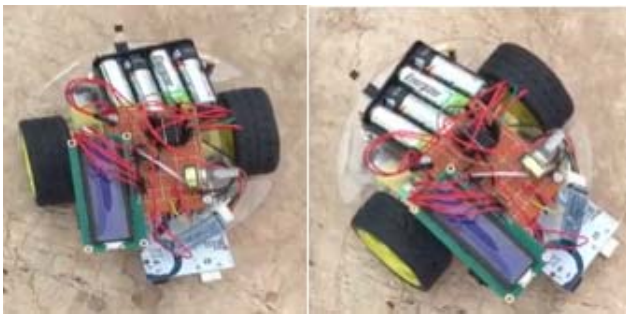

Fig. 3. Actual prototype of the MoBot.

IV. RESULTS AND DISCUSSION

The actual temperature of the model environment was measured for 10 trials by the mercury-type thermometer and compared with the LM35 sensor to compute for the accuracy. The LCD specified the numerical value of the temperature. Varying temperature values were set at the set point temperature. Results are tabulated as shown in Table I.

TABLE I
TEMPERATURE SENSOR ACCURACY

Trial No.	Set Point (°C)	Mercury Thermometer	Digital Thermometer (LM 35)	Error	% Error
1	10	10	10.1	0.1	1.00
2	15	15	15.6	0.6	4.00
3	20	20	20.9	0.9	4.50
4	25	25	25.4	0.4	1.60
5	30	30	30.5	0.5	1.67
6	35	35	35.2	0.2	0.57
7	40	40	40.1	0.1	0.25
8	45	45	45.3	0.3	0.67
9	50	50	50.6	0.6	1.20
10	55	55	55.8	0.8	1.45

Hence, from the above configuration, the total percentage error is at 1.69% and the temperature sensor accuracy of the LM35 is at 98.31%. As seen in Figure 4, the result was satisfactory.

Testing methods should also be considered in the implementation of the project. The group used a hairdryer and a pack of ice to vary the temperature measured by the sensor for demonstration purposes. Relying on normal temperatures or outside temperature without means of controlling the measured temperature can or most likely exhibit errors.

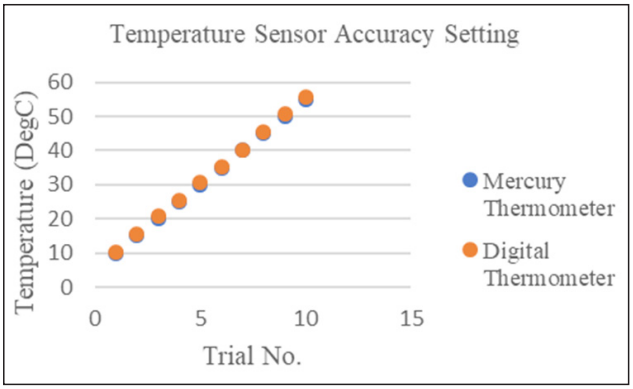

Fig. 4. Graph for temperature sensor accuracy test.

The temperature-based MoBot was able to work properly and was able to drive and vary the speed of the motor based on the temperature that it got from the sensor as seen in Table II. There are other ways to drive a motor based on temperature, one of which is using a thermistor, but we resorted to using a temperature sensor instead for we think it is accurate enough to give us the correct readings needed. The program used was self-made and is working properly.

TABLE II
Motor Speed Controller Through PWM Values

Trial No.	Set Point (°C)	LM 35	PWM	MOBOT Action
1	10	10.1	0	Stop
2	15	15.6	0	Stop
3	20	20.9	0	Stop
4	25	25.4	128	Clockwise
5	30	30.5	128	Clockwise
6	35	35.2	128	Counter-clockwise
7	40	40.1	255	Forward
8	45	45.3	255	Forward
9	50	50.6	255	Forward
10	55	55.8	255	Forward

TABLE III
MoBoT Decision Table

Temperature (°C)	Left Wheel	Right Wheel	Action
0–24.9	0	0	Stop
25.0–30.9	0	1	Turn clockwise
31.0–35.9	1	0	Turn counter-clockwise
36.0–above	1	1	Move forward

Based on the given MoBot decision table from Table III, Table II shows the corresponding PWM and sample movement of the MoBot.

Table III shows the sample movement of the MoBot and its corresponding temperature ranges. Sample MoBot action shows that the system can act depending on the temperature of the prescribed environment.

V. Conclusion

Students or simply enthusiasts of making MoBots should also consider making a temperature-controlled MoBot. In making this type of project, temperature sensitivity, testing methods, MoBot maneuvering, and chassis specifications should be carefully considered.

To accurately and coherently display the state of the MoBot, the temperature bounds must be accurately specified. Because of limited control over a certain range of temperature, the range of temperature that the MoBot can work in should also be limited.

The weight of the MoBot chassis must also be considered in the making of this project. Always consider if the motor can successfully drive the MoBot and display several values of its duty cycle.

In addition, the group knows that the MoBot is very limited in terms of its maneuvering capabilities. Further improvements can make the MoBot go left or right or even avoid obstacles to avoid being stuck in collision.

The MoBot was also able to move forward and backward and stayed stationary in varying speeds, depending on the temperature that the sensor gathered.

Acknowledgment

The authors would like to thank the Dr. Jonathan Dungca, dean of the Gokongwei College of Engineering, and Engr. Alexander C. Abad, chairman of the Department of Electronics and Communications Engineering, of De La Salle University–Manila.

REFERENCES

[1] S. Fan et al, "An improved control system for modular multilevel converters with new modulation strategy and voltage balancing control," *IEEE Transactions on Power Electronics,* vol. 30, no. 1, pp. 358–371, 2015.

[2] Z. Liang, C. Zhou, S. Zhao, T. Liu, and Z. Wang, "Analysis of temperature effect on electromagnetic susceptibility of microcontroller," in *Environmental Electromagnetics (CEEM), 2015 7th Asia-Pacific Conference on*, pp. 254–257, Nov. 2015.

[3] M. F. L. Abdullah and L. M. Poh, *"Mobile robot temperature sensing application via Bluetooth,"* International Journal of Smart Home, vol. 5, no. 3, pp. 39–48, 2011.

[4] F. Baylon, J. M. G. Dy, R. D. Quidilla, R. A. D. San Pascual, and A. E. Dulay, "Implementation of a portable automobile exhaust emission analyzer," in *Presented during the ECE Student Forum, DLSU*, Dec. 2006.

[5] M. Ang, L. Limkaichong, W. Perez, L. Sayson, N. Tampo, N. Bugtai, and E. Estanislao-Clark, "Development of robotic arm rehabilitation machine with biofeedback that addresses the question on Filipino elderly patient motivation," in *ICSR*, pp. 401–409, Nov. 2010.

[6] J. Kim, M. M. Sabry, D. Atienza, K. Vaidyanathan, and K. Gross, "Global fan speed control considering non-ideal temperature measurements in enterprise servers," in *2014 IEEE Design, Automation & Test in Europe Conference & Exhibition (DATE)*, Dresden, pp. 1–6, 2014.

[7] G. R. George (2010). *Temperature based DC motor speed control*, doctoral dissertation, UMP.

[8] K. R. Asha, P. S. Tasleem, A. V. R. Kumar, S. M. Swamy, and K. R. Rekha, "Real time speed control of a DC motor by temperature variation using LabVIEW and Arduino," in *2017 IEEE International Conference on Recent Advances in Electronics and Communication Technology (ICRAECT)*. Bangalore, pp. 72–75, 2017.

[9] J. Shao, D. Nolan, M. Teissier, and D. Swanson, "A novel microcontroller-based sensorless brushless DC (BLDC) motor drive for automotive fuel pumps," *IEEE Transactions on Industry Applications*, vol. 39, no. 6, pp. 1734–1740, 2003.

[10] S. Masaraddi and M. S. Aspalli, "Cascaded H-bridge multilevel inverter using PIC16F877A controller," *International Journal on Emerging Technologies*, vol. 6, no. 2, p. 249, 2015.

[11] C. Liu, W. Ren, B. Zhang, and C. Lv, "The application of soil temperature measurement by LM35 temperature sensors," in *Electronic and Mechanical Engineering and Information Technology (EMEIT), 2011 International Conference on*, vol. 4 pp. 1825–1828, Aug. 2011.

[12] S. S. Pande, R. Shukla, B. S. Waseem, and S. Jain, "Design and implementation of microcontroller based temperature controller for industrial application," *International Journal of Engineering, Management & Medical Research (IJEMMR)*, vol. 1, no. 4, 2015.

[13] A. L. Amoo, H. A. Guda, H. A. Sambo, and T. L. G. Soh, "Design and implementation of a room temperature control system: Microcontroller-based," in *2014 IEEE Student Conference on Research and Development*, Batu Ferringhi, pp. 1–6, 2014.

[14] A. Pimpalgaonkar, M. Jha, N. Shukla, and K. Asthana, "A precision temperature controller using embedded system," *International Journal of Scientific and Research Publications*, vol. 3, no. 12, pp. 1–3, 2013.

[15] T. Instruments. "L293D datasheet," 2010. [Online]. Available: http://www.Alldatasheet. com/datasheet-pdf/pdf/112910/TI/L293D.html. [Accessed: Sept. 5, 2015].

The Contributors

Alexander C. Abad is a graduate of BS Electronics and Communications Engineering at St. Louis University-Baguio City. He finished his MS in Electronics and Communications Engineering at De La Salle University - Manila and currently taking up his PhD in ECE at DLSU. His field of interest includes robotics, machine intelligence, machine vision, mixed-signal electronics and IC design.

Timothy M. Amado is a faculty member of the Electronics Engineering Department of the College of Engineering at the Technological University of the Philippines-Manila. He earned his BSECE degree at TUP-Manila where he graduated Magna Cum Laude, and his MSECE degree at Mapua University (formerly Mapua Institute of Technology). He is currently taking his PhD in ECE at Mapua University. He is also a recipient of the DOST Academic Excellence Award, Special Award in Engineering and TUP Academic Excellence Award. His research interest are Data Analytics, Machine Learning, and Deep Learning.

Argel A. Bandala is an Associate Professor and Research Faculty of the Electronics Engineering Department at De La Salle University. He received his Master of Science in Electronics and Communications Engineering in year 2012 and Doctor of Philosophy in Electronics and Communications Engineering in year 2015 at De La Salle University. He is the current Vice Chair of The Institute of Electrical and Electronics Engineers (IEEE) Philippines Section and Secretary of Computational Intelligence Society Philippine Chapter. He is also a member of IEEE Robotics and Automation Society. His main works are "Implementation of Varied Particle Container for Smoothed Particle Hydrodynamics-Based Aggregation for Unmanned Aerial Vehicle Quadrotor Swarm" and "Swarming Algorithm for Unmanned Aerial Vehicle (UAV) Quadrotors – Swarm Behavior for Aggregation, Foraging, Formation, and Tracking."

Robert Kerwin C. Billones is currently taking his PhD-ECE in De La Salle University in the area of artificial intelligence and vision systems. He received his Master of Science (Electronics and Communications Engineering) from De La Salle University. He currently works as part-time faculty in the Electronics Engineering Department of De La Salle University, and as science research specialist in Department of Science and Technology for the CATCH-ALL project under the intelligent transport systems program.

Melvin K. Cabatuan received his B.Sc. degree in Electronics and Communications Engineering (ECE) from Cebu Institute of Technology, Cebu, Philippines, in 2004; MS degree in Engineering from Nara Institute of Science and Technology (NAIST), Nara, Japan, in 2010; and Ph.D. degree in ECE from De La Salle University (DLSU) - Manila in 2016. He joined the Electronics and Communications Engineering Department of DLSU in 2011, where he is currently an Assistant Professor. His current research interest involves Machine/Deep Learning, Computer Graphics, and Computer Vision applications to Health Informatics, Education Technology, Game/Graphic Content Development, and Mobile Computing. He is knowledgeable in programming languages - C/Cpp, Java, and MatLab/Octave scripting. He has more than 5 years of experience in computer vision application development with OpenCV library in the mobile framework.

Jose Santos R. Carandang VI currently works at the Department of Biology, De La Salle University. He does research in Ecology, Evolutionary Biology and Zoology. Their current project is "An assessment and evaluation of the cyto-genotoxic effects of E waste in Manila, Philippines using different bio-monitoring models."

Julien L. Carandang is a candidate for Doctor of Philosophy in Development Studies in De La Salle University. He also took his Master of Arts in Development Policy in De La Salle University. His Bachelor of Arts in Consular and Diplomatic Affairs was obtained in De La Salle University-College of Saint Benilde.

Elmer P. Dadios is a University Fellow and Professor at De La Salle University. He is also the President of Neuronemech, Inc. In 1996, he received his Doctor of Philosophy from Loughborough University. In 1997, he was an Exchange

Scientist in Japan Society for the Promotion of Science, Tokyo Institute of Technology. He served as the Director of Engineering Graduate School, De La Salle University in 1998–1999 and Director of School of Engineering, De La Salle University in 2003–2004. He is also the General Chair for HNICEM in 2003, 2005, 2007, 2009, 2011, 2013. His main works are "Fuzzy Logic – Controls, Concepts, Theories and Applications," ISBN: 978-95351-0396-7, 2012. "Fuzzy Logic – Algorithms, Techniques and Implementations," ISBN: 978-953-510393-6, 2012. "Fuzzy Logic – Emerging Technologies and Applications," ISBN: 978-953-51-03370, 2012. His research interests includes; Robotics, Mechatronics, Automation, Intelligent Systems, Neural Networks, Fuzzy Logic, Genetic Algorithms, Evolutionary Computation, and IT. He is a Senior Member in The Institute of Electrical and Electronics Engineers (IEEE) and Founder and current Chair of IEEE Computational Intelligence Society, Philippines. He is a member of IEEE Region 10 Executive Committee and Founder and President of The Mechatronics and Robotics Society of the Philippines

Ma. Ellenita G. De Castro is currently holding a rank of Assistant Professorial Lecturer 2 at the Biology Department of De La Salle University-Manila. At present, she is completing a dissertation research entitled "Ecophysiology and Silvicultural Requirements of a Nickel Hyperaccumulating Plant, *Brackenridgea palustris* ssp. foxworthyi as a Potential Bioremediation Agent" to obtain her doctoral degree in Biology. Among her field of interests include phytoremediation, mycoremediation, impacts of environment of embryonic development and environmental rehabilitation. She was part of the recently completed research project entitled Screening of Indigenous Plant as Biodiesel Feedstock under the CHED-PHERNet Sustainability Studies Program and at present she is actively involved in a research projects entitled "The feasibility of using bamboo as a low-cost, environment-friendly alternative to polyvinyl chloride (PVC) pipes in hydrophonic vegetable production," an interdisciplinary research funded by the DLSU University Research Coordination Office (URCO). Since 2014, Ms. De Castro already co-authored a total of nine (9) papers in various ISI and Scopus-listed journals and had presented several papers in local conferences. With regards to her administrative capacity, Ms. De Castro serves as the Senior Project Technical Staff at the Program Management Unit of CHED-PHERNet Sustainability Studies Program specifically tasks to liase DLSU to CHED Main Office, a task she performs since 2009.

Angelo R. dela Cruz received his B.Sc. and M.Sc. in Electronics and Communications Engineering degrees from Mapua Institute of Technology Manila in 2000, and from De La Salle University Manila in 2007 respectively. He received his Ph.D. in Electrical and Electronics Engineering from the University of the Philippines, Diliman in 2014. He is a licensed Electronics Engineer and an active member of the Institute of the Electrical and Electronics Engineers (IEEE) and Institute of Electronics Engineers in the Philippines (IECEP). His primary research interests are image and video coding and compression, cross-layer error-control optimization, and adaptive signal processing for digital communication system design. He has presented and published notable research papers in international conferences and journal publications in the area of multimedia signal processing and communications.

Jay Robert B. del Rosario was born at Imus in Cavite, Philippines, on October 11, 1982. In 2003, he continued his study in Manila and earned a degree in Bachelor of Science in Computer Engineering and Master of Information Technology at Technological University of the Philippines. He obtained his Certificate in Mechatronics in Milan, Italy late 2010 after passing the Mechatronics Specialist Exam. Mr. del Rosario was a former Professor and chairman of Mechatronics and Robotics Society in the Kingdom of Bahrain and Kingdom of Saudi Arabia from 2008–2011. He has been in the teaching profession for 12 years and currently pursuing his PhD in Electronics and Communications Engineering at De La Salle University-Manila, and PhD in Education major in Educational Management at Cavite State University-Indang, Cavite. His research interests include Mechatronics, Computer Systems Architecture, Webpage Design and Development, Software Engineering, Industrial Automation and Computational Intelligence. Most of his research articles can be viewed in Scopus, Google Scholar and Researchgate and a Professional Member of IEEE and Red Cross-Philippines.

Dennis S. Erasga is Associate Professor of Environmental Sociology at the De La Salle University (DLSU), Manila, Philippines. He is a Salzburg Global Seminar Fellow (Biography as Mirror of Society, 2006). He has publications on social theory, ecoconstructionism, literature as critique of science, and a theory of social action in Philippine sociology-"pakiramdaman" including two books: *From Grain to Nature: A Rice-Based History of Environmental Discourse in the Philippines*, 1946–2005 (2012) and *Sociological Landscape: Theories, Realities and Trends* (2013). Professor Erasga obtained his PhD in Environmental Science from the University of the Philippines, Los Banos. He is currently teaching graduate and undergraduate theory and sociology courses at the Behavioral Sciences Department, De La Salle University. He holds several professorial chairs the latest of which was the Pao Shih Tien Chair in Organizational Development.

Jean Clifford B. Espiritu received the B.Sc. in Electronics Engineering from De La Salle University - Manila in 2017.

He has since designed and fabricated commercialized Printed Circuit Boards for smart motor controller. He, together with his colleagues, has developed and published a research paper about a Fuzzy Logic Buck and Boost Converter using Arduino. His research interests include power electronics, schematic and PCB Design, and PCB Fabrication.

Laurence A. Gan Lim is a Full Professor of the Mechanical Engineering Department at De La Salle University. He obtained his Doctor of Philosophy in Computer Science at Coventry University. He is the Chair of the Institute of Electrical and Electronics Engineers (IEEE, Philippines). He is also a member of the Philippine Society of Mechanical Engineers (PSME). His main work is "Implementatio of GA-KSOM and ANFIS in the classification of colonic histopathological images."

Balintawak S. Gareza is a practicing anesthesiologist and presently the chair of the Division of Family and Community Medicine. She is the pioneer of research culture in the College of Medicine since its opening in 2002. Her effort in the field of academic research has earned the medical students' citations and awards in various research competitions in the National level.

Jomel A. Lorenzo Jr. received the B.Sc. in Electronics Engineering from De La Salle University - Manila in 2017. He has since developed BLDC motor control algorithms and designed embedded systems software in Arduino and Dave. He has received the best paper award and other rewards in DLSU Technology Fair 2017. His research interests include embedded systems, motor control, and battery systems management.

Noriel C. Mallari graduated with BS Electronics and Communications Engineering and MS Electronics and Communications Engineering from De La Salle University (DLSU), Manila, Philippines in 2006 and 2012, respectively. He is currently a PhD student in Electronics and Communications Engineering in DLSU. He is also an Assistant Professor of the Electronics and Communications Engineering Department, Gokongwei College of Engineering of DLSU. His research interests are controls and power management for electric vehicles and renewable energy applications.

Isidro Antonio V. Marfori III graduated with BS-Mechanical engineering and MS-Mechanical Engineering at De La Salle University-Manila in 2002 and 2009, respectively. He is currently a candidate for PHD in Mechanical Engineering at De La Salle University. He is also an Assistant Professor in the Mechanical Engineering Department of DLSU-Manila. His research interests are micro hydro power plants and other renewable energy, alternative personal transportation systems, and advances on computer-aided design.

Michael B. Ples is a medical practitioner in the field of Otolaryngology-Head and Neck Surgery. He is a medical and surgical fellow of the Philippine Academy of Medical Specialist Inc. and the International College of Surgeons-Philippine Section. His research interest are in the fields of medical science, animal physiology, and natural products.

Eric Camilo R. Punzalan obtained his bachelor's degree in chemistry in 1964 from De La Salle University (DLSU) as a COCOFED full scholar. He served as a junior faculty member of the same department shortly thereafter before leaving for the United States in 1988. After finishing graduate studies at the University of Connecticut under Prof William F. Bailey and a post-doctoral research stint at the University of Chicago with Prof Philip Eaton, he returned to the Philippines under the Balik Scientist Program of the Department of Science and Technology (DOST). He specializes in organic/organometallic chemistry and environmental science. He returned to DLSU Chemistry Department and served as Research Director for the College of Science from 1999 to 2005. During this period, he instituted the DLSU Research Congress and revived the college journal now known as the *Manila Journal of Science* (MJS).

Kristofferson M. Reyes received the B.Sc. in Computer Engineering from De La Salle University - Manila in 2017. He has since developed several Android applications, the notable ones being an Information Bank, "InfoBank," which serves as a logged and tracker of computers that go in and out of any IT department, and an e-bike app, "AdaptivEbike," which works in conjunction with a specific model of the e-bike in order to display, gather, and control the response of the e-bike. His research interests include artificial intelligence, cloud computing, and mobile software applications.

Edison A. Roxas received his Bachelor of Science in Electronics and Communications degree from the Technological Institute of the Philippines - Manila, and his Master of Science in Electronics and Communications degree from De La Salle University. He is a member of the Institute of Electronics Engineers in the Philippines (IECEP) and the Institute of Electrical and Electronics Engineers (IEEE). He is an active researcher and participated in several funded research grants either as main proponent or research assistant. His research interests focus on Machine Learning and Computer Vision applied in Biomedical Engineering, Transport and Traffic Management Engineering. At present, he is focused on finishing his Doctor of Philosophy in Electronics and Communications degree at De La Salle University.

Edwin Sybingco is a faculty of the DLSU ECE Department. He is currently taking his PhD in De La Salle University in the area of Digital Signal Processing (DSP) focusing on Big Data and Intelligent Systems. He received his Master of Science (Electronics and Communications Engineering) from De La Salle University. He already published more than 30 scientific papers internationally in the field of DSP, Machine Vision, Computational Intelligence, and robotics.

Romeo G. Teruel is a faculty member of the Business Economics department, University of St. La Salle. He is also the research director and assistant vice-chancellor for research at University of St. La Salle.

Ira C. Valenzuela received her Bachelor of Science in Electronics Engineering from Technological University of the Philippines in 2012 and Master of Science in Electronics and Communications Engineering from Mapúa Institute of Technology in 2015. She is currently working towards her Doctor of Philosophy in Electronics and Communications Engineering at De La Salle University in the area of computational intelligence. Her research interests are materials design, IC design, microelectronics, artificial intelligence, and evolutionary computing.

Ryan Rhay P. Vicerra is an Associate Professor of the Manufacturing Engineering and Management Department at De La Salle University. He received his Master of Science in Electronics and Communications Engineering in year 2008 and Doctor of Philosophy in Electronics and Communications Engineering in year 2015 at De La Salle University. He is a member of The Institute of Electrical and Electronics Engineers (IEEE) Philippines Section and Computational Intelligence Society Philippine Chapter. His main works are "Swarm intelligence for underwater swarm robot system," "Development of an underwater swarm robot system," and "Simulation of slime mold swarm intelligence."

Guidelines for Contributors

1. The Journal on Computational Innovations and Engineering Applications (JCIEA) aims to promote the development of new and creative ideas on the use of technology in solving problems in the field of computational applications, computational intelligence, electronics and information and communications technology (ICT), manufacturing engineering, energy and environment, robotics, control and automation, and all their related fields. Manuscript submissions should, therefore, be in pursuit of the same goal and within the related fields.
2. JCIEA only accepts manuscripts written in English. The responsibility for copyediting manuscripts, as well as obtaining reproduction permissions for the use of graphics and other materials from their references, will fall on the author.
3. Authors must also remember to cite all references and ensure that their paper submission has not been previously published or is undergoing peer review for another publication.
4. Manuscripts should include a unique title, an abstract, some keywords, an introduction and discussion of the study, a presentation and discussion of results, and a conclusion. Authors may also include an acknowledgement of funding organizations or consultants, if needed.
5. Manuscripts may be sent to *jciea.dlsu@gmail.com* or *jciea@dlsu.edu.ph* as either an MS Word file (*.doc or *.docx) or a LaTeX file (*.tex), including its supporting files.
6. Manuscripts in either file format should have the following features:

- Single-spaced, two-column format with 1-inch margin on all sides on letter-sized template
- Font to be used is Times New Roman, size 11
- Graphs (*.eps, *.svg), tables (*.csv), and images (*.jpg, *.png) should be saved and sent apart from the MS Word file.
- Citations and references should be submitted in IEEE or APA format.
- Submission of these references in a BibTeX format is preferred.

7. Manuscript should be eight to twelve (8–12) pages long, including all figures, tables, and references. Manuscripts exceeding the 12-page limit will require permissions from the editors.
8. Authors must include their full names and affiliations in the manuscript. They may include a 150- to 200-word biography to be included in the back portion of the journal.

Call for Papers

SCOPES AND TOPICS

Artificial Intelligence

Agents and Multi-agent Systems
Computational Intelligence
Genetic and Evolutionary Algorithms
Data Mining
Expert Systems
Fuzzy Logic
Machine Learning
Machine/Computer Vision
Natural Language Processing
Neural Networks

Emerging Technology Trends

Big Data Analytics
Biomedical, Health Care and Assistive Technologies
Cloud Computing
Human-to-Machine Interfaces
Internet of Things
Intelligent Transport Systems
Smart Cities
Smart Grids
Smart Farm Technologies
Virtual/Augmented Reality
Wireless Sensor Networks

Energy and Environment

Environmental Informatics
Environmental Systems Management
Green Technology
Industrial Ecology
Life Cycle Assessment and Material Flow Analysis
Nanotechnology and Nanomaterials
Renewable and Non-renewable Energy Sources
Solid Waste Management
Sustainability Models

Engineering, Information, and Communications Technology

Bioinformatics and Bioengineering
Biomedical Engineering
Biometrics
Business Intelligence
Computer-Aided Network Design
Computing Architectures and Systems
Cyber/Internet Security
Data Analytics
Decision Support Systems
Digital/Analog Signal Processing
E-Commerce Application Fields
E-Learning and Mobile Learning Tools
Electronic Circuits and Systems Engineering
Electronic Waste
Gamification
Image and Video Processing
Information and Communications Technology
Mechatronics Engineering
Power and Energy
Robotics, Control, and Automation
Sensing and Sensor Networks
Virtual Learning Environments
Web Analytics

For inquiries and paper submissions, email us at **jciea@dlsu.edu.ph** or visit at www.dlsu.edu.ph/offices/publishing-house/journals/jciea